DOCTORAL THESIS

EXTRACTION OF CHITIN AND PREPARATION OF ITS DERIVATIVES FROM ARTHROPODS FOR CIRCULAR ECONOMY APPLICATIONS

Samia ELOUALI

Jury Members

President	**R. JALAL**	Cadi ayyad University
Secretary	**H. CHAIRI**	University of Abdelmalek Essaidi
Examiner	**A. EL ABBASSI**	Cadi Ayyad University
Examiner	**E. LIZUNDIA**	University of the Basque Country
Examiner	**Q. ZHOU**	Royal Institute of Technology (KTH)
Thesis Director	**J-M. RAQUEZ**	University of Mons
Co-Director	**E. EL MOUDEN**	Cadi Ayyad University
Expert	**M. RHAZI**	Cadi Ayyad University

Dédicace

À mon père, Mohamed Elouali, à celui qui a toujours été ma force dans les moments de doute, mon refuge dans les tempêtes et la lumière qui a guidé chacun de mes pas. Si ce travail existe aujourd'hui, c'est parce que tu as cru en moi avant même que je n'y croie moi-même.

À mes frères et sœurs : Yassine, Soufiane, Kaoutar, Badr et Meryem, vous êtes une part de mon équilibre, de ma force et de mon courage. Votre présence n'a jamais cessé de m'accompagner.

À mes tantes Naima et Latifa, et à mon oncle Mustapha, pour votre présence précieuse, et pour tout ce que vous représentez dans mon parcours.

À mon mari, Zakaria Erraji, pour ton soutien indéfectible, ta patience et ta présence constante à mes côtés. Merci d'avoir été mon pilier, de m'avoir encouragée dans chaque étape et d'avoir partagé avec moi les sacrifices et les espoirs liés à ce parcours.

À vous, qui avez été là, dans l'ombre comme dans la lumière, ce travail vous appartient.

Acknowledgments

This journey is not only the story of a PhD, but the story of people who believed in me, supported me and walked beside me every step of the way. I would first like to express my deepest gratitude to Professor Mohammed Rhazi. This journey began with you during my Master's studies, when you introduced me to the world of chitin and chitosan. Since then, we have continued this adventure together. Thank you for your trust, for giving me this opportunity, and for allowing me to grow under your guidance. Working with you has always been a true pleasure and a great honor.

My sincere thanks go to my promotor, Professor Jean-Marie Raquez, for creating such an inspiring and stimulating scientific environment. Thank you for welcoming me into your laboratory, for your continuous support, and for believing in this work throughout this journey. Your guidance has been essential in shaping both this thesis and my scientific path.

I would also like to warmly thank Professor El Hassan El Mouden for accepting to take over the administrative supervision of my thesis after the retirement of Professor Rhazi. Your presence, your support, and your kindness during this transition have meant a lot to me.

To Dr. Samira Benali, words will never be enough. You have been far more than a supervisor to me. From my very first day in Mons until today, you have been a mentor, a guide, and a constant source of strength. You supported me beyond science, believed in me during difficult moments, and helped me grow both professionally and personally. Thank you for your patience, your trust, and your unwavering support. And I truly believe that the best is yet to come, and I am grateful that we will continue building it together.

I would like to express my sincere gratitude to Professor Khadija El Hariri, Director of the École Normale Supérieure of Marrakech, for her warm welcome, her constant support, and her encouragement throughout my academic journey. I would not be here today without you. You have always been a role model and a true source of inspiration.

I would also like to thank Mrs. Lalla Khadija Ahioud for her support, motivation, and presence. Thank you for everything you have done for me and for all ENS students. Your kindness has truly marked my journey. I would like to sincerely thank Mr. Hassan Lamtai and Mr. Sébastien Moins for their invaluable technical assistance in the laboratory throughout my doctoral work.

I am deeply grateful to ARES (Académie de Recherche et d'Enseignement Supérieur) for funding this research, and to the entire AQUA'MAR project team for the collaborative and supportive environment we built together. Special thanks to my colleagues Maryam Bousaid and Imad Zaouite, and to Professors Hicham Chairi, Igor Eeckhaut and Matthias Gosselin. And once again, thank you, Dr. Samira Benali, for everything.

I would like to thank my colleagues from the Équipe des Macromolécules Naturelles (EMN): Dr. Youssef Ait Hamdan, Dr. Soukaina Elkadaoui and Manar Azzi, for the shared moments and support.

I am also grateful to all members of the SMPC group: Rosica Mincheva, Noémie Hergue, Sylvie Dufour, Gédice Fernand, Djahida Lerari, Lola, Imade Armadi, Yosra Ajbar, Jacques-Kevin Wandji and Yousra Nait Hammou, who supported me, especially during my first steps at UMONS. A special thank you to Nathalie Vanderest for her constant help and kindness.

I would like to thank the Biological Structures and Biomimetics workgroup, directed by Professor Jan-Henning Dirks. I am especially grateful to Dr. Jendrian Riedel, Christoph Bruns and Jonas Unterholzner for the enriching scientific internship I had at HSB Bremen (University of Applied Sciences). This experience allowed me to develop a deeper critical understanding of structure–function relationships and to acquire valuable skills in advanced characterization techniques.

My sincere thanks also go to Professor Sam Van Wassenbergh and Dr. Joaquim Sanctorum from the University of Antwerp for introducing me to micro-CT techniques and helping me find the ideal laboratory for my scientific stay in Bremen.

I would like to thank Marlène Genlain and Maryse Demuynck for their support in the development and valorization of the patent arising from this work.

I also acknowledge the Near East Foundation, Emerging Business Factory, Enactus Morocco, and INDH for supporting the first pilot scale of SGW–ShrimpGreenWater, confirming the real-world potential of our process.

And finally, to those without whom none of this would have been possible.

À mon père, Mohamed Elouali, mon pilier, ma force et mon refuge.
Si je suis arrivée jusqu'à ce jour, c'est grâce à toi, après Dieu. Tes sacrifices, ton amour, ta présence constante et ton soutien inconditionnel ont été la lumière qui m'a guidée dans les moments les plus difficiles. Tu as toujours cru en moi, même lorsque je doutais, et c'est cette force que tu m'as transmise qui m'a permis d'avancer.

J’espère que ce travail te rendra fier, car chaque réussite que j’accomplis est le reflet de tout ce que tu m’as donné. Je t’aime plus que les mots ne pourront jamais l’exprimer.

To my brothers and sisters, Yassine, Soufiane, Kaoutar, Badr and Meryem, you have been my silent strength in every step of this journey. In moments of doubt and exhaustion, your words, your presence, and your unconditional support gave me the courage to keep going. Even from afar, I always felt you close to me. Thank you for being my foundation.

To my family, especially my aunts Naima and Latifa, and my uncle Mustapha, thank you for your love, your presence and your unwavering support from the beginning until the end of this journey.

To all the Elouali family, thank you for your encouragement and support throughout this path.

To my husband, Zakaria Erraji, for your unconditional support, your patience, and your constant presence by my side. Thank you for being my strength in moments of doubt, for encouraging me when I needed it most, and for sharing with me both the sacrifices and the hopes of this journey. This achievement is also yours.

To my in-laws, thank you for your kindness, your support, and for welcoming me as part of your family. Your presence and encouragement have meant a lot throughout this journey.

This work is as much yours as it is mine…

Abstract

This PhD thesis addresses the valorization of chitin-rich biomass within the framework of a sustainable and circular bioeconomy, with a particular focus on the development of an integrated strategy adapted to the Moroccan context. A novel autoclave-assisted process (AAP) was developed and optimized for the extraction of chitin and its conversion into chitosan from multiple biological sources, including marine by-products and terrestrial organisms. The proposed process demonstrated significant improvements compared to conventional extraction methods, notably through a drastic reduction in processing time, with deproteinization reduced from 18 hours to 75 minutes and deacetylation from 24 hours to 1 hour. In addition, reductions of 83% in chemical consumption and 80% in water usage were achieved, while maintaining a high protein removal efficiency of 94%. The extracted chitin exhibited high purity, preserved crystallinity, and favorable thermal properties, confirming the effectiveness of the process. These results are reflected in a high Industrial Feasibility Score (IFS), highlighting the strong potential of the AAP for industrial implementation. The influence of biomass origin on the physicochemical properties of chitin and chitosan was investigated, revealing significant variability in key parameters such as degree of deacetylation and molecular weight. This variability was leveraged for the design of advanced materials, leading to the development of an innovative three-dimensional (3D) chitosan scaffold. The resulting material exhibited outstanding adsorption performance toward inorganic pollutants, with maximum adsorption capacities reaching 860 $mg \cdot g^{-1}$ for Cu^{2+} and 576 $mg \cdot g^{-1}$ for Cr^{3+}, exceeding most values reported for conventional chitosan-based adsorbents. A marked selectivity toward multivalent ions was also demonstrated. Overall, this work establishes a coherent approach combining efficient extraction, material engineering and application development, and proposes a strategic framework for the implementation of a multi-feedstock chitin biorefinery in Morocco. By integrating process adaptability, resource diversity and high-value applications, this study contributes to the emergence of sustainable bio-based industries and highlights the potential of chitin as a key bioresource for future industrial systems.

Résumé

Cette thèse de doctorat porte sur la valorisation de biomasses riches en chitine dans le cadre d'une bioéconomie circulaire et durable, avec une attention particulière portée au développement d'une stratégie intégrée adaptée au contexte marocain. Un procédé innovant assisté par autoclave (AAP) a été développé et optimisé pour l'extraction de la chitine et sa conversion en chitosane à partir de diverses sources biologiques, incluant des sous-produits marins et des organismes terrestres. Le procédé développé a permis d'obtenir des améliorations significatives par rapport aux méthodes conventionnelles, notamment une réduction drastique du temps de traitement, avec une déprotéinisation passant de 18 heures à 75 minutes et une désacétylation de 24 heures à 1 heure. En parallèle, des réductions de 83 % de la consommation de réactifs chimiques et de 80 % de la consommation d'eau ont été obtenues, tout en maintenant une efficacité d'élimination des protéines de 94 %. La chitine extraite présente une haute pureté, une cristallinité préservée et des propriétés thermiques favorables, confirmant la performance du procédé. Ces résultats se traduisent par un score élevé de faisabilité industrielle (IFS), soulignant le fort potentiel du procédé AAP pour une mise à l'échelle industrielle. L'influence de l'origine biologique sur les propriétés physicochimiques de la chitine et du chitosane a été mise en évidence, révélant des variations significatives du degré de désacétylation et de la masse molaire. Cette variabilité a été exploitée pour la conception de matériaux avancés, conduisant au développement d'un scaffold tridimensionnel (3D) innovant à base de chitosane. Ce matériau a montré des performances remarquables en adsorption de polluants inorganiques, avec des capacités maximales atteignant 860 $mg \cdot g^{-1}$ pour Cu^{2+} et 576 $mg \cdot g^{-1}$ pour Cr^{3+}, dépassant la majorité des adsorbants à base de chitosane rapportés dans la littérature. Une sélectivité marquée envers les ions multivalents a également été observée. Dans l'ensemble, ce travail propose une approche cohérente combinant un procédé d'extraction performant, une ingénierie des matériaux et le développement d'applications à forte valeur ajoutée, tout en introduisant un cadre stratégique pour la mise en place d'une bioraffinerie de la chitine multi-ressources au Maroc. En intégrant l'adaptabilité des procédés, la diversité des ressources et le développement d'applications ciblées, cette étude contribue à l'émergence d'industries biosourcées durables et met en évidence le potentiel de la chitine comme ressource clé pour les systèmes industriels futurs.

ملخّص

تركّز هذه الأطروحة على تثمين الكتلة الحيوية الغنية بالكيتين في إطار اقتصاد حيوي دائري ومستدام، مع اهتمام خاص بتطوير استراتيجية متكاملة ملائمة للسياق المغربي. تم تطوير وتحسين عملية مبتكرة بمساعدة الأوتوكلاف (AAP) لاستخلاص الكيتين وتحويله إلى الكيتوزان انطلاقًا من مصادر بيولوجية متعددة، تشمل مخلفات بحرية وكائنات برية.

أظهرت العملية المقترحة تحسينات كبيرة مقارنة بالطرق التقليدية، خاصة من خلال تقليص كبير في زمن المعالجة، حيث تم تقليل زمن نزع البروتين من 18 ساعة إلى 75 دقيقة، وزمن نزع الأسيتيل من 24 ساعة إلى ساعة واحدة فقط. بالإضافة إلى ذلك، تم تحقيق انخفاض بنسبة 83% في استهلاك المواد الكيميائية و80% في استهلاك المياه، مع الحفاظ على كفاءة عالية في إزالة البروتين بلغت 94%. كما أظهرت الكيتين المستخلصة نقاوة عالية وبنية بلورية محفوظة وخصائص حرارية جيدة، مما يدل (IFS)، مما يؤكد فعالية العملية. وتعكس هذه النتائج الحصول على مؤشر مرتفع لقابلية التطبيق الصناعي على الإمكانات الكبيرة لهذه العملية للتطبيق على نطاق صناعي.

كما تم دراسة تأثير مصدر الكتلة الحيوية على الخصائص الفيزيائية والكيميائية للكيتين والكيتوزان، حيث تم تسجيل اختلافات ملحوظة في درجة نزع الأسيتيل والكتلة الجزيئية. وقد تم استغلال هذه الاختلافات في تصميم مواد متقدمة، مما أدى إلى تطوير هيكل ثلاثي الأبعاد (3D) مبتكر من الكيتوزان. وقد أظهر هذا الهيكل أداءً متميزًا في امتزاز الملوثات غير العضوية، حيث بلغت سعة الامتزاز القصوى 860 ملغ/غ لأيونات النحاس و576 ملغ/غ لأيونات الكروم، وهي قيم تتجاوز معظم ما ورد في الأدبيات العلمية للمواد المعتمدة على الكيتوزان. كما تم تسجيل انتقائية واضحة تجاه الأيونات متعددة الشحنة.

بشكل عام، يقدم هذا العمل مقاربة متكاملة تجمع بين تطوير عملية استخراج فعالة، وهندسة مواد متقدمة، وتطبيقات ذات قيمة مضافة عالية، مع اقتراح إطار استراتيجي لإنشاء مصفاة حيوية متعددة المصادر للكيتين في المغرب. ومن خلال دمج مرونة العمليات، وتنوع الموارد، وتطوير تطبيقات مستهدفة، تساهم هذه الدراسة في دعم ظهور صناعات حيوية مستدامة وتبرز الإمكانات الكبيرة للكيتين كمورد أساسي للأنظمة الصناعية المستقبلية.

Dissemination & Communication

List of Publications- Thesis related

- S. Elouali, Y. Ait Hamdan, S. Benali, P. Lhomme, M. Gosselin, J.M. Raquez, M. Rhazi, Extraction of chitin and chitosan from *Hermetia illucens* breeding waste: A greener approach for industrial application, Int. J. Biol. Macromol. 285 (2025) 138302. https://doi.org/10.1016/J.IJBIOMAC.2024.138302.
- S. Elouali, I. Armadi, S. Benali, Y. Paint, J.H. Dirks, P. Lhomme, M. Rhazi, E.H Mouden, J.M. Raquez, Influence of autoclave-assisted process and the chitin fibers orientation on the physicochemical properties of chitin and chitosan from different Bioresources. Bioresource Technology Journal. ***Submited***
- S. Elouali, S. Benali, M. Rhazi, J.M. Raquez, Bioengineered chitosan scaffolds for tunable and sustainable heavy metal removal from water. *Nature communications.* ***Submited***

List of Publications- Collaborations and other works

- S. Elouali, H. Ait Ali Ouydir, Y. Ait Hamdan, N. Eladlani, M. Rhazi, Chitosan from *Periplaneta americana L.*: a sustainable solution for heavy metals removal, EuroMediterr J Environ Integr (2024). https://doi.org/10.1007/s41207-024-00645-6.
- S. Elouali, Y. Ait Hamdan, M. Belmajdoub, M. Rhazi, Green chitosan extraction from *Hermetia illucens* breeding waste (prepupal cases): Characterization and bioadsorption activity, Int. J. Biol. Macromol. 281 (2024) 136449. https://doi.org/10.1016/j.ijbiomac.2024.136449.
- S. Elouali, O. Dahbane, Y. Ait Hamdan, N. Eladlani, M. Rhazi, Exploring the potential use of chitosan derived from *Hermetia illucens* waste for olive oil mill wastewater treatment, EuroMediterr. J. Environ. Integr. (2024). https://doi.org/10.1007/s41207-024-00593-1.
- S. Elouali, J. Elarabi, F. El Amerany, Y. Ait Hamdan, N. Eladlani, S. Benali, H. Lamtai, E.H. El Mouden, J.-M. Raquez, M. Rhazi, Chitosan-enhanced hydroponic cultivation of *Ocimum basilicum L.*: a sustainable approach for improved growth, quality and antioxidant activity, EuroMediterr. J. Environ. Integr. 10 (2025) 4551–4564. https://doi.org/10.1007/s41207-025-00809-y.
- S. Elouali, S. Benali, Y. Ait Hamdan, M. Bousaid, M. Salam, M.A. Elhidan, E.H El Mouden, J.M. Raquez, M. Rhazi. Chitosan from *Tityus tenuimanus*: Moroccan Scorpion with Dual Cu(II) and Hg(II) Bioadsorption and Antimicrobial Activity, EuroMediterr. J. Environ. Integr. (2026). ***Accepted***

- Y Ait Hamdan, H. Oudadesse, S. Elouali, N. Eladlani, B. Lefeuvre, M. Rhazi, Exploring the potential of chitosan from royal shrimp waste for elaboration of chitosan/bioglass biocomposite: Characterization and "in vitro" bioactivity, Int. J. Biol. Macromol. (2024) 134909. https://doi.org/10.1016/j.ijbiomac.2024.134909.
- Y Ait Hamdan, S. Elouali, N. Eladlani, B. Lefeuvre, H. Oudadesse, M. Rhazi, Investigation on *Akis granulifera* (Coleoptera, Sahlberg, 1823) as a potential source of chitin and chitosan: Extraction, characterization and hydrogel formation, Int. J. Biol. Macromol. 252 (2023) 126292. https://doi.org/10.1016/J.IJBIOMAC.2023.126292.
- Y. Ait Hamdan, S. Elouali, H. Oudadesse, B. Lefeuvre, M. Rhazi, Exploring the potential of chitosan/aragonite biocomposite derived from cuttlebone waste: Elaboration, physicochemical properties and in vitro bioactivity, Int. J. Biol. Macromol. 267 (2024) 131554. https://doi.org/10.1016/J.IJBIOMAC.2024.131554.
- Y.A. Hamdan, H. Oudadesse, L. Jawad, K. Smimih, H. Kabdy, S. Elouali, N. Eladlani, M. Rhazi, Chitosan-Based Biomaterials for Tissue Engineering of Glial Cells, in: 2023: pp. 416–441. https://doi.org/10.4018/978-1-6684-9675-6.ch021.
- Y.A. Hamdan, B. El-Mansoury, S. Elouali, K. Rachmoune, A. Belbachir, H. Oudadesse, M. Rhazi, A review of chitosan polysaccharides: Neuropharmacological implications and tissue regeneration, Int. J. Biol. Macromol. (2024) 135356. https://doi.org/10.1016/J.IJBIOMAC.2024.135356.
- Y.A. Hamdan, S. Elouali, A. Ben Maloui, B. El-Mansoury, H. Oudadesse, M. Rhazi, Chitosan and its derivatives as potential neuro-protective agents for the treatment of Parkinson's disease, 2023. https://doi.org/10.4018/978-1-6684-5156-4.ch015.
- M. Salam, V. Grossule, S. Elouali, F. Wang, S. Benali, J.-M. Raquez, W. Yakti, V. Bolletta, M. Henjak, F. Hayat, Q. Wang, Sustainable biowaste management: Uncovering the environmental footprint of traditional and emerging waste managing technologies, Environmental Chemistry and Ecotoxicology 7 (2025) 1684–1700. https://doi.org/10.1016/j.enceco.2025.07.012.
- M. Salam, V. Grossule, C. Li, D. Renault, A.E. Mahmoud, S. Elouali, F. Wang, S. Ullah, V. Bolletta, Y. Cao, Toxicity and bioconversion: Meta-analytical insights into microplastic effects on black soldier fly rearing, Science of The Total Environment 1011 (2026) 181120.https://doi.org/10.1016/j.scitotenv.2025.181120.
- B. El-Mansoury, K. Smimih, Y.A. Hamdan, A. El Khiat, S. Elouali, H. El Fatimi, A. Draoui, O. El Hiba, A.R. Jayakumar, The interplay between environmental pollutants, gut microbiota, and infections: Current concepts and therapies, 2023. https://doi.org/10.4018/978-1-7998-9414-8.ch008.

- Y. Ait Hamdan, H. Oudadesse, S. Elouali, K. Smimih, H. El Ghachi, A.J.S.D. Gnimassoun, R.A. Ramdane, N. Eladlani, M. Rhazi, Chitosan Polysaccharides, in: 2023: pp. 400–415. https://doi.org/10.4018/978-1-6684-9675-6.ch020.
- I. Armadi, S. Elouali, A. Abana, A. El Housseini, S. Loqman, A. Belbachir, Overview of Biomaterials Classification, Properties, and Biomedical Applications, in: Innovations and Applications of Advanced Biomaterials in Healthcare and Engineering, IGI Global Scientific Publishing, 2025: pp. 51–90. https://doi.org/10.4018/979-8-3373-1305-4.ch002.
- Y. Ait Hamdan, I. Armadi, khawla Rachmoune, F.E. Elamrani, M. Mekouar, A. El Housseini, A. Moufakkir, S. Elouali, S. Loqman, A. Belbachir, M. Rhazi, Therapeutic Implications of Chitosan and Its Derivatives, in: Biomedical Applications and Toxicity of Polymers, Nanoparticles, Biomaterials, and Metal Ions, IGI Global Scientific Publishing, 2025: pp. 205–232. https://doi.org/10.4018/979-8-3373-0055-9.ch009.
- Y.A. Hamdan, M. Rhazi, H. Kabdy, A. Benmaloui, S. Elouali, J. Laadraoui, Z.H. Ahmad, N. Eladlani, H. Oudadesse, Investigation of Potential Neuroprotective Role of Chitosan-Based Biomaterials and Their Derivatives by Targeting Glial Cells, in: 2023: pp. 375–399. https://doi.org/10.4018/978-1-6684-9675-6.ch019.
- F. El Amerany, S. Elouali, Y.A. Hamdan, I. Janah, M. Rhazi, Reducing the Toxicity of Heavy Metals and Metalloids on Grain Crops by Breeding, in: Plant Stress Tolerance, CRC Press, Boca Raton, 2025: pp. 327–342. https://doi.org/10.1201/9781003457237-16.

Patent applications

- Porous chitosan scaffold for water purification. European Patent Application P1804-UK Scoremet

Participation to congress- Poster presentations

- ELOUALI S., AIT ALI OUYDIR H., AIT HAMDAN Y., ELADLANI N., RHAZI M., RAQUEZ J.M. "Valorization of waste from *Periplaneta Americana L.* as a new chitinous source applicated in the treatment of a real effluent". Poster, International conference on Water-Energy-Food-Ecosystem Nexus in the mediterranean region (WEFE2023), Marrakech, Morocco, 15-17.11.2023
- AIT HAMDAN Y., ELOUALI S., ELADLANI N.,OUDADESSE H., RHAZI M., RAQUEZ J.M. "Valorization of natural resources based cuttlefish bone waste by producing active biomolecules: chitin, chitosan and aragonite". Poster,

International conference on Water-Energy-Food-Ecosystem Nexus in the mediterranean region (WEFE2023), Marrakech, Morocco, 15-17.11.2023

- ELOUALI S., AIT HAMDAN Y., ELADLANI N., RHAZI M., RAQUEZ J.M. "Revealing the Potential of Chitin and Chitosan: Sustainable Extraction and Transformation of Marine Waste for Climate Action". Poster, International conference on Water-Energy-Food-Ecosystem Nexus in the mediterranean region (WEFE2023), Marrakech, Morocco, 15-17.11.2023
- ELOUALI S., BOUSAID M., BENALI S., RAQUEZ J.M., RHAZI M. "Exploring arthropods as an alpha-chitin and beta-chitin sources for sustainable aquaculture nets production", poster presentation, BPG annual meeting, Blankenberge, Belgium, 30-31.05.2024
- ELOUALI S., AIT HAMDAN Y., BENALI S., LHOMME P., GOSSELIN M., RAQUEZ J.M., RHAZI M. "Sustainable extraction of chitin and chitosan from *Hermetia illucens* breeding waste: Controlled properties and Eco-friendly approach", poster presentation, the 2024 PhD Scientific Day, Louvain-la-Neuve, Belgium, 31.10.2024
- ELOUALI S., AIT HAMDAN Y., BENALI S., LHOMME P., GOSSELIN M., RAQUEZ J.M., RHAZI M. "Extraction of chitin and chitosan from *Hermetia illucens* breeding waste: a greener approach for industrial application", poster presentation, BPG 2025, Houffalize, Belgium, 26-27.05.2025

Participation to congress- Oral presentations

- ELOUALI S., AIT HAMDAN Y., ELADLANI N., RHAZI M., RAQUEZ J.M. " Complexation of Mercury by Chitosan extracted from scorpion species". Oral presentation, 5th International conference on Advanced Materials for Photonics, Sensing and Energy Conversion Energy Applications (AMPSECA'2023), Marrakech, Morocco, 25-26.05.2023
- ELOUALI S., AIT HAMDAN Y., ELADLANI N., RHAZI M., RAQUEZ J.M. "Chitosan Derived from *Hermetia illucens* waste: A novel approch to mitigate heavy metal pollution". Oral presentation, International conference on Water-Energy-Food-Ecosystem Nexus in the mediterranean region (WEFE2023), Marrakech, Morocco, 15-17.11.2023
- ELOUALI S., DAHBANE O., AIT HAMDAN Y., ELADLANI N., RHAZI M., RAQUEZ J.M. "The promising pretreatment of olive mill wastewater by chitosan produced from *Hermetia illucens* prepupal cases". Oral presentation, International conference on Water-Energy-Food-Ecosystem Nexus in the mediterranean region (WEFE2023), Marrakech, Morocco, 15-17.11.2023
- ELOUALI S., BENALI S., RAQUEZ J.M., RHAZI M., "Exploring arthropods as an alpha-chitin and beta-chitin sources for circular economy applications", Oral

presentation, International Conference on Multidisciplinary Sciences and Technological Developments ICMUSTED 2024, Bayburt, Turkey, 13-15.12.2024

Table of Contents

List of Abbreviations

AAP: Autoclave-Assisted Process

ANOVA: Analysis of Variance

BA: *Buthus atlantis*

BSF: Black Soldier Fly

CHT: Chitin

CHS: Chitosan

DA: Degree of Acetylation

DTG: Derivative Thermogravimetry

DTG_{max}: Maximum Degradation Temperature

EDX: Energy Dispersive X-ray Spectroscopy

ESEM: Environmental Scanning Electron Microscopy

FTIR: Fourier Transform Infrared Spectroscopy

HI: *Hermetia illucens*

I_{Cr}: Crystallinity Index

IFS: Industrial Feasibility Score

KOH: Potassium Hydroxide

NaOH: Sodium Hydroxide

HCl: Hydrochloric Acid

Mv: Viscosity-average Molecular Weight

NMR: Nuclear Magnetic Resonance

^{1}H-NMR: Proton Nuclear Magnetic Resonance

POM: Polarized Optical Microscopy

PL: *Parapenaeus longirostris*

PP: *Pollicipes pollicipes*

RM: Raw Material

Sc: Scaffold

SEM: Scanning Electron Microscopy

SM: *Scorpio mogadorensis*

SO: *Sepia officinalis*

SS: *Sardina pilchardus*

TDS: Total Dissolved Solids

TG: Thermogravimetric Analysis

TRL: Technology Readiness Level

UV-Vis: Ultraviolet–Visible Spectroscopy

XRD: X-ray Diffraction

3D: Three-Dimensional

Tables list

Figures List

Part 1: General Introduction

The continuous growth of the global population, together with increasing industrialization and urbanization, has led to a rising demand for materials largely derived from petroleum resources. This dependence raises two major challenges. On one hand, fossil resources are finite and unevenly distributed worldwide, leading to economic dependence of many countries on petroleum-exporting regions and contributing to geopolitical tensions [1,2]. On the other hand, petroleum-based materials generate persistent waste, which accumulate in the environment and cause long-term ecological damage [3].

These limitations highlight the need to rethink current production models and to reduce our reliance on fossil resources. One possible pathway consists in shifting toward renewable and locally available bioresources. In this context, biomass represents a promising alternative, as it is widely accessible and can be exploited according to regional specificities. Unlike petroleum, being concentrated in specific areas of the world, biomass is distributed across all countries, offering the opportunity to develop more autonomous and sustainable production systems based on local resources.

This transition is closely related to the concept of circular bioeconomy, which promotes the valorization of biological resources and organic residues into value-added products [4]. By integrating principles of resource efficiency, recycling and reuse, this approach aims to reduce waste, while maintaining materials within productive cycles for as long as possible **(figure 1)**. In this framework, the concept of biorefinery plays a central role, as it refers to the integrated processing of biomass into a spectrum of valuable products, including materials, chemicals and energy. Biorefinery approaches enable the efficient utilization of biomass by maximizing the value extracted from biological resources, while minimizing waste generation [4,5]. Such a transition is strongly supported by international initiatives, particularly the United Nations

Sustainable Development Goals (SDGs), adopted in 2015 by more than 190 countries [6]. Among these, SDG 6 (Clean Water and Sanitation), SDG 9 (Industry, Innovation and Infrastructure), and SDG 12 (Responsible Consumption and Production) emphasize the importance of developing sustainable materials and environmentally responsible industrial processes.

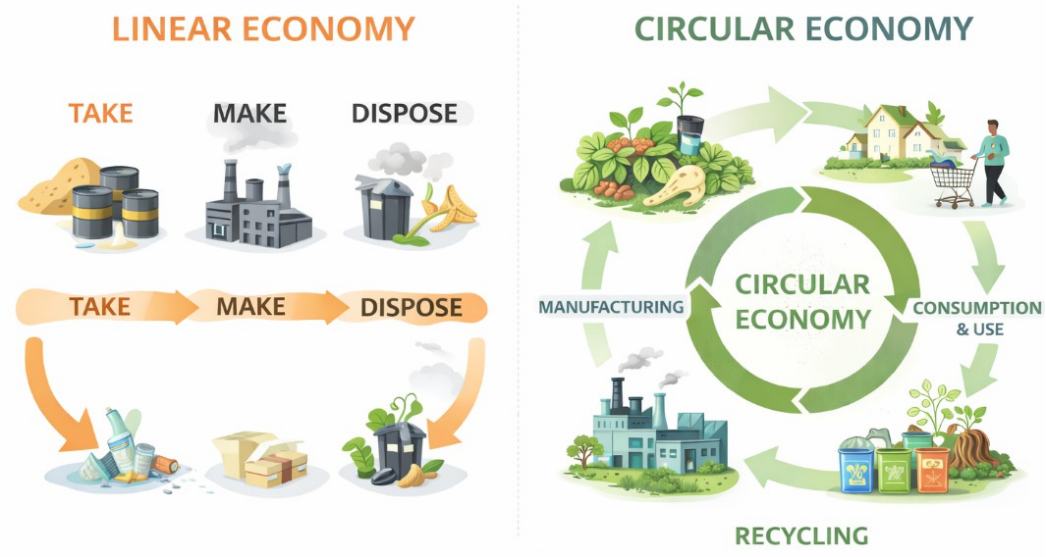

Figure 1. Schematic representation of resource flows in linear and circular economical systems

Within this framework, an important question arises: which biological resources can be mobilized to replace petroleum-based materials? The answer largely depends on the availability and diversity of biomass resources within each country. Indeed, biomass is not uniformly distributed and its nature varies according to geographical, climatic and economic contexts. Depending on these factors, different types of biomass can be valorized, including lignocellulosic resources such as wood, agricultural residues and marine biomass. This context-dependent availability highlights the importance of developing locally adapted strategies based on the specific bioresources accessible in each country. Among these, marine biomass represents a particularly relevant resource in regions where fishing and seafood processing activities generate large quantities of organic waste.

These marine by-products, including arthropods biomass such as crustacean shells, and cephalopod residues, are rich in valuable biopolymers. Among them, chitin stands out as one of the most abundant natural polysaccharides [7]. It can be extracted from various biological sources and transformed into functional materials with a wide range of applications. The growing interest in chitin and its derivatives is reflected in their increasing industrial importance. In 2020, the global market for chitin and chitosan was estimated at USD 42.24 billion and is projected to reach approximately USD 69.30 billion by 2028 [8], highlighting their strong commercial potential.

In this context, Morocco offers particularly favorable conditions for the development of chitin-based valorization strategies. The country benefits from an extensive coastline along both the Atlantic Ocean and the Mediterranean Sea, supporting important fisheries and seafood processing industries that generate significant quantities of marine by-products, including shrimp shells, crab residues and cephalopod wastes [9]. These aquatic biomass residues constitute an abundant and locally available bioresource that remains largely underexploited. Their valorization represents a promising pathway toward the implementation of a circular bioeconomy based on marine resources. In this perspective, the development of a chitin biorefinery approach appears particularly relevant, as it would enable the conversion of this biomass into high-value products while minimizing waste and improving resource efficiency. Such an approach would allow Morocco to rely on its own bioresources to reduce dependence on petroleum-derived materials and to develop sustainable and locally adapted production systems. In this context, a central question arises: what strategies can be developed today to enable the effective implementation of a chitin biorefinery in Morocco, allowing this bioresource to be sustainably exploited and integrated into future bio-based industry?

The present doctoral research was conducted within the framework of the AQUA'MAR project (ARES-PRD) entitled "(Re)dynamization of Moroccan

Aquaculture through the Valorization of Natural Resources from Arthropods". This Moroccan-Belgian collaborative project aims to promote the sustainable development of aquaculture and marine biotechnology through the valorization of locally available biological resources, by integrating the expertise of Moroccan and Belgian research institutions (University of Cadi Ayyad and University of Mons). Within this context, the objective of this thesis was to evaluate the potential of chitin derived from different Arthropods including *Hermetia illucens* breeding residues, generated during the production of insect-based feed for aquaculture, as a valuable bioresource for the development of functional materials. To address this objective, the thesis first provides a comprehensive state of the art on chitin-rich bioresources, their extraction strategies and their potential application production systems. The state of the art is presented in the following chapter in order to further detail and critically analyze the different aspects discussed above.

Part 2: State Of The Art

1. Chitin and its derivatives

1.1. Discovery, historical background and chemical structure

Chitin is one of the most abundant natural polysaccharides in the biosphere and constitutes a major structural component in numerous biological systems. The scientific discovery of chitin dates back to 1811, when the French chemist Henri Braconnot isolated a previously unknown substance from mushroom cell walls, which he initially termed "fungine". Later, in 1823, the substance was also identified in insect cuticles by Auguste Odier, who introduced the term chitin, derived from the Greek word chiton, meaning protective covering or tunic. Since then, chitin has been recognized as a key structural biopolymer present in a wide range of organisms, including arthropods, fungi, mollusks and certain algae.

Structurally, chitin is a linear polysaccharide composed of β-(1→4)-linked N-acetyl-D-glucosamine units **(figure 2)**, forming long polymer chains analogous to cellulose but differing in the substitution of the hydroxyl group at the C-2 position by an acetamide group [10]. This molecular architecture promotes the formation of highly ordered crystalline domains through extensive intra- and intermolecular hydrogen bonding interactions between adjacent chains. As a consequence, chitin exhibits remarkable structural stability and mechanical resistance, properties that are essential for its biological function as a reinforcing element in protective exoskeletons and structural matrices.

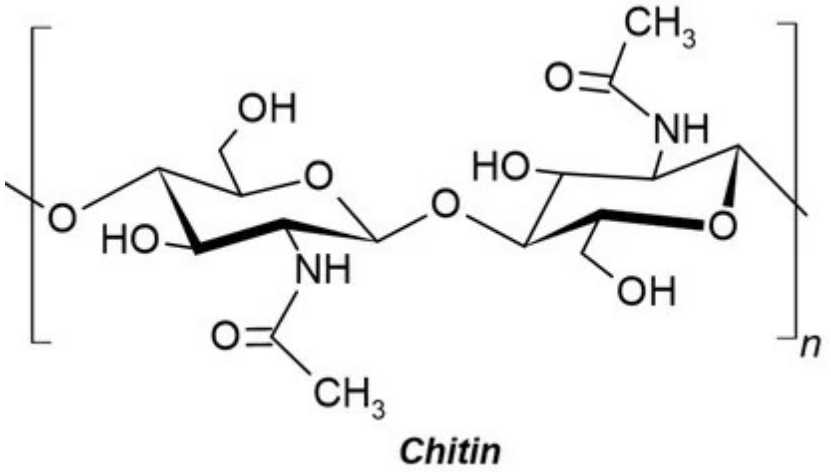

Figure 2. Chemical structure of chitin

At the supramolecular level, individual chitin chains assemble into microfibrils and nanofibrillar bundles, which are embedded within a proteinaceous matrix in biological tissues. This hierarchical organization leads to the formation of highly ordered crystalline microfibrils that confer exceptional stiffness and chemical resistance to the polymer [11]. Such a dense hydrogen-bonding network significantly reduces solubility in most common solvents, which explains why native chitin is generally considered chemically inert and requires specific treatments to enable its transformation into functional derivatives [12–14].

1.2. Conversion of chitin into chitosan

Although chitin is abundant in Nature, its direct industrial applications remain limited due to its poor solubility in most solvents [15]. This limitation is primarily related to the strong hydrogen-bonding network between polymer chains and the high crystallinity of the material. To overcome this limitation, chitin is commonly transformed into chitosan, which represents the most widely utilized derivative of chitin. From a historical perspective, the conversion of chitin into chitosan was first reported in 1859 by the French physiologist Charles Rouget, who demonstrated that treating chitin with concentrated alkaline solutions leads to a modified form of chitin

that becomes soluble in acidic media [16]. This discovery laid the foundation for the development of chitosan as a distinct and functional derivative of chitin. The industrial production of chitosan emerged much later, notably in Japan in the early 1970s, where the abundance of crustacean waste from seafood processing industries provided a readily available raw material [17]. This context, combined with a strong seafood industry and early investments in biomaterials and industrial biotechnology, enabled Japan to play a pioneering role in the large-scale production and commercialization of chitin and chitosan, significantly contributing to their global development [18].

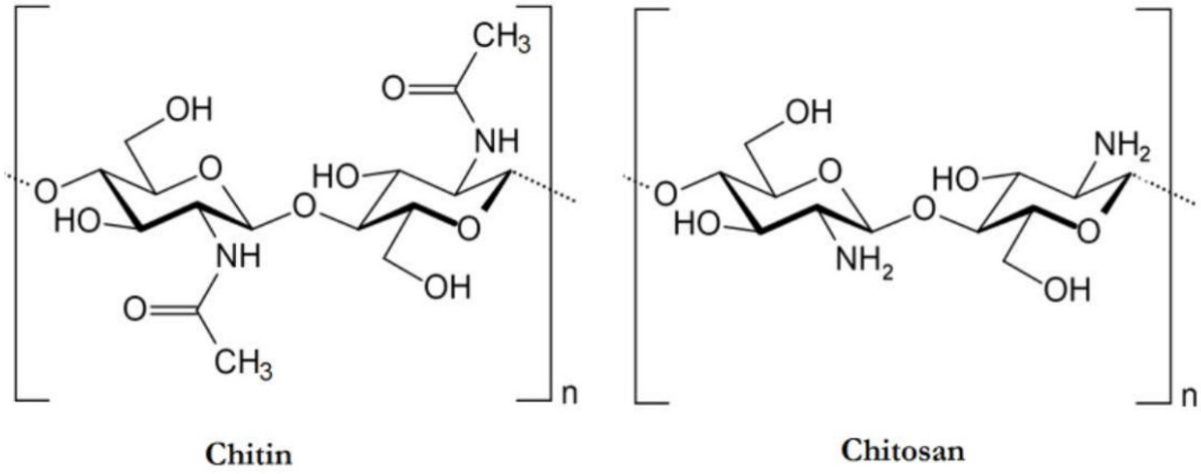

Figure 3. Chemical structure of chitin and chitosan

Chitosan is then obtained through the partial or complete deacetylation of chitin, typically performed under alkaline conditions. During this process, acetyl groups attached to the amino functions of N-acetylglucosamine units are removed, generating D-glucosamine residues containing free primary amine groups along the polymer backbone [19]. As a result, chitosan becomes a copolymer composed of glucosamine and N-acetylglucosamine units, whose relative proportions depend on the degree of acetylation **(figure 3)**.

1.3. Key properties of chitin derivatives

The wide range of technological applications attributed to chitin and chitosan is closely associated with their distinctive physicochemical and biological properties. These characteristics arise from the molecular structure of the polymer backbone and the presence of reactive functional groups distributed along the chains. Parameters such as the degree of acetylation, molecular weight, crystallinity and thermal behavior strongly influence the physicochemical performance of these biopolymers and determine their suitability for various applications. In addition to these structural parameters, chitin and chitosan exhibit several functional properties including biodegradability, antimicrobial activity, antioxidant behavior and strong chelating capacity toward metal ions, which significantly broaden their application potential in sustainable material systems [20].

1.3.1. Degree of acetylation (DA)

The degree of acetylation (DA) represents one of the most critical parameters controlling the properties of chitin and chitosan. It corresponds to the proportion of acetylated N-acetyl-D-glucosamine units relative to deacetylated glucosamine residues along the polymer chain [21]. Native chitin typically presents a high degree of acetylation, often exceeding 90%, whereas chitosan is characterized by lower acetylation levels due to the deacetylation process applied during extraction.

Variations in the degree of acetylation strongly affect several physicochemical characteristics, including solubility, charge density, intermolecular interactions and chemical reactivity [22]. When the degree of acetylation decreases, a higher number of free amino groups becomes available along the polymer backbone. In acidic environments, these amino groups become protonated, generating a polycationic structure, which favorize interaction with molecules such as proteins, microbial cell membranes and dissolved metal ions [23]. As a consequence, the degree of acetylation

plays a fundamental role in determining the adsorption capacity, biological activity and chemical functionality of chitosan-based materials.

1.3.2. Molecular weight (Mv)

The molecular weight (Mv) of chitin and chitosan is another essential parameter influencing their physicochemical behavior. Molecular weight directly affects solution viscosity, mechanical strength, diffusion properties and the ability of the polymer chains to interact with other molecules [24]. High Mv chitosan generally exhibits enhanced viscosity and improved mechanical properties, making it suitable for applications such as film formation, membrane fabrication and coating technologies [25]. Conversely, lower Mv chitosan or chitosan oligomers often demonstrate increased solubility and improved biological activity due to their higher mobility and greater ability to penetrate biological membranes [26]. The Mv distribution of chitosan can be influenced by extraction conditions, alkaline treatment and depolymerization processes such as enzymatic hydrolysis or oxidative degradation [27]. Consequently, controlling molecular weight represents an important strategy for tailoring the functional properties of chitosan for specific industrial or biomedical applications.

1.3.3. Crystallinity and chitin fiber orientation

Chitin occurs naturally in several crystalline polymorphic forms depending on the spatial arrangement of its polymer chains during biosynthesis. Three main allomorphic structures have been identified: α-chitin, β-chitin and γ-chitin [28] **(figure 4)**. Among these forms, α-chitin is the most common and thermodynamically stable structure, typically found in crustacean shells and insect cuticles. In this configuration, adjacent polymer chains are arranged in an antiparallel orientation, resulting in strong intersheet hydrogen bonding that produces a highly compact crystalline structure with limited swelling capacity. In contrast, β-chitin, which is mainly found in cephalopods such as squid pens and cuttlefish structures [29], exhibits a parallel chain

arrangement with weaker hydrogen bonding interactions. This structural configuration generates a more open crystalline lattice, making β-chitin more reactive and more susceptible to chemical modification. The third form, γ-chitin, is comparatively rare and consists of a combination of parallel and antiparallel chain arrangements. Although less frequently encountered, γ-chitin has been identified in specific biological structures such as insect cocoons and certain fungal cell walls.

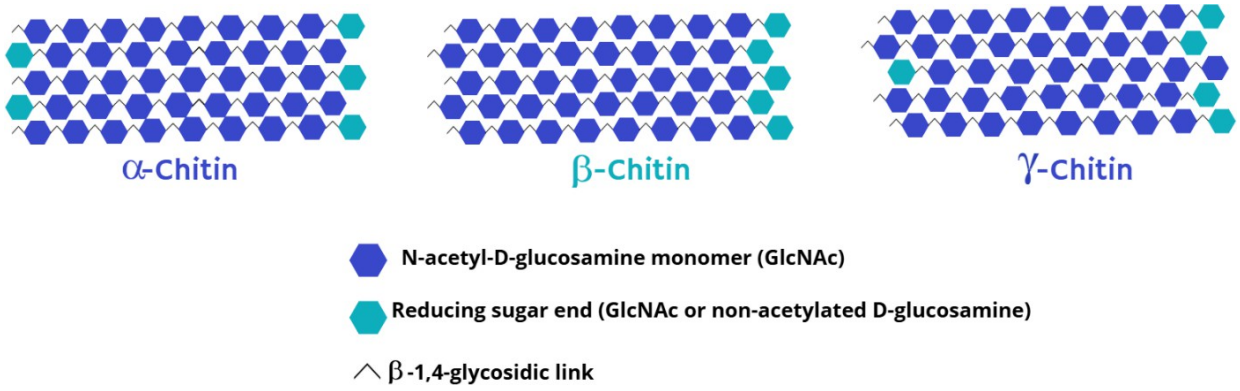

Figure 4. Polymorphic forms of chitin

During the conversion of chitin into chitosan, a partial disruption of these crystalline regions occurs as a result of the deacetylation process. This transformation typically leads to a decrease in crystallinity and increases the accessibility of reactive functional groups along the polymer chains. Changes in crystallinity therefore influence key material properties, including water absorption capacity, chemical reactivity and mechanical performance [30].

Beyond polymorphism, the spatial orientation of chitin microfibrils within biological matrices represents another crucial structural parameter influencing material performance. In most arthropod exoskeletons, chitin nanofibrils are arranged in layered helicoidal architectures known as Bouligand structures, where successive fibrillar layers are rotated by small angles relative to each other. Other spatial

orientations have been reported such as parallel, parabolic and helicoidal [31,32] **(figure 5)**.

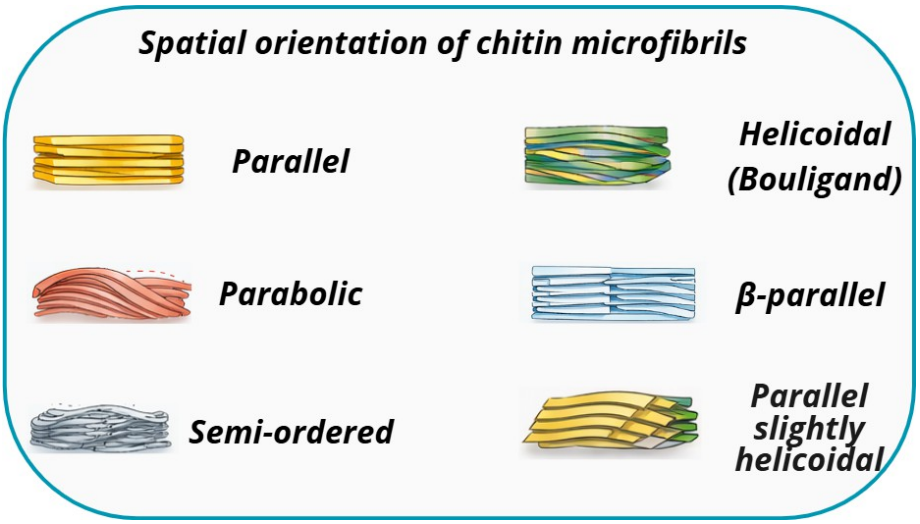

Figure 5. Spatial orientation of chitin microfibils

Such hierarchical structuring results in highly organized nanofibrillar assemblies embedded within protein matrices, where fiber alignment governs mechanical stiffness, permeability and fracture behavior [33]. Variations in microfibril orientation influence the packing density of crystalline domains, hydrogen-bonding interactions between polymer sheets and crystallite coherence length, thereby modulating both crystallinity and macroscopic material properties [34].

Despite the extensive literature describing the polymorphism, crystallinity and hierarchical organization of chitin, these structural features have been predominantly studied in a separated manner. In particular, although different microfibrillar architectures and polymorphic forms have been widely reported, their evolution during extraction and conversion processes remains insufficiently understood. More importantly, no clear link has been systematically established between these structural characteristics, especially microfibril orientation, and the resulting functional properties of chitin- and chitosan-based materials. Since fiber orientation is known to

influence key properties such as mechanical strength, porosity and mass transfer behavior, establishing this structure–property relationship is essential for the rational design of functional materials.

1.3.4. Thermal properties

Chitin and chitosan exhibit relatively high thermal stability compared with many other naturally-occurring biopolymers. Their thermal behavior typically involves a two-stage degradation process, including initial dehydration step, followed by decomposition of the polymer backbone at higher temperatures [35,36]. The thermal stability of these materials depends strongly on structural parameters such as DA, crystallinity and Mv, which govern intermolecular interactions and chain mobility [37]. Due to its highly ordered crystalline structure and strong intermolecular hydrogen bonding, chitin generally shows higher thermal stability than chitosan. In contrast, chitosan exhibits slightly lower degradation temperatures because the deacetylation process disrupts the ordered crystalline structure of the polymer and reduce the extent of hydrogen bonding interactions within the polymer matrix [38]. Understanding these thermal characteristics is essential for optimizing material processing conditions. For instance, as reported by *Râpa and Vasile (2020)*, during solvent casting of chitosan-based films, drying temperatures must be carefully controlled (typically below 100 °C) to avoid premature thermal degradation and to preserve film integrity [39]. Similarly, the thermal stability of chitin and chitosan based materials directly affects the mechanical performance and structural stability of films obtained by solution casting [40]. In coating technologies, thermal resistance determines the appropriate curing and drying conditions required to ensure uniform film formation without degradation. Moreover, in the fabrication of porous structures such as freeze-dried chitosan scaffolds, thermal transitions and degradation temperatures play a crucial role in controlling pore morphology and preventing structural collapse, thereby influencing the final material properties.

Furthermore, the thermal properties of chitin depend significantly on its polymorphic form. In particular, β-chitin exhibits lower thermal stability, with maximum degradation temperatures generally not exceeding approximately 350 °C [41]. This lower stability is attributed to its parallel-chain arrangement and weaker intermolecular hydrogen bonding, which results in a less compact crystalline structure. In contrast, α-chitin, characterized by an antiparallel chain arrangement and a highly ordered crystalline structure, exhibits higher thermal stability due to stronger intra and intermolecular hydrogen bonding [42,43]. Consequently, the tighter molecular packing in α-chitin requires higher energy to initiate thermal degradation, leading to higher decomposition temperatures compared to β-chitin.

1.3.5. Biodegradability and biocompatibility

One of the most attractive features of chitin and chitosan is their biodegradable and biocompatible nature. These biopolymers can be enzymatically degraded by naturally occurring enzymes such as chitinases, lysozymes and other glycosidases, leading to the formation of oligomers and glucosamine derivatives [44]. These degradation products are generally non-toxic and can be metabolized by living organisms. The biodegradability of chitin and chitosan makes them particularly suitable for applications requiring environmentally friendly materials. Their degradation products exhibit minimal ecological persistence and can be reintegrated into natural biochemical cycles.

1.3.6. Antimicrobial and antioxidant activities

Chitosan is widely recognized for its intrinsic antimicrobial activity against a broad range of microorganisms including Gram-positive and Gram-negative bacteria, fungi and certain viruses. This antimicrobial effect is mainly attributed to the polycationic nature of chitosan, which enables strong electrostatic interactions with charged microbial cell membranes. These interactions can disrupt membrane integrity, increase

permeability and ultimately inhibit microbial growth [45]. In addition to antimicrobial activity, chitosan and several of its derivatives exhibit antioxidant properties, which are associated with their capacity to scavenge reactive oxygen species and chelate transition metal ions involved in oxidative reactions. These antioxidant characteristics have leveraged considerable interest in fields such as food preservation, biomedical materials and pharmaceutical formulations that will be discussed below [46].

1.3.7. Chelating and bioadsorption capacity

Chitosan is known for its strong chelating ability toward metal ions and various environmental pollutants [47,48]. The presence of amino and hydroxyl functional groups along the polymer backbone allows chitosan to interact with metal ions through mechanisms such as ion exchange, complexation and electrostatic attraction [49]. These interactions make chitosan as an efficient bioadsorbent for environmental remediation, particularly in the removal of heavy metals such as lead, cadmium, copper and chromium from contaminated water [47,50,51]. Numerous studies have demonstrated that adsorption efficiency depends strongly on structural parameters such as DA, Mv and surface morphology of the material [52,53].

1.4. Main derivatives of chitin and chitosan

Although native chitin and chitosan possess several intrinsic physicochemical and biological properties, their direct application in advanced technological fields often requires structural or morphological modifications. In many cases, the native polymer structure does not provide the optimal reactivity, surface area, or selectivity needed for specific applications. Consequently, various derivatives and engineered forms of chitin and chitosan have been developed in order to tailor their functional properties and enhance their performance in targeted applications. These modifications may involve chemical functionalization of the polymer backbone or the fabrication of materials with specific architectures and morphologies. In environmental applications,

for example, chitosan derivatives are frequently designed to improve selectivity and adsorption capacity toward specific metal ions or pollutants, through the introduction of functional groups capable of forming coordination complexes with metal species [54]. In agricultural applications, structural modification of chitosan can enhance its bioactivity as a plant growth stimulator or elicitor of plant defense mechanisms, thereby improving crop productivity and resistance to environmental stress [55]. Similarly, in biomedical and pharmaceutical fields, chitin and chitosan derivatives are often engineered to optimize properties such as biocompatibility, controlled drug release, mechanical stability, and interaction with biological tissues [56]. Beyond chemical modification, the versatility of chitin and chitosan also arises from their ability to be processed into a wide range of structural forms and functional materials. These include films, nanoparticles, hydrogels, beads, porous scaffolds and composite materials **(figure 6)**, each offering specific structural characteristics that can be exploited for different applications [57–60].

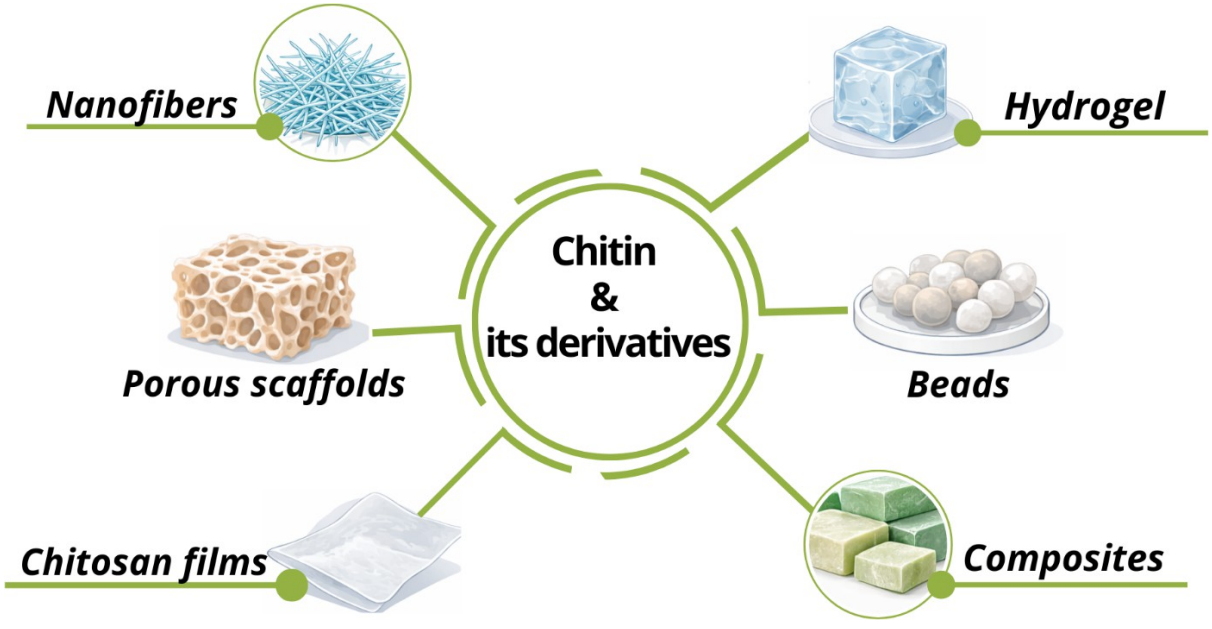

Figure 6. Derivatives of chitin and chitosan

One of the most common forms of chitosan-based materials is chitosan films, which are obtained through solution casting [61]. Due to their excellent film-forming ability, flexibility and antimicrobial properties, chitosan films have been extensively investigated for applications in biomedical coatings and barrier materials [62]. Another important class of derivatives involves nano-structured chitin and chitosan materials. These nanostructures can be produced in different morphologies, primarily as nanocrystals or nanofibers, depending on the extraction and processing methods used [63]. They exhibit extremely high surface area and enhanced reactivity [64]. These features make them particularly attractive for applications in nanocomposites, biomedical materials and advanced adsorption systems. The nanoscale structure also facilitates interactions with biological membranes and improves the dispersion of these materials within polymer matrices.

Hydrogels consist of three-dimensional polymer networks formed through either chemical crosslinking (covalent bonds) or physical interactions such as ionic bonding, hydrogen bonding and chain entanglement between polymer chains [65,66]. In the case of chitosan, network formation is primarily governed by interactions involving its reactive amino (-NH_2) and hydroxyl (–OH) groups, which can participate in crosslinking reactions or electrostatic interactions with multivalent ions [67]. These interconnected structures enable the hydrogel to absorb large quantities of water while maintaining structural integrity [68]. Their high-water retention capacity, biocompatibility and tunable porosity make them particularly suitable for applications such as drug delivery systems, wound dressings, tissue engineering and environmental remediation [69]. Chitosan can also be processed into beads or microspheres, typically through ionic gelation or precipitation techniques. In ionic gelation, chitosan chains are crosslinked through electrostatic interactions between protonated amino groups (-NH_3^+) and multivalent anions such as tripolyphosphate (TPP) [47], leading to the formation of stable hydrogel beads. In precipitation-based

methods, chitosan is first dissolved in acidic solution and then dropped into an alkaline medium (e.g., NaOH), where deprotonation of amino groups induces polymer aggregation and solid bead formation [58,70]. These spherical structures are widely used as adsorbents or carriers due to their high surface area and accessible functional groups. Chitosan beads have demonstrated high efficiency in the removal of heavy metals, dyes and other contaminants from aqueous solutions, making them promising materials for water purification technologies [47,58].

Another promising class of materials derived from chitosan is three-dimensional porous scaffolds, which are typically obtained through techniques such as freeze-drying (lyophilization), gas foaming or phase separation. In particular, freeze-drying involves the removal of solvent from a frozen chitosan solution, leading to the formation of an interconnected porous network. The resulting structure is characterized by high porosity and pore interconnectivity, which are key parameters for facilitating cell infiltration and mass transfer [71,72]. Chitosan scaffolds have attracted considerable interest in biomedical engineering, particularly in tissue regeneration and wound healing applications due to their biocompatibility, biodegradability and structural similarity to components of the extracellular matrix [73,74]. In environmental applications, porous scaffolds can also function as highly efficient adsorbent materials capable of capturing pollutants from contaminated water. However, this potential remains insufficiently explored in the literature. In addition to these forms, chitin and chitosan are frequently combined with other natural or synthetic polymers to produce composite materials with enhanced properties.

2. Extraction and processing of chitin and chitosan

Several technological strategies have been developed to extract chitin and chitosan. These approaches aim to remove minerals, lipids, protein fractions and acetyl groups. The main extraction routes currently reported in the literature include conventional

chemical extraction, biological or green extraction methods such as enzymatic extraction and DES & ionic liquid solvents, and emerging intensified technologies like ultrasound assisted process, microwave assisted process and autoclave assisted process, as illustrated in **figure 7**.

Figure 7. Extraction techniques of chitin and chitosan

Conventional chemical extraction remains the dominant industrial process due to its operational simplicity and high extraction efficiency. This method typically relies on sequential acid and alkaline treatments to remove mineral salts and proteins from the biomass. Despite its widespread use, chemical extraction requires significant quantities of reagents and generates large volumes of effluents, raising important environmental concerns [75,76]. To reduce chemical consumption and improve environmental performance, biological extraction approaches have been explored. Enzymatic treatments using microbial or marine proteases can remove protein fractions from crustacean shells under milder conditions while preserving polymer integrity [77,78].

In parallel, several process intensification technologies have been developed to accelerate extraction reactions and improve process efficiency. Microwave-assisted extraction has been reported to significantly reduce processing time during the demineralization, deproteinization and deacetylation steps [79]. In a recent study, chitosan with a degree of deacetylation of approximately 82.7% was produced in about 24 min using microwave irradiation, compared with 6–7 h required by conventional heating [80]. A comparative overview of the principal extraction methods, including their main principles, advantages and limitations, is summarized in **Table 1**.

Table 1. Comparison of the main extraction methods used for chitin and chitosan production

Extraction method	Experimental conditions	Advantages	Limitations	Ref
Conventional chemical extraction	-Demineralization: 3 M HCl, 75 °C, 2 h -Deproteinization: 10% NaOH, 80 °C, 2 h -Deacetylation: 50% NaOH, 100 °C, 2.5 h	-High extraction efficiency -Industrially established -Reproducible	-High consumption of acids and bases -Large volumes of wastewater -Possible polymer degradation	[80]
Autoclave-assisted extraction	Deproteinization using 2.5 M NaOH under autoclave conditions (121 °C, 15 psi, 20 min) followed by acid demineralization	-Faster protein removal -Improved process efficiency	The method is limited only in shrimp shells source	[77]
	Deacetylation using 50% NaOH in 1h	-Faster and efficient deacetylation (DA=5%)		[81]
Enzymatic extraction	-Protease-assisted deproteinization using microbial enzymes -3 h hydrolysis at 45 °C	-Mild conditions -Preserves polymer molecular weight	-High enzyme cost -Slower than chemical extraction	[77]
Microwave-assisted extraction	-Demineralization: 3 M HCl, 500 W, 8 min -Deproteinization: NaOH, 160–350 W, 8 min -Deacetylation: NaOH 50%, 350 W, 8 min	-Strong reduction in processing time (minutes instead of hours) -Energy-efficient	-Requires microwave equipment -Scaling up remains challenging	[80]

Ultrasound-assisted extraction	Ultrasonic treatment 20–40 kHz for ~30–60 min combined with acid/alkali extraction	-Enhanced mass transfer -Reduced chemical usage	-Energy demand -Process optimization required	[82]
Fermentation-based extraction	Lactic acid fermentation 4–6 days for simultaneous demineralization and deproteinization	-Low chemical consumption -Environmentally friendly	-Long processing time -limited industrial scalability	[83]

Despite the promising results reported for intensified extraction techniques, several limitations remain, particularly regarding their industrial applicability. In industrial contexts, process selection is primarily driven by efficiency, productivity and cost, while sustainability and environmental impacts are still considered as secondary considerations in many cases. Although alternative extraction methods have been proposed to reduce chemical consumption and processing time, their implementation at large scale remains limited. Recent comparative studies have further highlighted the potential of autoclave-assisted processes for chitin deacetylation. In particular, a study conducted on shrimp shell biomass demonstrated that autoclave-assisted treatment can achieve a high deacetylation (DA=5%), compared to conventional thermochemical methods (DA= 19%) and microwave-assisted processes (DA=33%) [81]. This enhanced performance is attributed to the combined effect of elevated temperature and pressure, which improves alkali diffusion into the crystalline structure and promotes more efficient removal of acetyl groups.

However, it is important to note that in these studies, including those reported by Younes et al., [77], the deacetylation step is carried out using highly concentrated sodium hydroxide solutions (50% NaOH), following conventional Kurita-type protocols [84]. While being effective, these conditions are known to induce partial depolymerization of chitosan chains, leading to a decrease in molecular weight [85]. In contrast, alternative deacetylation approaches such as the Broussignac process, based on mixtures of KOH, ethanol and ethylene glycol, have been reported to provide

efficient deacetylation while better preserving the polymer chain length, resulting in higher molecular weight chitosan [86]. Nevertheless, such alternative chemistries have not yet been investigated under autoclave-assisted conditions.

Moreover, the application of autoclave-assisted extraction remains largely limited to shrimp shell biomass, with no comprehensive studies evaluating its performance across different chitin sources. This restricts the assessment of its robustness and limits its current technological readiness level (TRL). In addition, key parameters such as water consumption, energy demand and overall environmental impact of the process are rarely evaluated, making it difficult to determine its real sustainability compared to conventional extraction methods. Furthermore, most studies focus primarily on extraction yield, without systematically investigating how processing conditions influence the structural and functional properties of the final chitin and chitosan materials. Beyond the extraction process itself, the biological origin of the raw material is also a critical factor influencing the properties of the final product. The interplay between biomass source and extraction method therefore remains insufficiently understood and deserves further investigation.

3. Arthropods biomass as a source of chitin

3.1. Main industrial sources

Arthropods constitute the most important reservoirs due to the structural role of chitin in their exoskeletons [87]. Industrial production of chitin has therefore historically relied on arthropod biomass, particularly marine crustaceans such as shrimp, crabs and lobsters, whose shells contain significant amounts of chitin embedded within a matrix of proteins, minerals and pigments [88]. Crustacean processing industries generate large quantities of shell waste during seafood preparation. These residues typically represent 40–60% of the total biomass of crustaceans and contain chitin contents ranging from approximately 20 to 30% of the dry weight, making them the primary commercial source for industrial chitin extraction [87,89].

Recently, other arthropod groups have increasingly attracted scientific attention as alternative chitin sources. Insects represent one of the most promising emerging resources, particularly in the context of the rapid expansion of insect farming industries for animal feed and organic waste recycling. Species such as BSF produce substantial quantities of exoskeletal residues during their life cycle, especially in the pupal stage, which are rich in chitin and can be valorized for biopolymer production [90]. Other arthropod resources have also been investigated, including terrestrial organisms such as scorpions and beetles whose exoskeletons contain structurally organized chitin [91]. Although these resources remain less explored compared with marine crustaceans and insects, they provide interesting perspectives for diversifying chitin supply chains and expanding the range of available biomass feedstocks. Beyond arthropods, cephalopod by-products such as squid pens and cuttlefish bones are also recognized as valuable marine resources containing chitin in the β-polymorphic form [92]. These residues are generated in large quantities by seafood processing industries

3.2. Advantages and limitations of each source

Although several biological sources can provide chitin, their industrial relevance depends on factors such as availability, extraction efficiency, chemical composition and environmental sustainability. Each biomass source presents specific advantages as well as certain limitations that must be considered when evaluating its potential for large-scale chitin production. A comparative overview of the main advantages and limitations associated with these different sources is presented in **table 2**, highlighting the main characteristics influencing their suitability for chitin production.

Table 2. Advantages and disadvantages of each chitin source

Source	Advantages	Disadvantages	Ref
	- Well-established extraction methods with high efficiency	- Seasonal availability can limit supply	**[93,94]**

Crustaceans (Shrimp, Crab, Lobster)	- High chitin content (up to 30% of dry weight) - Commercially available and widely used in various industries - Good mechanical properties of extracted chitin, making it suitable for diverse applications	- Potential allergens (e.g., tropomyosin) that may pose health risks - Requires harsh chemical treatments (HCl) due to the high mineral content that may damage chitin structure and lead to environmental pollution	
Insects (e.g., BSF puparia)	- Year-round availability, allowing for consistent supply - Higher chitin content in some species (up to 40% of dry weight) - More sustainable and eco-friendly, with lower carbon footprint - Potential for higher yields and simpler extraction processes compared to crustaceans	- Less established extraction methods compared to crustaceans, requiring further optimization - Variability in chitin quality depending on species and extraction method - Limited commercial availability and market acceptance, affecting scalability	**[95–97]**
Fungi (e.g., Termitomyces, Ganoderma)	- Renewable and sustainable source with minimal environmental impact - Absence of allergenic proteins, making it safer for consumption - More environmentally friendly with lower disposal costs and potential for waste substrate utilization	- Lower chitin content compared to crustaceans and insects (typically around 5-10% of dry weight) - Extraction methods still being optimized, with less standardization - Potential risks of pathogenic fungi if not handled properly	**[95]**
Squid Pens	- Renewable source with minimal environmental impact and year-round	- Lower chitin content compared to crustaceans (typically around 15-20%)	**[98]**

	- Can be processed with fewer environmental concerns compared to crustaceans	- Limited commercial use and availability, affecting market viability - Extraction methods may not be as well-developed as those for crustaceans

3.3. Potential of Moroccan bioresources

Morocco possesses significant natural resources that could support the development of sustainable chitin supply chains within a circular bioeconomy framework. The country benefits from an extensive coastline of approximately 3 500 km along both the Atlantic Ocean and the Mediterranean Sea, supporting one of the most important fisheries sectors in Africa [99]. This sector generates large quantities of marine by-products originating from seafood processing industries, including crustacean shells, cephalopod structures and other chitin-containing residues that remain partially underutilized. Several investigations conducted on Moroccan marine resources have highlighted the considerable quantities of chitinous waste generated by seafood processing activities. In Northern Morocco, shrimp decortication units located between Larache and Tangier produce large volumes of shell residues that can be valorized through chitin extraction. These wastes represent a significant industrial resource, with an estimated potential of approximately 950 tons of purified chitin per year, which could subsequently yield around 700 tons of chitosan after deacetylation [9]. The recovery of chitin from such residues represents an effective strategy to transform seafood processing waste into high-value biomaterials while reducing the environmental burden associated with their disposal.

Cephalopod processing residues also constitute an important but still underexploited source of chitin along the Moroccan coast. Studies focusing on cuttlefish processing units in Dakhla, one of the main cephalopod fishing areas in Morocco, demonstrated that the large quantities of discarded cuttlebones could potentially generate around 77

tons of β-chitin annually, which may subsequently be converted into approximately 60 tons of chitosan depending on the extraction and deacetylation processes employed [92]. In addition to their abundance, these residues are particularly interesting because they contain β-chitin, a polymorphic form characterized by a more open crystalline structure and higher reactivity compared with the α-chitin typically obtained from crustaceans [87].

At a smaller geographic scale, investigations carried out in the coastal city of Essaouira between 2012 and 2013 further illustrate the local potential of seafood waste valorization. Surveys conducted in several seafood restaurants revealed that considerable quantities of chitin-rich residues are generated annually, including approximately 17 370 kg of shrimp waste, 22 680 kg of squilla residues, and 43 740 kg of spider crab shells, in addition to smaller quantities of squid pens and cuttlebones [100]. Although these values correspond to a limited urban area, they highlight the substantial availability of chitinous biomass that could be recovered through integrated valorization strategies. Beyond marine resources, Morocco also offers favorable conditions for the development of alternative chitin sources. The increasing interest in insect farming for animal feed production and organic waste recycling provides new opportunities for generating chitin-rich residues, particularly from species such as BSF. These residues could be integrated into sustainable biomass valorization systems, enabling the conversion of organic waste streams into functional biomaterials while supporting circular bioeconomy principles [101].

4. Main applications

Chitin and its derivatives have been widely explored in various scientific and industrial sectors, including biomedicine, agriculture, food technology and environmental remediation. Their versatility and adaptability allow them to be processed into different material forms such as films, nanoparticles, hydrogels, beads

and porous scaffolds, which significantly expands their range of applications **(figure 8)**.

In biomedical fields, these polymers have been extensively investigated for applications such as drug delivery systems, wound dressings and tissue engineering scaffolds. Chitosan-based materials provide a favorable environment for cell adhesion and proliferation, while their antimicrobial properties contribute to reducing the risk of infection in medical devices and wound healing applications. In agriculture, chitosan has attracted increasing attention as a natural plant biostimulant and elicitor of plant defense responses. Its application can stimulate plant growth, enhance resistance to pathogens and improve tolerance to environmental stresses. Chitosan-based formulations are therefore considered promising environmentally friendly alternatives to conventional agrochemicals.

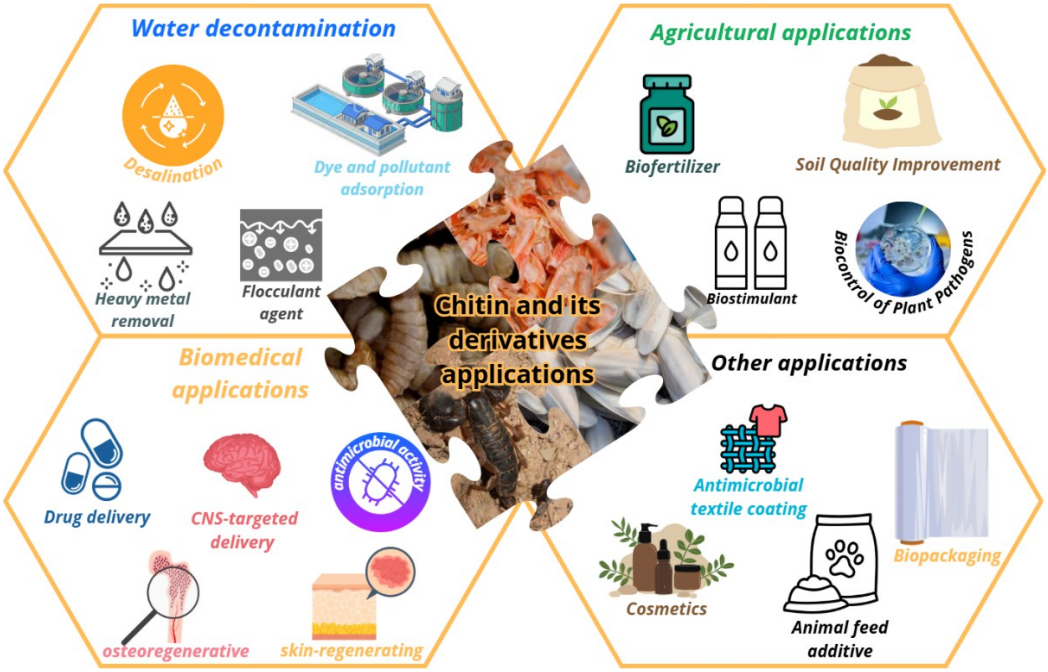

Figure 8. Chitin and its derivatives applications

In the food sector, chitosan is commonly investigated for the development of biodegradable packaging materials and edible coatings [102,103]. Thanks to its film-forming ability and antimicrobial activity, chitosan can be used to produce protective

films capable of extending the shelf life of perishable food products and reducing microbial contamination [104,105].

Water contamination represents one of the major environmental challenges associated with industrial development and intensive agricultural activities. Aquatic systems act as vectors for the dispersion of pollutants, including heavy metals, salts, dyes and emerging contaminants, which can accumulate in ecosystems and enter the food chain **(figure 9)**.

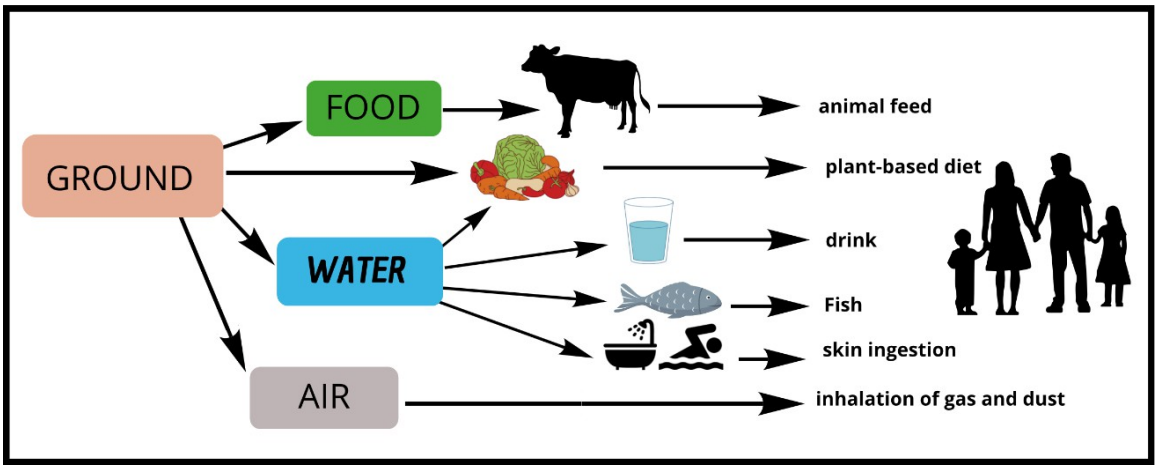

Figure 9. Water vector contamination in ecosystems

Among the inorganic contaminants frequently detected in natural and industrial waters, metal and non-metal ions such as Cu^{2+}, Cr^{3+}, Ca^{2+}, Pb^{2+}, Cd^{2+}, K^{+}, Mg^{2+} and Na^{+} are commonly encountered and represent important environmental challenges [106]. Some of these elements are essential micronutrients at trace concentrations but become toxic when present at elevated levels [107]. For instance, copper (Cu^{2+}) plays a role in several enzymatic processes. However, excessive exposure may induce oxidative stress, liver damage and neurological disorders [108]. Chromium (Cr^{3+}) is generally considered less toxic than hexavalent chromium, yet high concentrations may still cause metabolic disturbances and cellular toxicity [109]. In contrast, metals such as lead (Pb^{2+}) and cadmium (Cd^{2+}) are highly toxic even at low concentrations. Lead exposure is associated with severe neurological effects and developmental disorders,

while cadmium accumulation can lead to kidney dysfunction, bone demineralization and carcinogenic effects [110].

In addition to heavy metals, alkaline and alkaline-earth ions such as Ca^{2+}, Mg^{2+}, Na^{+} and K^{+} play an important role in determining water hardness and salinity [111]. Although these ions are essential for biological processes and plant nutrition, excessive concentrations can significantly alter water quality. High levels of sodium and magnesium salts contribute to water salinization and soil degradation, which may reduce agricultural productivity and disturb nutrient uptake in plants [112]. Similarly, elevated calcium and potassium concentrations can influence ionic balance in irrigation water and hydroponic nutrient solutions, affecting plant growth and crop quality. Because these ions frequently coexist in contaminated or saline waters, the development of efficient materials capable of selectively removing or regulating their concentration is essential for water purification and sustainable agricultural practices [113].

Among the various materials investigated for water purification, chitosan-based adsorbents have attracted considerable attention due to their unique physicochemical properties and environmental compatibility. Chitosan is a naturally derived polysaccharide characterized by the presence of a high density of reactive amino (–NH_2) and hydroxyl (–OH) functional groups, which can interact strongly with metal ions through mechanisms such as chelation, ion exchange and electrostatic interactions. These functional groups provide numerous active sites for binding contaminants, enabling efficient adsorption of metal ions from aqueous solutions. One of the main advantages of chitosan as a bioadsorbent lies in its high affinity toward transition metal ions, particularly heavy metals such as Pb^{2+}, Cd^{2+}, Cu^{2+} and Cr^{3+}. The coordination between metal ions and amino groups present along the chitosan backbone leads to the formation of stable complexes, allowing effective removal of these contaminants even at relatively low concentrations. In addition, the adsorption

performance of chitosan can be significantly enhanced through chemical modification, crosslinking or the incorporation of functional groups, which improve its stability and selectivity toward specific pollutants. A comparative overview of some chitin derivatives used for the removal of heavy metals and salinity-related ions from water is summarized in **Table 3.**

Table 3. Representative chitin derivatives and chitosan-based materials used for water treatment applications

Chitin derivatives	Structural characteristics	Target pollutants	Key advantages	Reference
Chitosan beads	Porous spherical structure	Pb^{2+}, Cu^{2+}, Cd^{2+}	High adsorption capacity and easy recovery	[114]
Crosslinked chitosan	Chemically stabilized polymer network	Pb^{2+}, Cr^{3+}	Improved stability in acidic conditions	[115]
Magnetic chitosan composites	Chitosan + Fe_3O_4 nanoparticles	Pb^{2+}, Cu^{2+}	Easy magnetic separation after adsorption	[116,117]
Functionalized chitosan (thiol/carboxyl)	Modified functional groups	Pb^{2+}, Hg^{2+}, Cd^{2+}	Improved selectivity toward metal ions	[115]
Chitosan membranes	Thin porous filtration material	Salts, metal ions	Removal efficiency between 100 and 400$mg.g^{-1}$	[118]

5. Role of chitin and chitosan in the circular economy and sustainability

Chitin and chitosan have emerged as key bio-based polymers that enable the valorization of chitin-rich biomass generated by marine, agricultural and industrial activities [87,89]. Large quantities of such residues are produced annually from seafood processing industries, insect farming and other arthropod resources, representing an important yet underexploited source of renewable biomaterials.

Figure 10. Integration of chitin and chitosan in the circular bioeconomy framework

The recovery of chitin from these biological residues exemplifies a circular bioeconomy approach in which waste streams are converted into high-value biopolymers. This strategy contributes to reducing environmental pollution associated with seafood and insect farming waste while simultaneously generating sustainable materials for industrial applications [101]. As illustrated in **figure 10**, chitin and chitosan valorization integrates several stages of the circular economy, including biomass waste recycling, bio-based material production and the development of environmentally friendly technologies. Beyond resource efficiency, the sustainable exploitation of

chitin-rich biomass also contributes to several United Nations Sustainable Development Goals (SDGs). The development of chitosan-based materials for environmental technologies supports SDG 6 (Clean Water and Sanitation), while the advancement of bio-based polymer technologies promotes SDG 9 (Industry, Innovation and Infrastructure). Furthermore, the transformation of biological waste into valuable biomaterials aligns with SDG 12 (Responsible Consumption and Production) by encouraging sustainable resource management and waste reduction. Overall, the integration of chitin and chitosan production within biomass valorization strategies represents a promising pathway toward the development of sustainable materials and circular bioeconomy systems. By linking waste recycling, renewable biomaterials and environmental technologies, these biopolymers illustrate how biological resources can contribute to more sustainable industrial models.

6. Conclusion

The literature review highlights that chitin and its derivatives represent highly promising bio-based materials due to their abundance, biodegradability and versatile physicochemical properties. Their capacity to be processed into a wide range of functional materials, including films, hydrogels, beads and porous scaffolds, enables applications across multiple fields such as biomedicine, agriculture, food packaging and environmental remediation. In particular, their strong chelating ability and adsorption performance position chitosan-based materials as attractive candidates for water treatment applications. However, despite these advantages, several scientific and technological limitations remain. First, the relationship between the structural organization of chitin, especially crystallinity and microfibril orientation, and the final properties of derived materials remains insufficiently understood. Most studies describe these structural features independently, without establishing a clear structure–property relationship, which limits the rational design of high-performance materials. Second, although numerous extraction methods have been developed, the selection of an optimal process remains challenging. Conventional chemical extraction

is still dominant at the industrial scale due to its efficiency and reproducibility, despite its significant environmental impact. Emerging techniques such as microwave-, ultrasound- and autoclave-assisted processes have demonstrated promising results in terms of time reduction and process intensification. In particular, autoclave-assisted extraction has shown high efficiency in deacetylation and protein removal. Nevertheless, its application remains limited to specific biomass sources, mainly shrimp shells, and relies on conventional high-concentration alkaline treatments that may induce polymer degradation. Moreover, key parameters such as water consumption, energy demand and overall environmental performance are rarely evaluated, making it difficult to assess the true sustainability and scalability of these processes. In addition, alternative deacetylation strategies, such as the Broussignac process, have demonstrated the ability to preserve higher molecular weight chitosan compared to conventional methods. However, their integration with intensified processes such as autoclave-assisted extraction has not yet been explored, highlighting an important gap in process optimization. Furthermore, most studies focus on single biomass sources, predominantly marine crustaceans, while the variability of chitin properties depending on the biological origin remains underexplored. The interplay between biomass source and extraction conditions and its impact on the structural and functional properties of chitin and chitosan, therefore represents a critical knowledge gap. Finally, although chitosan-based materials have been widely investigated, some promising forms such as porous scaffolds remain insufficiently explored for environmental applications, particularly in water treatment systems. Overall, these limitations highlight the need for integrated approaches that combine (i) the valorization of diverse biomass sources within a circular economy approach, (ii) the development of efficient and sustainable extraction processes and (iii) a better understanding of structure–property relationships in chitin-derived materials. In this context, particular attention should also be given to the development of advanced material architectures, such as three-dimensional porous scaffolds, which offer

significant potential for the adsorption and removal of heavy metals and dissolved salts from aqueous media. Moreover, the properties of chitosan derived from different biological sources, including molecular weight, degree of acetylation and intrinsic structural organization, play a key role in the formation of such porous architectures and directly influence their adsorption performance. Such approaches are essential to enable the transition toward scalable and sustainable chitin biorefineries within a circular bioeconomy framework.

Part 3: Objectives And Proposed Scientific Strategy

In the context of the transition toward a circular bioeconomy, the valorization of chitin-rich biomass represents a promising pathway for the development of sustainable polymeric materials capable of reducing dependence on petroleum-derived resources. Among these materials, chitin and its derivative chitosan have attracted increasing attention due to their abundance, biodegradability and versatile physicochemical properties, as well as their ability to be processed into a wide range of functional structures. In particular, their strong chelating capacity and chemical functionality make them highly relevant for environmental applications such as water treatment, where efficient removal of heavy metals and dissolved salts remains a major challenge.

However, as highlighted in the state of the art, several scientific and technological limitations still hinder the large-scale deployment of chitin-based materials. Current production systems remain largely dependent on a limited number of biomass sources, mainly marine crustaceans, and on conventional extraction processes characterized by high chemical consumption and environmental impact. Emerging techniques, although promising, remain insufficiently explored in terms of scalability, sustainability and adaptability to diverse biomass sources. In addition, the influence of both biomass origin and processing conditions on the structural organization and functional properties of chitin and chitosan remains poorly understood. In particular, the lack of clear correlations between key parameters such as degree of acetylation, molecular weight, crystallinity and microfibril orientation and the performance of derived materials limits the rational design of high-performance systems.

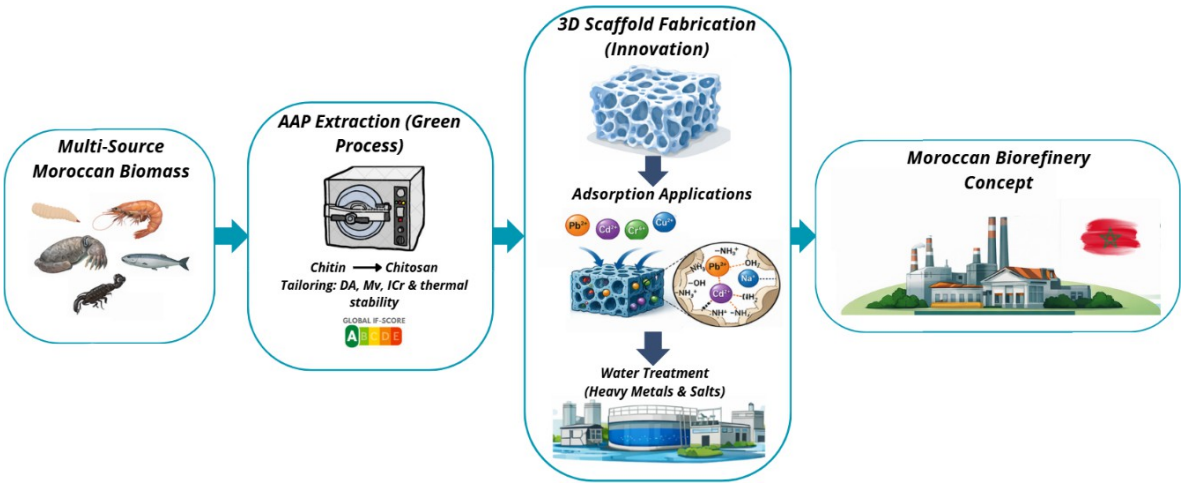

Figure 11. Integrated research strategy for the valorization of chitin-rich biomass: from resource diversification to structure–property control and water treatment applications

Within this framework, the present work aims to develop an integrated approach combining biomass valorization, process intensification and material design, with a particular focus on Moroccan bioresources. The strategy adopted is based on a progressive methodology linking extraction process development, diversification of biomass sources, control of polymer properties and evaluation of functional applications.

In a first stage, an optimized autoclave-assisted extraction process was developed using *Hermetia illucens* breeding residues as a model biomass. This step aimed to improve extraction efficiency while significantly reducing processing time, chemical consumption and water usage. In this context, the developed process reaches a technology readiness level (TRL) of 3, corresponding to experimental validation at laboratory scale. In addition, a classification based on an industrial feasibility score (IFS) was proposed to evaluate the potential for scale-up, in which the autoclave-assisted process was ranked as IFS = A, indicating high industrial potential based on its performance in terms of efficiency, resource consumption and operational simplicity.

In a second stage, this extraction strategy was extended to a wide range of marine and terrestrial arthropod and cephalopod resources available in Morocco, while simultaneously investigating the control of chitosan properties through the optimization of deacetylation conditions. This approach enabled the evaluation of the influence of both biological origin and processing parameters on the physicochemical properties of chitin and chitosan. Particular attention was given to tailoring key structural parameters, including the degree of acetylation and molecular weight, while limiting polymer degradation and improving material processability. This combined strategy highlights the role of biomass variability and process conditions in governing material performance.

In the final stage, the extracted chitosans were processed into three-dimensional porous scaffolds and evaluated as functional materials for water treatment applications. The objective was to exploit their interconnected porous architecture and surface functionality to enhance the adsorption of heavy metals and dissolved salts. Particular emphasis was placed on understanding how the origin of the biomass and the extraction conditions influence scaffold structure and, consequently, adsorption performance. In addition, this work led to the development of an innovative approach, subject to a patent application, for the design of chitosan-based materials and processes. As a final outcome, this research proposes a set of key tools and methodological guidelines for the implementation of a Moroccan chitin biorefinery, integrating biomass valorization, process optimization and material development within a circular bioeconomy framework.

Through this structured approach, the present research establishes clear relationships between biomass source, extraction process, structural organization and material properties. By integrating process optimization, biomass diversification and functional material design, this work contributes to the development of efficient and sustainable chitin-based systems. More broadly, it supports the implementation of circular

bioeconomy strategies and the development of scalable chitin biorefineries based on locally available bioresources.

Part 4: Material & Methods

1. Raw Materials and Biomass Sources

1.1. Taxonomic classification

In this study, several animal species were investigated as potential sources of chitin and its derivatives, including marine organisms (*Parapenaeus longirostris*, *Pollicipes pollicipes*, *Sepia officinalis*, *Sardina pilchardus*), insects (*Hermetia illucens*), as well as arachnids (*Buthus atlantis* and *Scorpio mogadorensis*), all of which are representative of fauna found in Moroccan ecosystems, particularly along the Atlantic and Mediterranean coasts as well as in terrestrial habitats. **Table 4** presents a comprehensive taxonomic classification of these species, ranging from kingdom to species, and incorporating intermediate ranks such as subphylum and subclass. This hierarchical framework highlights the taxonomic diversity of the selected organisms, which predominantly belong to the phyla Arthropoda, Mollusca and Chordata.

Table 4. Taxonomic classification of chitin and chitosan bioresources

	Black soldier fly	**Deep-water rose shrimp**	**Goose barnacles**	**Yellow scorpion**	**Black scorpion**	**Cuttlefish bone**	**Sardines scales**
Kingdom	Animalia	Animalia	Animalia	Animalia	Animalia	Animalia	Animalia
Phylum	Arthropoda	Arthropoda	Arthropoda	Arthropoda	Arthropoda	Mollusca	Chordata
Subphylum	Hexapoda	Crustacea	Crustacea	Chelicerata	Chelicerata	Conchifera	Vertebrata
Class	Insecta	Malacostraca	Thecostraca	Arachnida	Arachnida	Cephalopoda	Actinopterygii
Subclass	Pterygota	Eumalacotraca	Cirripedia	Dromopoda	Dromopoda	Coleoidea	Actinopteri
Order	Diptera	Decapoda	Scalpellifromes	Scorpiones	Scorpiones	Sepiida	Clupeiformes
Family	Stratiomyidae	Penaeidae	Pollicipedidae	Buthidae	Scorpionidae	Sepiidae	Clupeidae
Genus	Hermetia	parapenaeus	Pollicipes	Buthus	Scorpio	Sepia	Sardina
Espèce	*Hermetia illucens*	*Parapenaeus longirostris*	*Pollicipes pollicipes*	*Buthus atlantis*	*Scorpio mogadorensis*	*Sepia officinalis*	*Sardina pilchardus*

1.2. Arthropod Sources

1.2.1. *Hermetia illucens* (BSF)

Black soldier fly (BSF) larvae and puparia used in this study were supplied by EntomoNutris (Marrakech, Morocco). The larvae were reared from hatching until pupation on chick feed (Alf Sahel S.A) with a moisture content of 70%. Rearing was carried out in plastic containers (37 × 31 × 10 cm) at a density of 8.7 larvae·cm^{-2} (10,000 larvae per crate), under controlled environmental conditions of 28 °C and 60% relative humidity. Upon adult emergence, the puparial cases were collected, dried at 50 °C for 24 h, and finely ground using a Retsch RM 200 mortar grinder to obtain particle sizes ranging from 0.4 to 0.6 mm.

1.2.2. *Parapenaeus longirostris* shells (PL)

Parapenaeus longirostris shells were collected from restaurants located along the coasts of the Rabat–Salé–Kénitra region. After collection, the shells were thoroughly washed to remove impurities and subsequently dried at 80 °C for 24 h.

1.2.3. *Pollicipes pollicipes* (PP)

Pollicipes pollicipes, commonly known as barnacles, were collected from rocks along the coast of Dakhla in southern Morocco, where they are abundant. The collected samples were washed and then dried at 80 °C for 24 h.

1.2.4. Scorpion exoskeletons

Scorpio mogadorensis (SM) and *Buthus atlantis* (BA) are scorpion species endemic to Morocco, particularly in the Essaouira region. The specimens were collected from this area, and the soft tissues were removed from the ventral part. The remaining exoskeletons were then washed and dried at 80 °C.

1.3. Non-arthropod Moroccan sources

In addition to arthropod-derived materials, two non-arthropod biomasses from Moroccan origin were included for comparative purposes.

1.3.1. *Sepia officinalis* Cufllebone (SO)

Cuttlebone, a by-product of marine food processing, was obtained from *Sepia officinalis* collected from a restaurant in Rabat. The ventral and dorsal parts were separated and only the dorsal portion was retained. This fraction was washed, dried and ground prior to extraction.

1.3.2. *Sardina pilchardus* Scales (SS)

Scales of *Sardina pilchardus* were collected from the coast of Safi. The samples were carefully washed to remove adhering impurities and then dried at 80 °C to ensure complete dehydration.

2. Chemical Composition Analysis of Biomass

2.1. Ash content

Ash content was determined by incinerating samples at 550 °C at a constant rate of 50 °C every 30 min for 4 h, followed by cooling in a desiccator **[119]**. The ash content was calculated using the following equation (1):

$$\boldsymbol{Ash}\ (\%) = \frac{\mathbf{W2}-\boldsymbol{W0}}{\mathbf{W1}-\boldsymbol{W0}} \times \mathbf{100} \qquad \textbf{(1)}$$

Where W_0 is the constant weight of crucible, W_1 is the weight of the sample and crucible and W_2 is the weight of the ash and the crucible.

2.2. Water content

The water content was determined by dehydrating samples at 110 °C for 24 h. It was calculated based on the following equation (2):

$$\boldsymbol{Water}\ (\%) = \frac{\boldsymbol{mds}}{\boldsymbol{m_{rm}}} \times \boldsymbol{100} \qquad \textbf{(2)}$$

Where m_{ds} is the weight of dehydrated samples and m_{rm} is the weight of the raw material.

2.3. Lipid content

Lipid content was analyzed by a rotavapor (Heidolph) at 60 °C for 20 min after the defatting step **[120]**. The delipidation bath was then placed under the rotavapor to

remove the solvent; the remaining residue corresponded to the eliminated lipids. Lipid (%) content was calculated by weighing.

2.4. Protein content

Kjeldahl method has been employed following the procedure described by Liu et al. **[121]**, to determine the protein content in the BSF samples. 1g of the sample was subjected to catalytic heating to break down the proteins present in the raw material. Subsequently, 0.5 M of sulfuric acid was added to convert the released ammonia into ammonium sulfate. Alkaline distillation was employed to separate the free ammonia, which was then absorbed by boric acid and titrated with hydrochloric acid (0.1 M). The results are reported as a percentage.

2.5. Mineral content

Inductively Coupled Plasma Optical Emission Spectroscopy (ICP-OES), using the iCAP 7000 instrument from ThermoFisher Scientific, with a high sensitivity of <1 ppm, was utilized for the quantitative and qualitative determination of mineral content.

3. Chitin extraction procedures

3.1. Extraction from BSF puparia

Chitin extraction from *Hermetia illucens* puparia was performed using four different processes (P1–P4) to evaluate the influence of delipidation and reaction conditions. **(Table 5)**.

Table 5. Chitin extraction by processes P1, P2, P3 and P4

Processes	Delipidation	Demineralization	Deproteinization
P1	---	0.55M HCl / 25°C 1h / 1:200 (w/v)	1M NaOH / 80°C 18h / 1:20 (w/v)
P2	Hexane / 60°C 1h / 1:20 (w/v)	0.55M HCl / 25°C 1h / 1:20 (w/v)	1M NaOH / 80°C 18h / 1:20 (w/v)
P3	Methanol-chloroform / 25°C 1h / 1:20 (w/v)	0.55M HCl / 25°C 1h / 1:20 (w/v)	1M NaOH / 80°C 18h / 1:20 (w/v)
P4	Methanol-chlorofrom / 25°C	0.55M HéCl / 25°C 1h / 1:0 (w/v)	1M NaOH / 121°C-2.2 Bar

1h / 1:20 (w/v)	1h15 / 1:20 (w/v)

For delipidation, the Soxhlet extraction method using hexane solvent **[122]** and Folch method using Methanol-chloroform mixture 1:4 (v/v) as a solvent were selected. Demineralization was carried out using an HCl solution (0.55 M) with a ratio of 1:10 (w/v) at room temperature for 1h. The deproteinization step involved an alkaline treatment using repeated baths of NaOH solution (1M) at a ratio of 1:10 and maintained at 80°C under reflux heating and a 1M NaOH solution within an autoclave at 121°C for 15 min at a ratio of 1:20 (w/v). In parallel, deproteinization was carried out concurrently with the quantification of proteins removed at 595nm using the Bradford method **[123]**, a volume of 20 µL of each deproteinization bath is mixed with 3mL of Bradford solution (Coomassie Blue G-250, ethanol and water).

3.2. Extraction using autoclave-assisted process (AAP)

After confirming the high performance of autoclave assisted process, chitin extraction from *Parapenaeus longirostris, Pollicipes pollicipes, Scorpio mogadorensis, Buthus atlantis, Sepia officinalis, Hermetia illucens* larvae and *Sardina pilchardus* was carried out using an autoclave-assisted protocol involving successive demineralization, deproteinization and, when required, delipidation steps **(figure 12)**. Demineralization was performed using a 0.25 M HCl solution at a solid-to-liquid ratio of 1:40 (w/v) at room temperature for 1 h, with continuous monitoring of pH. The samples were then washed with distilled water until neutral pH and dried at 50 °C for 24 h. Deproteinization was subsequently carried out using a 1 M NaOH solution in an autoclave (SANOclav LaM-ECZ) at 121 °C and 2.2 bar for 15 min, with a solid-to-liquid ratio of 1:60 (w/v). This treatment was repeated until the filtrate became visually clear, indicating effective protein removal. The resulting chitin was washed with distilled water until neutral pH and dried again at 50 °C for 24 h. For lipid-rich biomasses, namely *Hermetia illucens* larvae and *Sardina pilchardus* scales, an additional delipidation step was performed using a methanol–chloroform mixture (1:4 v/v) at room temperature for 1 h.

All obtained chitins were washed until pH neutral and dried at 40°C for 24h. The chitins yield (%) was determined using the following equation (3):

$$\textbf{\textit{Chitin}}\ (\%) = \frac{\textbf{\textit{mchitin}}}{\textbf{\textit{m}}_{\textbf{\textit{raw material}}}} \times \textbf{\textit{100}} \qquad \textbf{(3)}$$

Where m_{chitin} represents the weight of chitin obtained after demineralization, delipidation and deproteinization steps, $m_{raw\ material}$ represents the weight of the insect material.

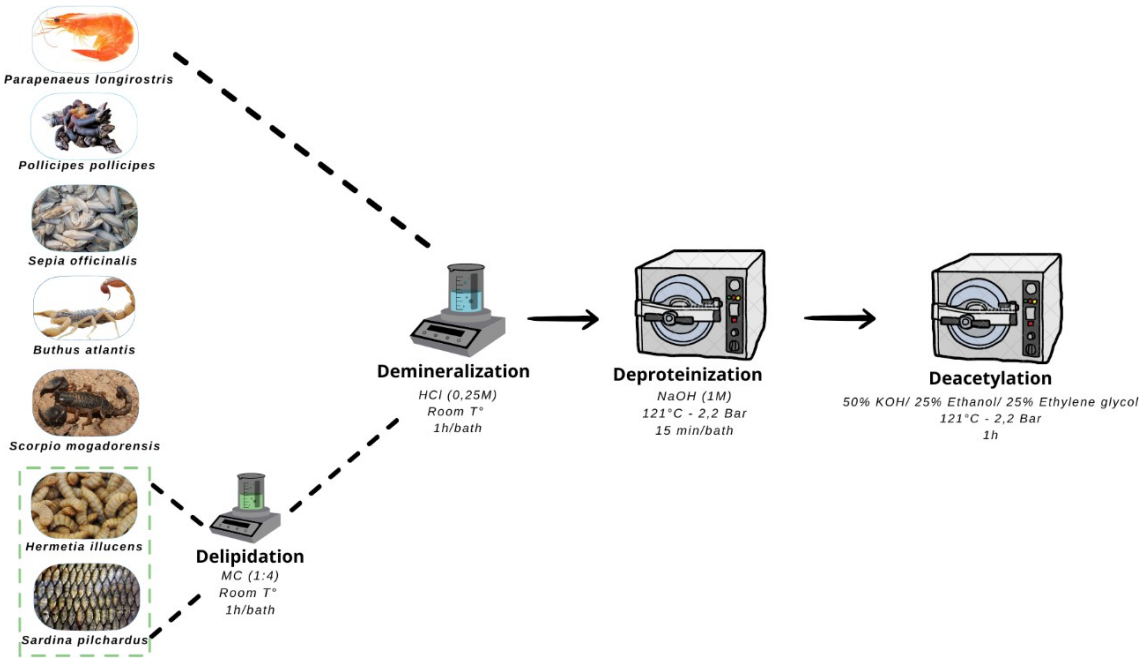

Figure 12. Chitin and chitosan extraction steps

4. Chitosan Preparation

Chitosans were prepared using two processes from BSF puparia. A mixture of 50% potassium hydroxide (KOH), 25% ethanol and 25% mono-ethylene glycol with a ratio of 1:60 (w/v) was used at 120°C for 24h under agitation. For P4 puparia deacetylation and other sources cited previously, the same mixture was used under autoclave conditions (121°C – 2.2bar) for 1h with a ratio of 1:10 (w/v) in an autoclave (SANOclav LaM-ECZ, which provided less than 6 times the quantity of chemical products for the deacetylation step. Chitosan samples were washed with distillate water until

neutrality and dried at 40°C for 24h. The chitosan yield (%) was determined using the following equation (4):

$$\boldsymbol{Chitosan}\,(\%) = \frac{\boldsymbol{mchitosan}}{\boldsymbol{m_{chitin}}} \times \boldsymbol{100} \qquad \textbf{(4)}$$

Where $m_{chitosan}$ represents the weight of chitosan obtained after deacetylation, m_{chitin} represents the weight of the chitin.

5. Preparation of chitosan-based materials

5.1.3D Scaffold preparation

Three-dimensional (3D) porous chitosan scaffolds were fabricated using a freeze-casting and lyophilization approach. The chitosan employed in this study was derived from *Buthus atlantis*, as described in the previous section, and was dissolved in 1% (v/v) acetic acid at a solid-to-liquid ratio of 1:100 (w:v) under continuous magnetic stirring at ambient temperature until complete solubilization and formation of a homogeneous solution. The resulting solution was cast into cylindrical molds (30 × 70 mm).

Two fabrication routes were investigated. In the first route (Sc I), the chitosan solution was frozen in the molds at -15 °C for 24 h to promote ice-crystal templating, followed by freeze-drying for 24 h to generate a highly porous structure at -60°C. In the second route (Sc II), the solution was directly subjected to freeze-drying for 24 h and subsequently neutralized by immersion in a 0.1 M NaOH bath **(figure 13)**. The obtained scaffolds were thoroughly rinsed with distilled water until neutral pH and freeze-dried again. The Sc I scaffolds exhibited a well-organized and interconnected porous architecture, which is advantageous for enhancing mass transfer and metal ion adsorption.

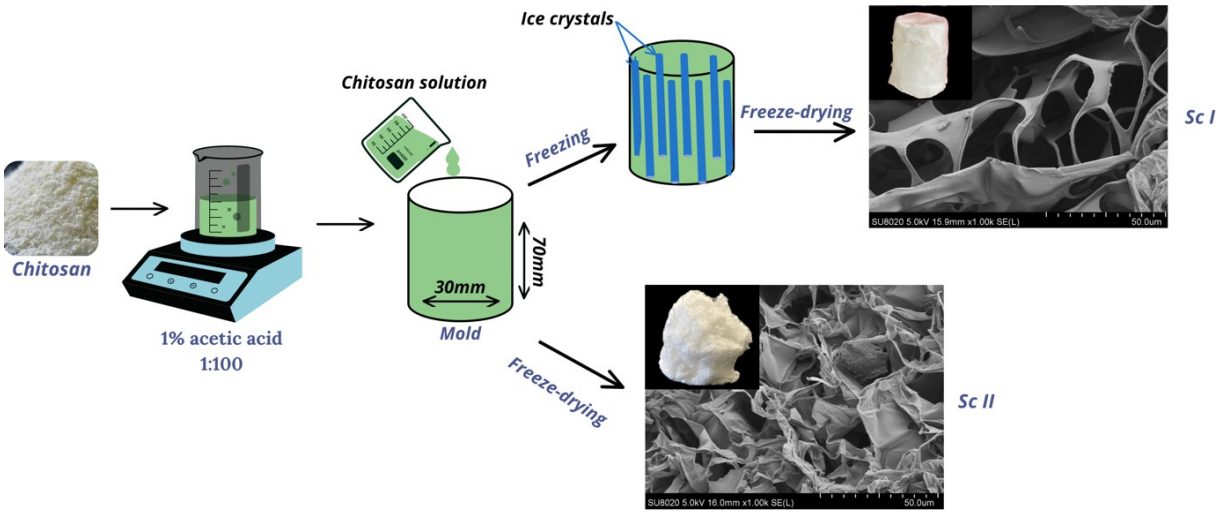

Figure 13. Preparation steps for chitosan scaffolds Sc I and Sc II

For comparative analysis, scaffolds were also prepared under identical conditions using chitosans derived from commercial chitosan extracted from shrimp shells, black soldier fly (*Hermetia illucens*) empty pupae and prepupae and *Pollicipes pollicipes*.

5.2. Film preparation

Chitosan films were prepared using the solvent casting technique. Chitosan derived from *Buthus atlantis*, as described previously, was dissolved in 1% (v/v) acetic acid at a solid-to-liquid ratio of 1:100 (w:v) under continuous magnetic stirring for 1 h at room temperature until complete dissolution and formation of a homogeneous solution. The resulting solution was then cast into polystyrene Petri dishes and allowed to dry under ambient conditions to form uniform films. After complete solvent evaporation, the dried films were neutralized by immersion in a 0.1 M NaOH solution to eliminate residual acetic acid. The films were subsequently rinsed thoroughly with distilled water until neutral pH and dried again at room temperature to obtain the final chitosan films.

6. Characterization Techniques

6.1. FTIR characterization

FTIR spectra were performed on Jasco 4600A Gemini FT-IR sampling spectrometer. The spectra allowed for the determination of the characteristic area of the acetylated amine function around 1655 cm^{-1}, and the reference peak of the amine function around 3450 cm^{-1}. Subsequently, the degree of acetylation (DA) was calculated using the following formula (5) **[124]**.

$$\boldsymbol{DA}\ (\%) = \frac{\boldsymbol{A1655}}{\boldsymbol{A3450}} \times \boldsymbol{115} \qquad \textbf{(5)}$$

6.2. SEM-EDX

Samples were analyzed in VEGA3 TESCAN device. The morphology of the prepared chitins (CHT P1, P2, P3 and P4) and chitosans (CHS P1, P2, P3 and P4) was observed by magnification at 50 μm.

6.3. Molecular weight determination

The Ubbelohde capillary viscometer (0.5-3 mm^2/s, 15-20 ml) was used to determine the viscometric molar mass of chitosan at 25 °C. The solution used is a mixture of 0.3 M acetic acid and 0.2 M sodium acetate **[125]**. The average molecular weight viscosity was calculated from the following Mark Houwink equation (6) **[126]**.

$$\boldsymbol{[\eta] = K.\ M^{a}} \qquad \textbf{(6)}$$

With [η] is the intrinsic viscosity, M is the viscometric molar mass. K and a are the viscometric constants determined in the literature **[22]**.

6.4. X-Ray Diffraction XRD analysis

The device used for recording the results is a Rigaku III diffractometer (Rigaku Corp, Japan) with Cu radiation (40 kV, 30 mA). Data were collected with a scan angle of 5° to 40°. The crystallinity index (I_{Cr}) is determined using the following **[127]**.

$$\boldsymbol{I_{Cr}}\ (\%) = \frac{\boldsymbol{Sc}}{\boldsymbol{St}} \times \mathbf{100} \qquad \textbf{(7)}$$

Where Sc is the area of the crystal domain and St is the area of the total domain.

6.5. Potentiometry titration

Chitosan was solubilized in a 0.1M HCl solution and then neutralized with a 0.1M NaOH solution. The titration curve showed two inflection points: the first corresponding to excess acid and the second to the neutralization of protonated chitosan **[128]**. The acetylation degree (DA) was calculated according to the equation (8) **[129]**.

$$\mathbf{DA}\ (\%) = \mathbf{1} - \frac{\mathbf{16{,}1\ (x_2 - x_1)}}{\mathbf{m - m'}} \times \mathbf{N} \qquad \mathbf{(8)}$$

Where N is the molarity of NaOH solution, m is the mass in grams of chitosan and m' is the mass of water content in a sample.

6.6. ^{1}H-NMR characterization

^{1}H-NMR was carried out on a 400 MHz Brucker, using D_2O/DCl (2%) to solubilize 20 mg of chitosan. The solution was heated at 70°C for 1h to accelerate the dissolution. NMR chemical shifts are reported in ppm **[130]**.

The integrals of the H-1-D peak and the integrals of the H-Acetyl peak serve as a basis to calculate the DA of chitosan following the equation (9) **[124]**.

$$\mathbf{DA\ (\%) =}\ \mathbf{1} - \frac{(\boldsymbol{H - 1 - D}\ )}{(\boldsymbol{H - 1 - D} + \mathbf{1/3}\ \boldsymbol{HAc})} \times \mathbf{100} \qquad \mathbf{(9)}$$

6.7. Thermal analysis

Thermogravimetry (TGA) measurements were performed using a TGA Q500 instrument under N_2 gas atmosphere at 0.1 MPa. The chitins and chitosans were heated from 20 to 600 °C with a heating rate of 20°C.min^{-1}.

7. Chitin fiber orientation analysis

7.1. ESEM

The microstructural organization of the chitin fibers in the cuticle was examined using an Environmental Scanning Electron Microscope (ESEM) (Thermo Scientific Quattro S). Small fragments of the scorpion cuticle were carefully isolated and mounted on aluminum stubs. The samples were observed under low-vacuum conditions without prior conductive coating in order to preserve the native

morphology of the chitinous structures. Images were recorded at different magnifications to visualize the hierarchical organization and orientation of the chitin fibers within the cuticular layers.

7.2. Polarized microscope

Thin sections of the cuticles were prepared using a cryotome (Bright Instruments, Starlet). The cuticle samples were first embedded and cryo-sectioned into slices with a thickness of approximately 10–20 µm, which is suitable for polarized light observation. The obtained sections were then mounted on microscope glass slides. The slices were then observed using a Nikon Eclipse polarized light microscope equipped with both bright-field and polarized light modes.

8. Adsorption Experiments

An initial concentration was prepared of 1 $g \cdot L^{-1}$. Then a total volume was used of 50 mL with 50 mg of scaffold form as a bioadsorbent for a contact time of 1 h: Na, Mg, K, Cd, Pb, Ca, Cr and Cu ions were used in the form of their chlorides, NaCl, $MgCl_2$, KCl, $CdCl_2$, $PbCl_2$, $CaCl_2$, $CrCl_3$ and $CuCl_2$ respectively, obtained from Sigma Aldrich with 98.99 % purity. This form was preferred because most sulfate salts were not soluble and nitrates could act as oxidants (**figure 14**).

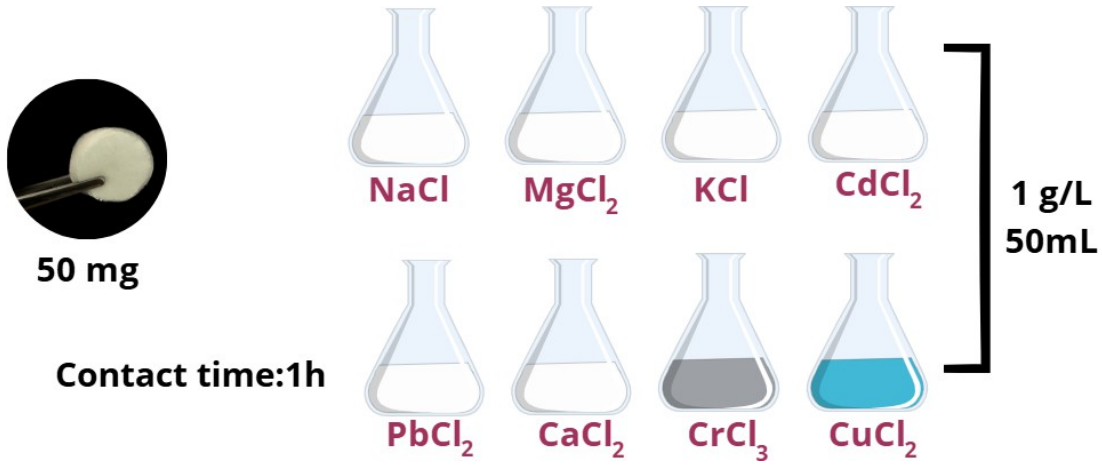

Figure 14. Conditions of adsorption tests

9. Analytical Measurements

9.1. Adsorption atomic spectroscopy

We employed ThermoFisher Scientific Flame Atomic Absorption Spectroscopy for Hydrides, conforming to the NF EN 1483 standard, dedicated to water quality identification and heavy metals and salts determination. The uptake rate and the adsorption capacity of metals by chitosan were calculated using the Equation (10) below:

$$\boldsymbol{Uptale\ rate}\ (\%) = \frac{\boldsymbol{Ci - Ct}}{\boldsymbol{C_i}} \times \mathbf{100} \qquad \textbf{(10)}$$

Where C_i is the initial concentration ($mg.L^{-1}$) and C_f is the final concentration ($mg.L^{-1}$)

9.2. UV-Visible spectroscopy

Metal ion concentration variations were evaluated using a UV–Vis spectrophotometer (UV-2600, Shimadzu). Quantification was performed based on calibration curves constructed from standard solutions prepared prior to analysis. In order to normalize the adsorption efficiency, the adsorption capacity of the chitosan-based scaffold was quantified for each tested salt using the equation (11):

$$\boldsymbol{Adsorption\ capacity}\ (\boldsymbol{mg\ g^{-1}}) = \frac{\boldsymbol{Ci - Ct}}{\boldsymbol{W}} \times \boldsymbol{V} \qquad \textbf{(11)}$$

Where C_i is the initial concentration ($mg.L^{-1}$), C_f is the final concentration ($mg.L^{-1}$), V is the solution volume (L) and W is the weight of the adsorbant.

9.3. TDS & Conductivity measurements

Total dissolved solids (TDS) and electrical conductivity (EC) were measured using a portable digital water quality meter (Furnetra) equipped with automatic temperature compensation.

10. Statistical Analysis

Statistical analysis of the data was carried out using GraphPad Prism version 9.00 software (San Diego, California, USA). Results are presented as mean ± SEM. An

analysis of variance (ANOVA) was performed, followed by Tukey post-hoc tests with a significance level of $p=0.05$.

Part 5: Results & Discussion

Chapter 1: High-yield, time-saving and water-efficient extraction of chitin and chitosan from *Hermetia illucens* breeding waste: A greener approach for industrial applications

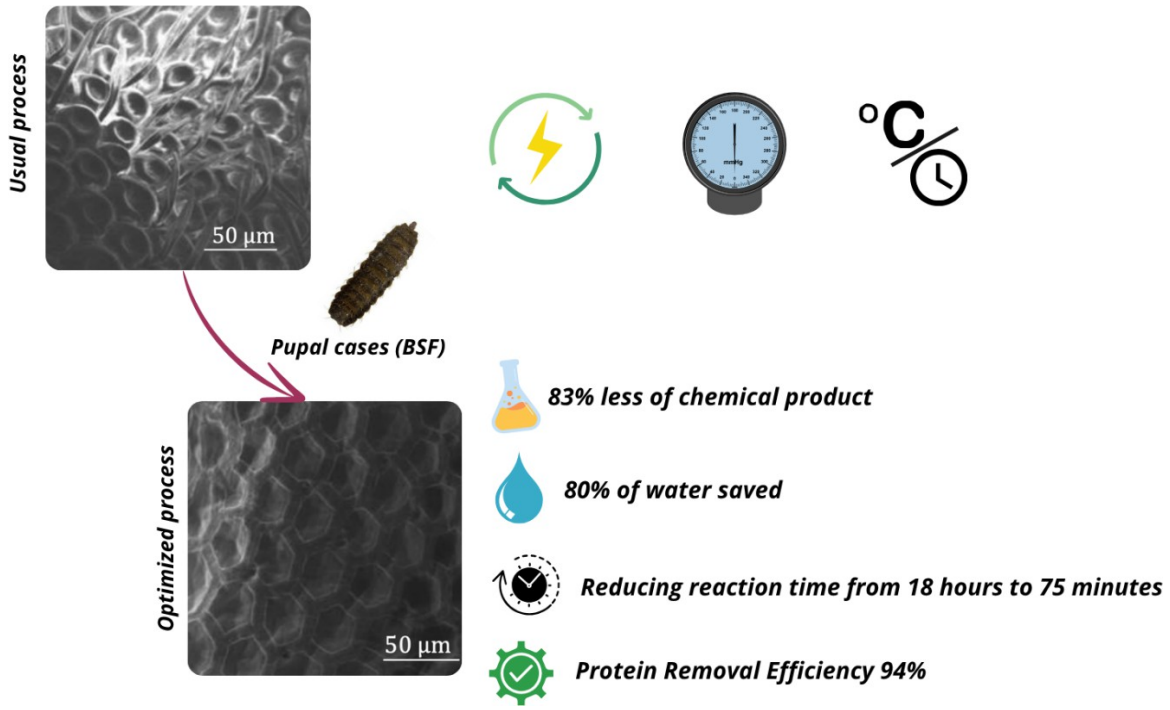

1. Introduction

BSF are one of the edible insects that play a pivotal role in organic waste recycling. It is recognized for its abundant proteins, lipids, minerals and chitin content [131], being considered as a key species in this regard. Additionally, BSF reproduce rapidly under suitable environmental conditions and could serve as alternative sources to produce chitin and chitosan [132]. Several research studies have been focused on obtaining chitin from its various stages, particularly the puparial cases, known as the third chitin-rich byproduct in the life cycle of the BSF. However, due to its richness in proteins, lipids and minerals, the pupal stage of *Hermetia illucens* requires more stringent conditions for the isolation of chitin, its purification, bleaching to eliminate impurities and pigments that resist extraction [133–135], which impact the quality and yield of both chitin and chitosan. Indeed, the major problem encountered in chitin chemistry lies on its preparation and extraction to obtain chitin with characteristics close to its native form in terms of molar mass, acetylation degree and crystalline properties. To address the need for sustainable scalability in chitin and chitosan production, this chapter explores alternative, rapid and eco-friendly extraction methods aimed at industrial feasibility. This approach was based on autoclave-assisted extraction, which has been adopted for the deproteinization step, resulting in a significant reduction in extraction duration compared to conventional methods [77] and for the sterilization of the raw material after the demineralization step by Lagat et al. [136] maintaining the high quality of chitin.

2. Chitin and chitosan production

Before any extraction process, it is essential to characterize the composition of the raw material, the steps of chitin and chitosan extraction are presented in **Figure 15** according to the chemical composition of the insect material.

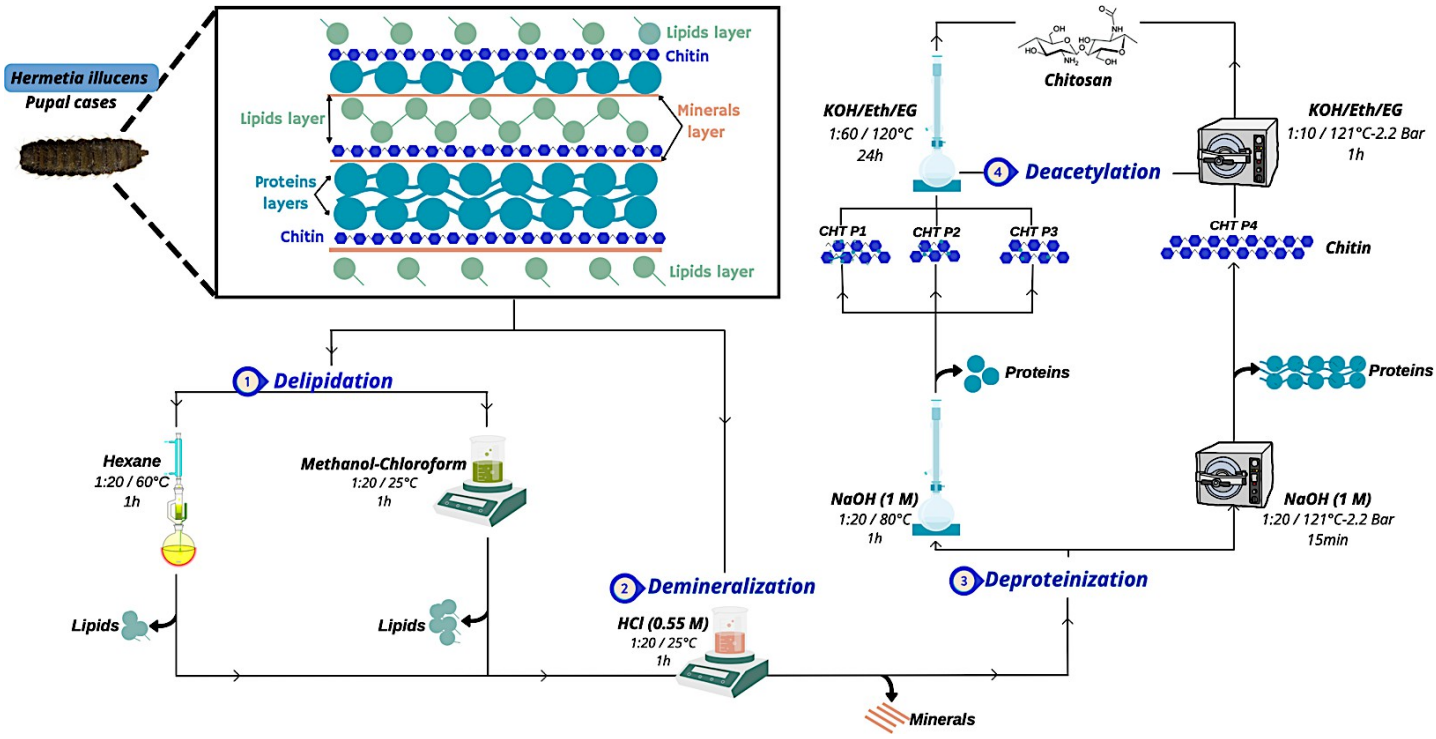

Figure 15. Steps for chitin extraction and chitosan elaboration from BSF (puparial cases)

2.1. Chemical composition of BSF Material

The analyses of BSF (puparial cases) show that they are composed of 7.80±0.02% of water, 16±0.01% of ash and 5.50±0.01% of lipid **(Table 6)**. Compared with the literature, the lipid content determined is close to that cited by Triunfo et al. [137], which is around 5%. Regarding this lipid content concerning the other stages of the BSF, the content of lipids remains lower than in other stages due to the transformation of lipids into an energy source during metamorphosis in the life cycle of these insects [90,121].

Table 6. Chemical composition of BSF puparial cases

	Lipid	Mineral	Protein	Water	Ash content	Other
Weight (%)	5.50±0.01	4.34±0.03	42.60±0.02	7.80±0.02	16±0.01	23.66±0.03

The pupal stage of BSF contains a total mineral content of 4.34±0.03% predominantly comprised of 1.37% K, 0.92% Cl and 0.78% Na. Additionally, tiny amounts of other

elements such as Mg, Ca, Al and P were detected at lower percentages varying from 0.19 to 0.49% **(Table 7)**. Generally, empty puparia of BSF is known for its low mineral content compared to other stages of BSF and other insects fed [121], which is confirmed by the absence of effervescence during the demineralization step. The lowest concentration of hydrochloric acid was used compared to the literature [138] reducing acid consumption by 75% in this step.

Table 7. Mineral content of BSF pupae

Minerals	K	Cl	Na	Mg	Ca	Al	P
(%)	1.32±0.01	0.92±0.01	0.78±0.00	0.49±0.02	0.30±0.02	0.29±0.01	0.19±0.00

The protein content for the insect material is around 42.60%, this value is correlated with that determined in *Hermetia illucens* larvae by Nafisah et al., with a content of 42.99% **[139]**, and by Liland et al., which is around 40% [140]. This data shows us the diversity of compounds contained in BSF puparial cases and confirms the significance of this study and the need to proceed with the elimination of lipids, minerals and even proteins and total impurities.

2.2. Assessment of process efficiency, kinetics and resource consumption

The kinetics of deproteinization were evaluated using four extraction processes (P1, P2, P3 and P4). The protein content for each extraction bath was quantified using the Bradford method, allowing the construction of individual curves for each method and a comparison of their efficiency and rate **(figure. 16)**. These observations revealed a progressive increase in the quantity of eliminated proteins across all four extraction processes compared to the respective baths. However, the deproteinization rate varies depending on the extraction process used.

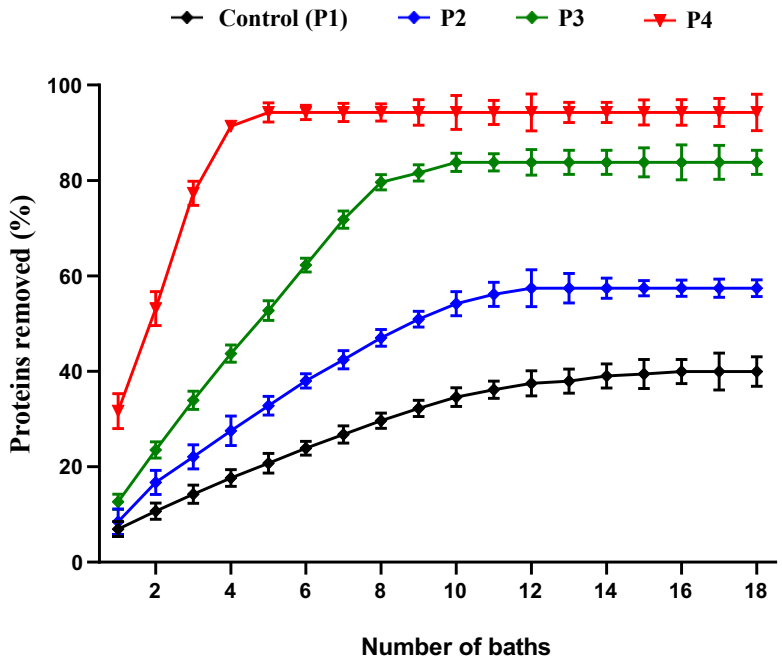

Figure 16. Kinetic of deproteinization step by processes P1, P2, P3 and P4

Even though the researcher relied on the disappearance of the bath coloration as evidence of deproteinization **[141]**, the kinetics studied by Bradford assay at 595 nm do not confirm it in this case. The baths were found to be colorless for processes P1, P2, P3, and P4 respectively at the 9th, 8th, 6th and 3rd baths. This confirms that the pupal stage of BSF remains rich in proteins **[121]**, whether responsible or not for the pigmentation of this species. After deproteinizing up to the 5th bath by process P4, the obtained chitin is clear and whitish in appearance **(figure 17)**. This was deemed unnecessary for whitening purposes. Notably, the autoclave process P4, emerged as the most proficient, successfully eliminating 94.25±3.79% of protein in just 5 baths for 75 minutes (15min/bath) **(figure 18)**. This method stands out as the most efficient process for rapid and economical deproteinization.

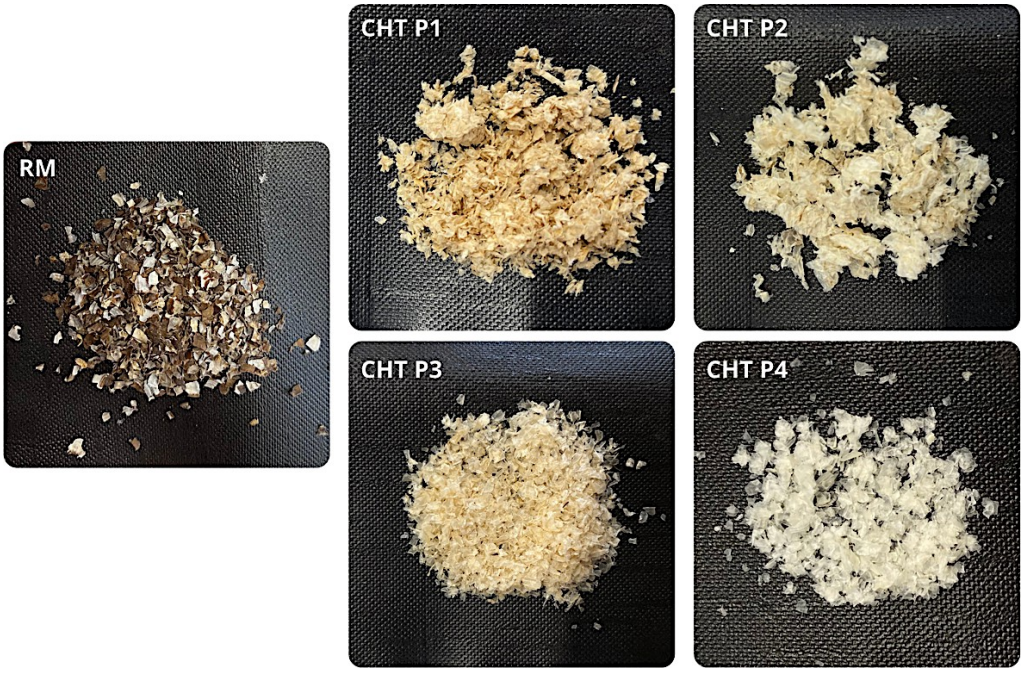

Figure 17. Visual comparison of raw material (RM) and chitin extracted through P1 (CHT P1), P2 (CHT P2), P3 (CHT P3) and P4 (CHT P4)

Based on the use of the flowmeter during the deproteinization step, a flow rate of 23 mL/min is used for reflux heating during this reaction to ensure the conservation of the solution used. A 100mL volume of distilled water is used to prepare the 1M NaOH solution for 5g of raw material, and 3L is also used for washing the deproteinized material after each bath. Projecting this onto the number of baths, which is systematically linked to the variation in water consumption during reflux, reaction, and washing, nearly 80L of distilled water is consumed to deproteinize 5g of *H. illucens* empty puparia with a low deproteinization efficiency of less than 40% by the usual process P1. However, an 80% reduction in water consumption is achieved by using process P4 – i.e. around 15L vs 80L for P1 - with a deproteinization efficiency more than 94%. Projected onto a normalization of water consumed for the production of 1 kg of chitin across the four processes **(figure 18)**, more than 1300 liters of water are saved by P4 (instead of P1).

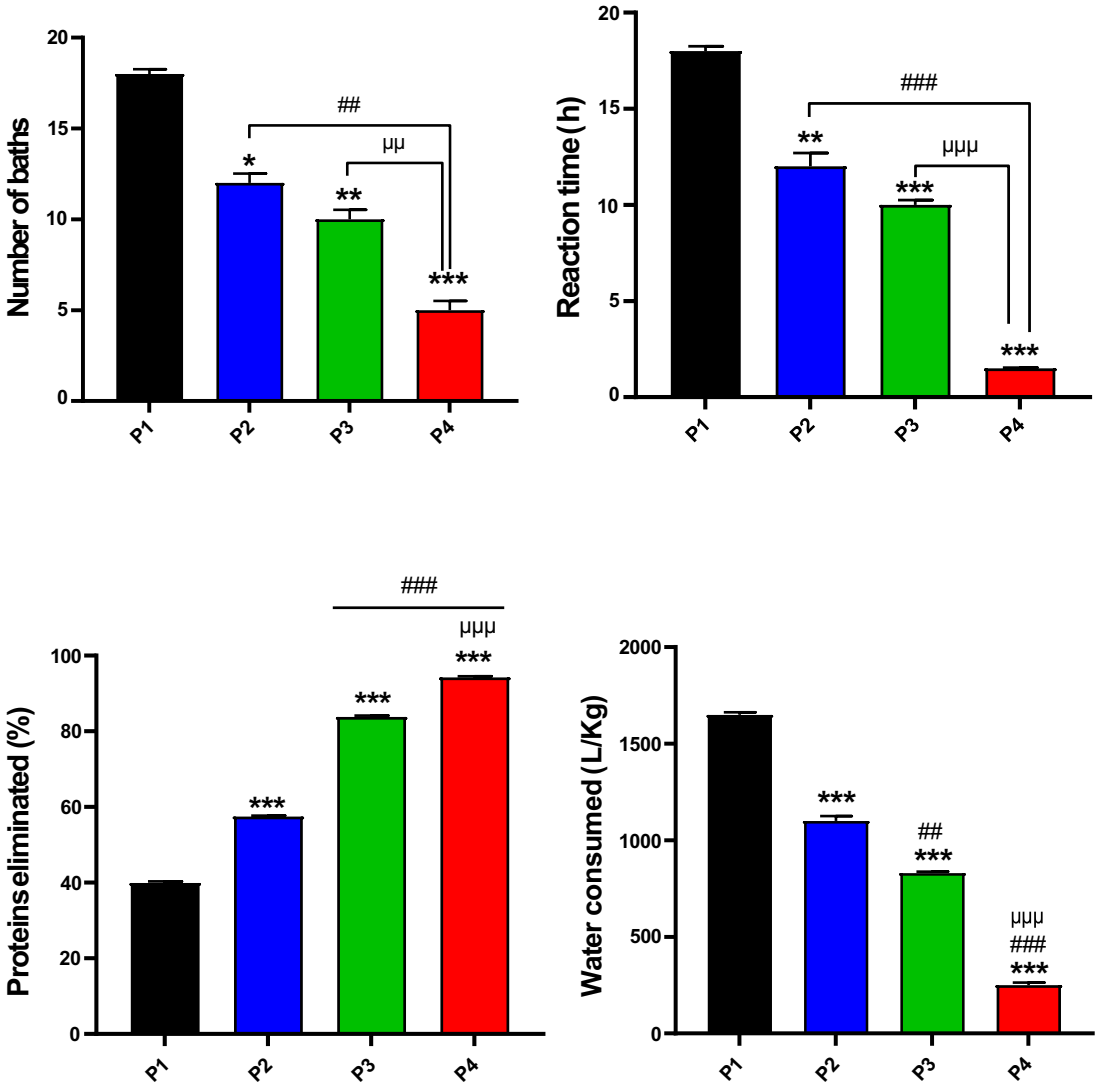

Figure 18. Histograms showing the Optimized factors during deproteinization step in the different processes (P1, P2, P3 and P4). Values are presented as means ± standard deviation Statistically significant differences ($p < 0.05$) from the P1 process (Control) are indicated by * from the P3 process by # and from the P4 process by (µ). Statistical evaluation was performed using a one-way ANOVA (p=0.05).

Following the protein analysis, process P4 exhibited the highest protein removal efficiency. Therefore, the elimination of proteins across the various processes can be ranked in the following order, where QPE is the quantity of proteins eliminated by each process:

QPE (P4) > QPE (P3) > QPE (P2) > QPE (P1)

From a performance standpoint, a significant difference is observed between the two lipid removal methods adopted in the extraction processes. This could be attributed to the heating involved in the Soxhlet protocol, which may degrade the material during delipidation. Considering this variance, a methanol-chloroform mixture in a 1:4 ratio was chosen for processes P3 and P4 to maintain a higher yield of 97.27%. Due to the low mineral content in the insect material, only one bath is utilized for this step. However, in terms of deproteinization, there is a considerable discrepancy in yield ranging from 19% to 41%.

2.3. Evaluation of extraction yields and stepwise recovery

Regarding the chitin yields obtained by the four processes **(Table 8)**, P4 shows the highest yield at 34.74± 1.15%. This yield is higher than the chitin yields reported in several studies on the extraction of chitin from BSF using chemical and biological methods [131,136,142,143]. However, chitosan yields (related to chitin) obtained vary from 68.57± 1.15 to 83.33± 1.15. This range is similar to the yield of chitosan prepared from *Tenebrio molitor* beetles, which typically falls between 76.43% and 78.26% **[144]**.

Table 8. Influence of different extraction processes on yields (%) after each step

Steps / Processes	Delipidation (%)	Demineralization (%)	Deproteinization (%)	Chitin yield (%)	Chitosan yield (%)
P1	–	53.50± 2.30	19.66± 0.58	13.84± 1.15	68.57± 1.15
P2	87.87± 0.62	69.34± 5.77 (*)	21.43± 0.57 *ns*	15.43± 0.07 *ns*	72.02± 0.57 *ns*
P3	97.27± 0.05 (#)	71.30± 0.05 (*)	34.58± 0.07 (*/#)	25.72± 1.15 (*/#)	74.37± 0.66 (*)
P4	97.27± 1.15 (#)	71.30± 1.15 (*)	41.70± 1.15 (*/#/μ)	34.74± 1.15 (*/#/μ)	83.33± 1.15 (*/#/μ)

*Values are presented as means ± standard deviation. Statistically significant differences (n= 3; p < 0.05) compared with the P1 process (Control) are indicated by * from the P3 process by #*

and from the P4 process by (μ). Statistical evaluation was performed using ANOVA with $p < 0.05$ considered statistically significant between control and treated groups.

3. Physicochemical properties

The XRD analysis of chitins (CHT P1, P2, P3 and P4) **(figure 19 (a))** shows two peaks at around 9° and 19°, corresponding to (020) and (110) reflection planes respectively [145]. Additionally, three low-intensity peaks were observed at 13°, 23° and 26°, corresponding to (021), (101) and (130) planes. These peaks exhibit the characteristic alpha chitin form [146]. Moreover, in CHT P1, a peak at 28° is observed, which could indicate interactions with mineral components present in this source that persist even after the demineralization step [147]. Following the deacetylation of chitins, the results of chitosan (CHS P1, P2, P3, and P4) show the disappearance of peaks around 9°, 13°, 19°, 23°, and 26° **(figure 19 (b))**, with the appearance of two new peaks at around 10° and 20°, which are characteristic of chitosan [148]. The peaks became less intense after deacetylation, indicating a difference in crystallinity between the original chitins and the resulting chitosan. Process P4 exhibited the most significant crystallinity difference, around 25.68%. This change can influence various physicochemical and functional properties of chitosan, including its solubility and viscosity [49]. In the CHS P1 spectrum, the presence of a peak around 22.8°, characteristic of chitin and corresponding to the (120) plane, suggests an incomplete transformation of chitin into chitosan. Additionally, a peak at 27° is observed in CHS P2, as well as in the CHS P3 spectra, with another peak at 23.7°, indicating impurities that could be attributed to minerals or persistent proteins/pigments in the chitosan [149]. In contrast, only the two

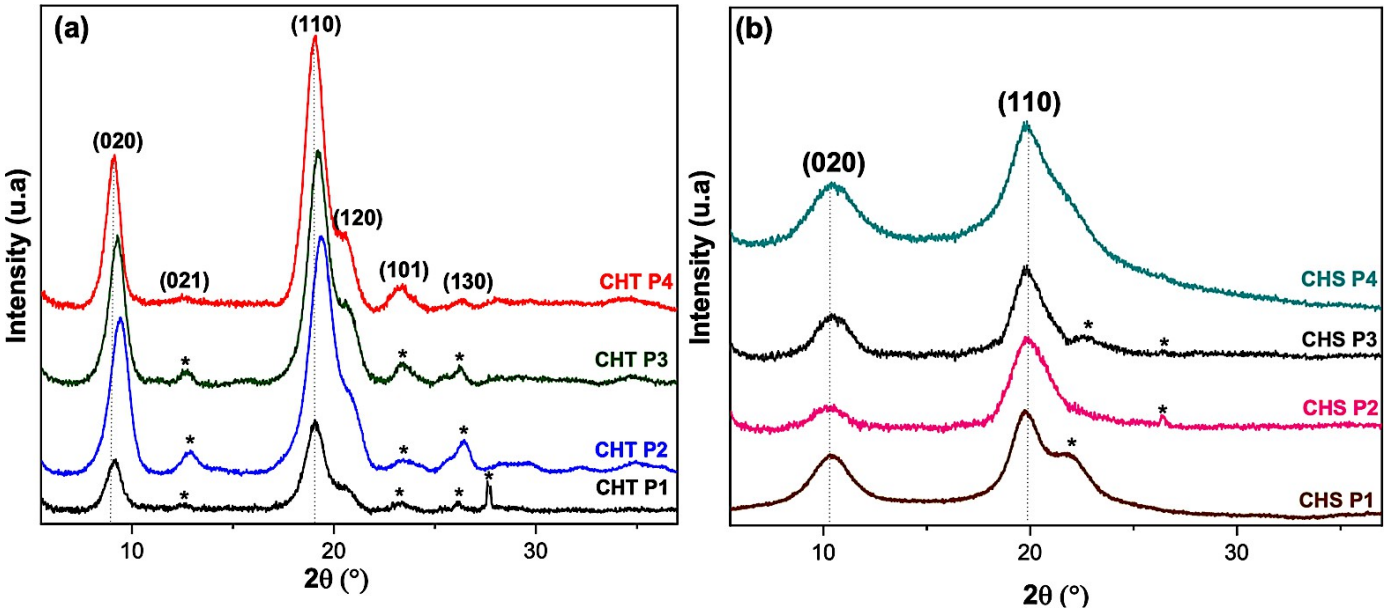

Figure 19. XRD spectra of chitins (a) and chitosans (b)

characteristic peaks of chitosan are observed in CHS P4, confirming that chitosan P4 is purer than P1, P2, and P3, with the highest crystallinity difference.

Based on the characteristic X-ray peak intensities of chitins and chitosans, the crystallinity indices (I_{Cr}) were calculated using equation (7). The results in **Table 9** show that the I_{Cr} values of chitin (CHT P1, P2, P3, and P4) are consistently higher than those of chitosan (CHS P1, P2, P3, and P4). These results are consistent with those of [130,150].

Table 9. XRD parameters of chitins and chitosans

	Chitin		Chitosan		Δ Crystallinity (%)
	2θ (°)	I_{Cr} (%)	2θ (°)	I_{Cr} (%)	
P1	9.1 19.06 23.16 26.6	53.3	10.32 19.72	34.8	18.5
P2	9.42	59.49			

	12.9 19.38 23.44 26.2		10.16 19.78	36.23	23.26
P3	9.3 12.6 19.14 23.28 26.44	62.23	10.4 19.84	45.3	16.93
P4	9.08 19.06 23.24 26.02	73.38	10.26 19.84	47.7	25.68

Further observation from the results of XRD analysis of chitin revealed a distinct contrast between delipidated chitin (CHT P2, P3 and P4) and non-delipidated chitin (CHT P1). Delipidated chitin exhibited well-defined and intense diffraction peaks, indicative of a highly ordered crystal structure. Conversely, non-delipidated chitin (CHT P1) exhibited less intense and less sharp peaks, suggestive of a less ordered crystal structure. These interpretations are similar for chitosan with (CHT P2, P3 and P4) and without any delipidation (CHT P1). These findings reinforce the important role of delipidation by obtaining a more ordered crystalline structure for both chitin and chitosan [151].

The peaks observed in all FTIR spectra **(figure 20 (a))** of chitins (CHT P1, P2, P3, and P4) included an amide I absorption band at 1659 cm^{-1}, corresponding to CO---HN intermolecular hydrogen bonds [147], and an amide II band at 1560 cm^{-1} [152]. Additionally, a broad band was observed at 3100-3600 cm^{-1}, corresponding to the stretching of -NH and -OH groups. The peak at 894 cm^{-1} represents a ring stretching band characteristic of the β-1,4 glycosidic bonds and the absorption peak around 1050 cm^{-1} is associated with the stretching vibration of the -C-O-C bridge of the glucosamine

ring [153]. Peaks at 3258 cm^{-1} and 3108 cm^{-1} correspond to the axial deformation of the NH group involved in intermolecular hydrogen bonds. The band observed at 1315 cm^{-1} indicates CO-NH deformation and the CH_2 grouping. These results are therefore consistent with those of [49,130,153]. Furthermore, the amide I band at 1659 cm^{-1} is distinctly split in the FTIR spectra, indicative of a doublet that results from differential hydrogen bonding. This splitting is a defining feature of α-chitin [154], thereby confirming the α-chitin structure in all isolated samples.

After the deacetylation of chitins, a significant change in the intensity of the bands was observed, along with the disappearance of some bands **(figure 20 (b))**. Specifically, the band observed at 3108 cm^{-1} disappeared. Additionally, the intensities of the bands at 1642 cm^{-1} and at 1560 cm^{-1} observed in the chitin spectra, decreased after deacetylation. These bands are indicative of chitosan [155,156]. The degree of acetylation (DA) of chitosans P1, P2, P3 and P4 was calculated using the equation (5) to be 9.09±0.18%, 6.33±0.05%, 6.35±0.78% and 5.80±0.07% respectively.

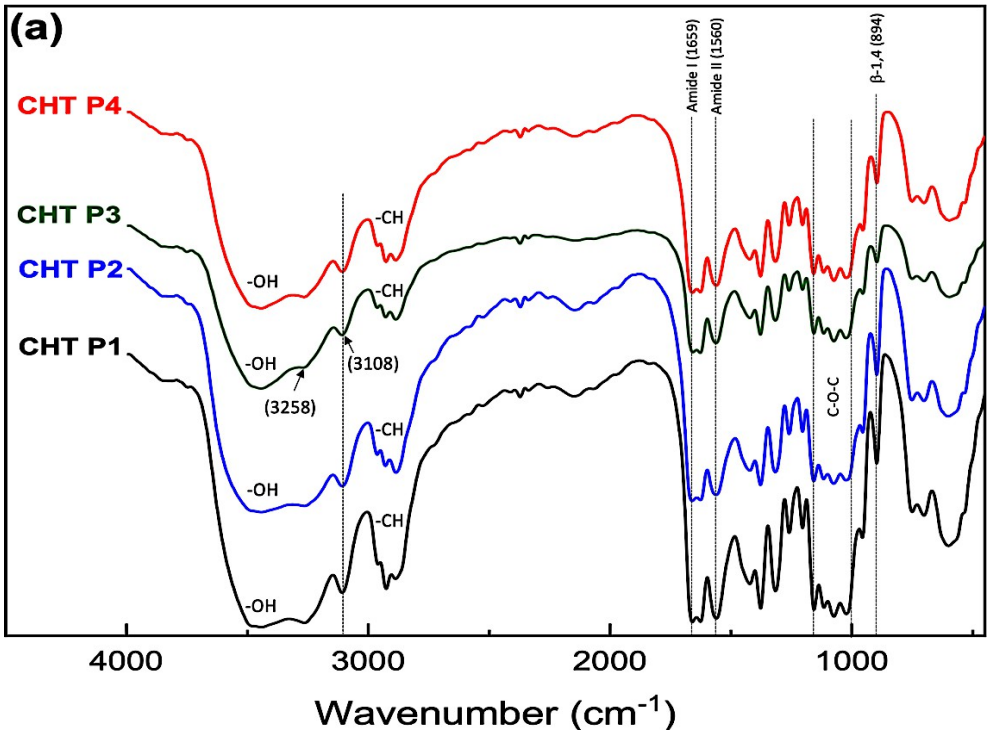

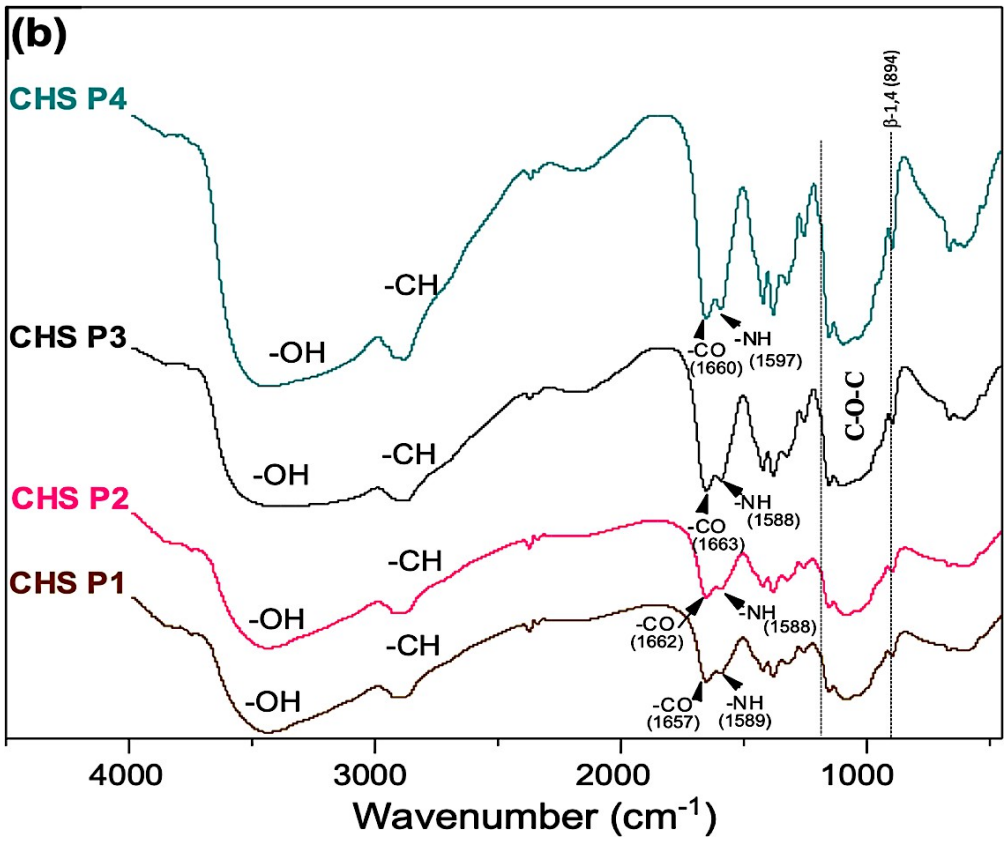

Figure 20. FTIR spectra of chitins (a) and chitosans (b)

^{1}H-NMR is considered to be the best and most accurate method currently available for calculating the degree of acetylation (DA) [157]. **Figure 21** shows the ^{1}H-NMR spectra of chitosans (CHS P1, P2, P3 and P4). A peak at 4.55 is assigned to the amine proton (H-1-D) with an integration value of 1.00 [150]. Additionally, protons at positions 1 to 6 in the molecule (H-1/6) are observed between 1.5 and 4 ppm [141]. The H-2 of the N-deacetylated units (H-2-D) appears at 1.08 ppm [157]. The acetyl proton peak (CH_3) is more intense in CHS P1 by comparing to CHS P4, with integration values of 0.16 for CHS P1, 0.15 for CHS P2, 0.12 for CHS P3 and 0.09 for CHS P4. The peak at 4.1 ppm is attributed to the solvent used. The DA of chitosans CHS P1, P2, P3 and P4 was calculated to be 5.04±0.02%, 4.77±0.20, 3.85±0.14 and 2.92±0.08 respectively. These results are in line with those calculated using FTIR method.

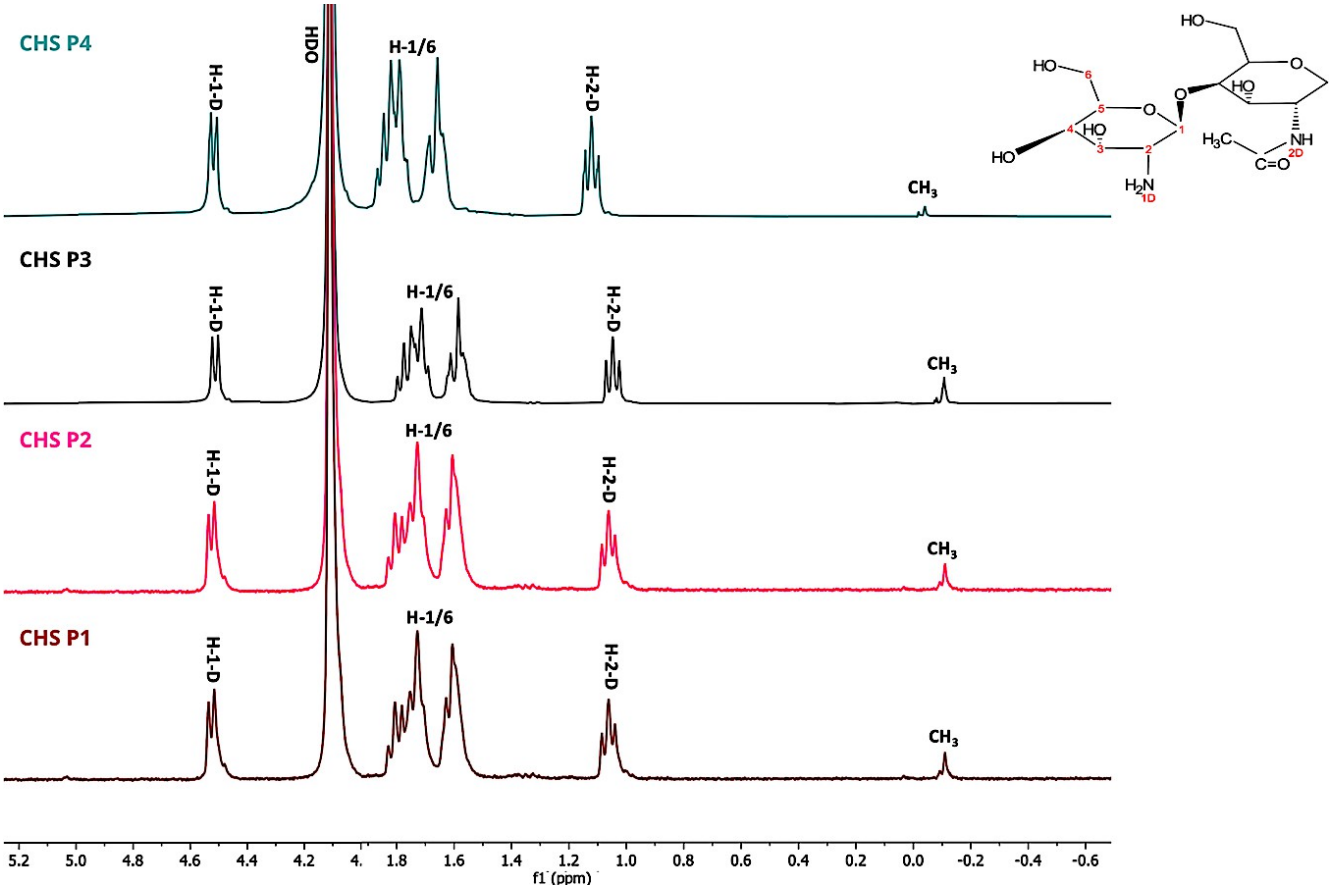

Figure 21. 1H-NMR spectra (400 MHz, 2% DCl, 70°C) of H. illucens chitosans (CHS) extracted by P1, P2, P3 and P4

The titration curves obtained from the recovered chitosan (CHS P1, P2, P3 and P4) **(figure 22)** show a clear difference between the two inflection points, which corresponds to the amount of acid consumed for the neutralization of the amine groups within the chitosan molecules [129]. The DA were calculated according to the equation (8) **(figure 23)**.

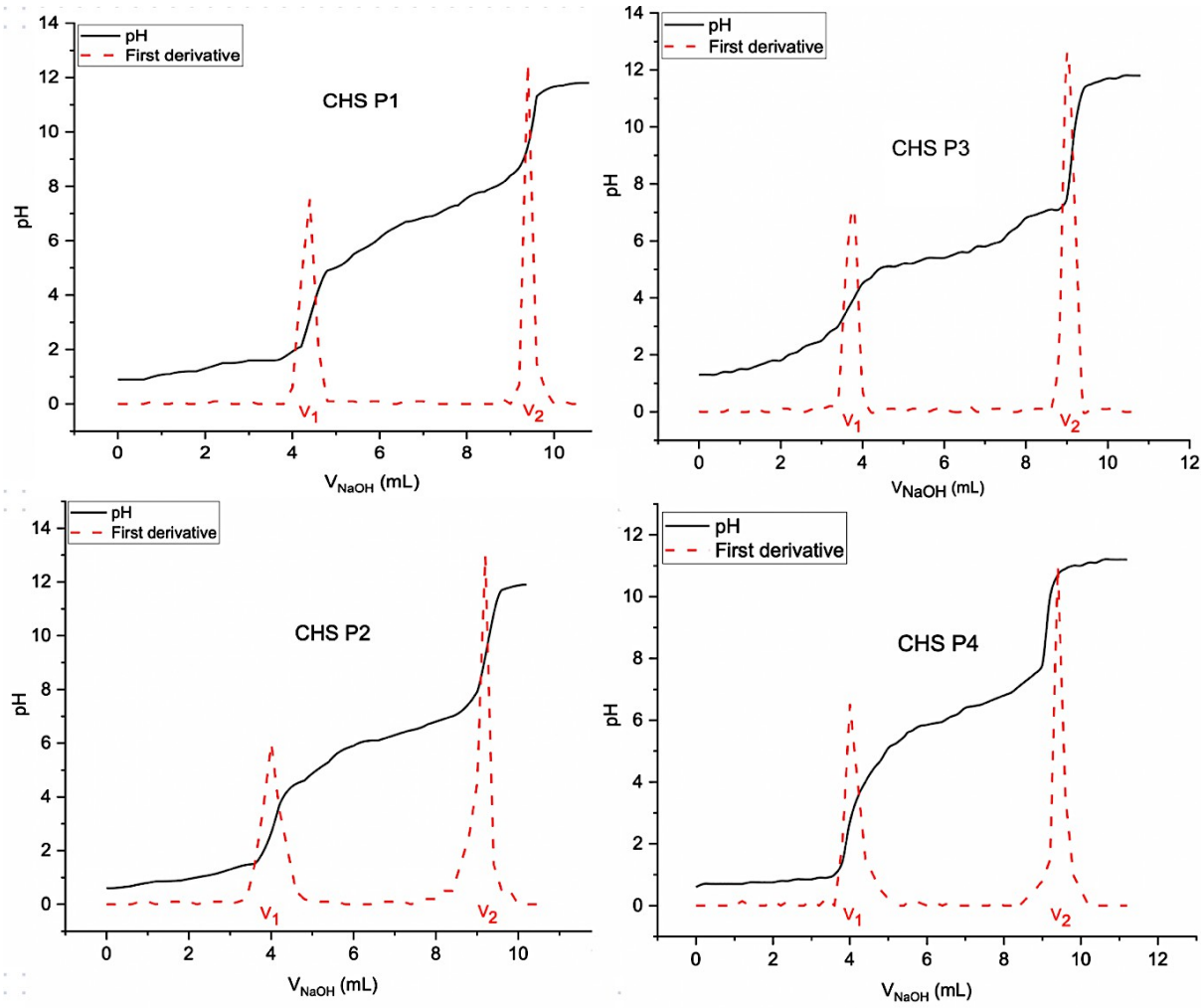

Figure 22. Potentiometry curves of chitosans P1, P2, P3 and P4

Figure 23 presents the DA determined for the different types of chitosan (CHS P1, CHS P2, CHS P3 and CHS P4). These results are in consistent with the literature for the same categories of beetle species [158][159]. The DA values obtained by the three methods show slight differences, which could be attributed to the precision, accuracy, and reliability of each method [130]. However, the trend of these values is coherent, and the results indicate that CHS P4 is the most deacetylated compared to CHS P1, P2, and P3. This property could be advantageous for environmental applications, such as heavy metal removal and as a plant fortifier [160,161], due to the presence of free amine groups that can rapidly exchange with metals and be protonated to facilitate solubilization.

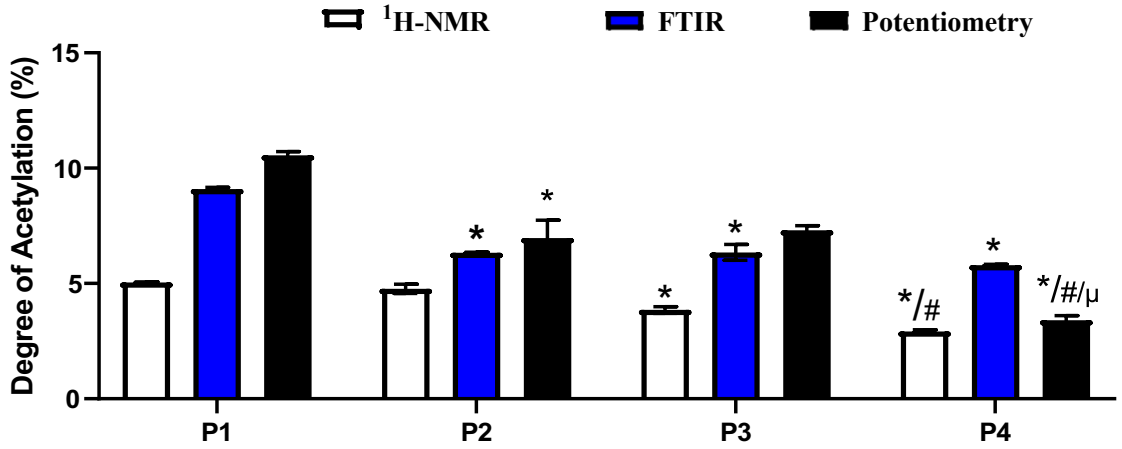

Figure 23. Histograms showing the comparison of degree of acetylation (DA) values according to three methods: FTIR, 1H-NMR, and Potentiometry. Values are expressed as means ± standard deviation. Statistically significant differences (n=5 ; $p < 0.05$) compared to to the P3 process by #, and compared to the P4 process by (μ). Statistical evaluation was performed using one-way ANOVA (p=0.05).

From the SEM images **(Figure 24)**, a contrast emerged between the delipidated chitin (CHT P2, P3 and P4) and non-delipidated chitin (CHT P1). Delipidated chitin shows a smoother surface and more regular organization. The lipids associated to chitin form an irregular and granular layer, which gives a rough appearance to the surface observed in SEM. Removal of these lipids reveals a chitin with a more uniform and regular surface, highlighting the high structural purity of the chitinous matrix. Additionally, delipidated chitins (CHT P2, P3 and P4) revealed fine details such as pores and ridges present on the surface contributing to a more homogeneous structure and smoother appearance [151].

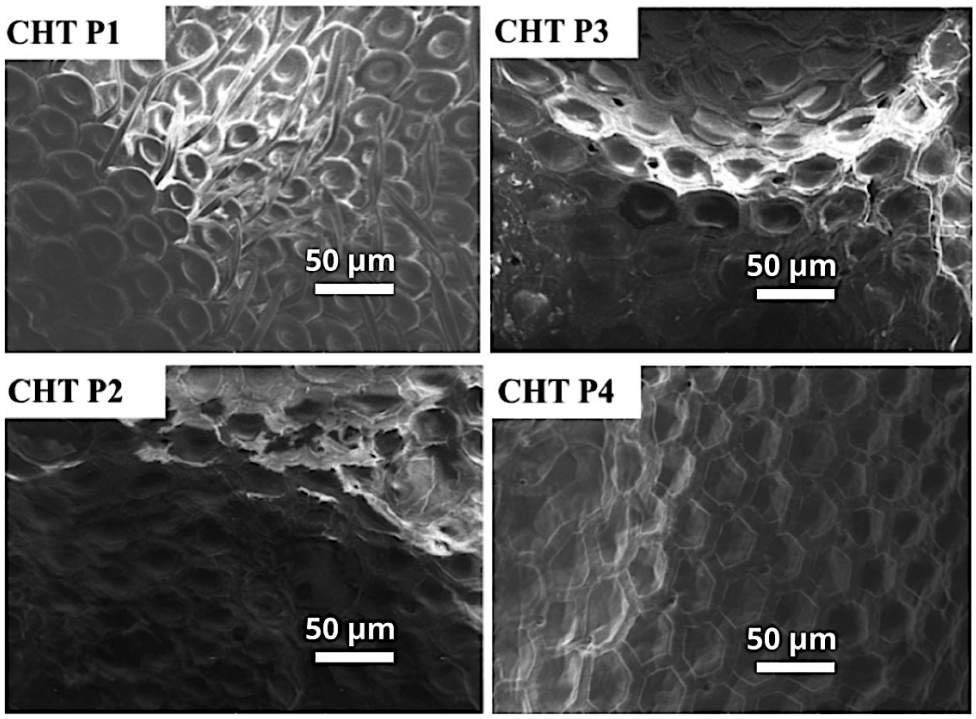

Figure 24. SEM images of chitins P1, P2, P3 and P4

The SEM images of chitosan (P1, P2, P3 and P4) show relatively uniform structures with heterogeneous surface presenting disorganized microfibrils, consequently reflecting a reduction in the crystallinity index **(Table 8)**. Additionally, the presence of lighter pores was notable on the surface, particularly evident in for chitosan from process P2 and P3 **(figure 25)**.

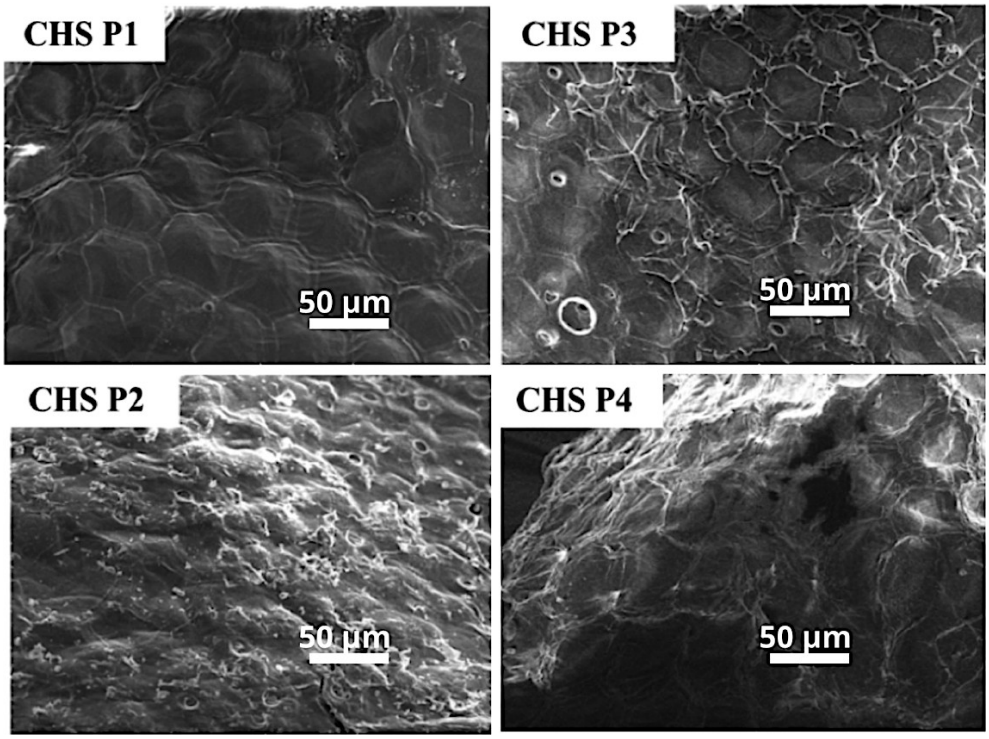

Figure 25. SEM images of chitosans P1, P2, P3 and P4

After plotting the curves of reduced viscosity as a function of the concentration of chitosan solution (P1, P2, P3 and P4), it was possible to deduce the value of the viscometric molar mass of each chitosan by applying the previous equation. Upon the obtained results, a noteworthy trend emerges: the viscometric molar mass of chitosan varies according to the production processes and can be categorized in the following order:

$$M_v \text{ CHS P4} > M_v \text{ CHS P1} > M_v \text{ CHS P3} > M_v \text{ CHS P2}$$

Process 2 led to a high degradation of chitosan P2 compared to other processes, resulting in a lower viscometric molar mass of 95 316 $g.mol^{-1}$ **(Fig. 26)**. This degradation can be attributed to the use of hexane during the delipidation step. The interactions between apolar hexane and polar groups of chitosan disrupt its chemical structure **[162]**. This results in the breakdown of chemical bonds within the polymer, thereby weakening its strength and mechanical properties. This renders the biopolymer brittle and susceptible to deformation.

Conversely, the chitosan P4 was obtained by the autoclave process, as evidenced by the higher viscometric molar mass of 220 378 g.mol^{-1} **(figure 26)**. This can be attributed to the shorter duration of the deacetylation step (1h), this molar mass is considered a good quality for commercial use from shrimp, as it falls within the typical molecular weight range for commercial chitosan products [163,164].

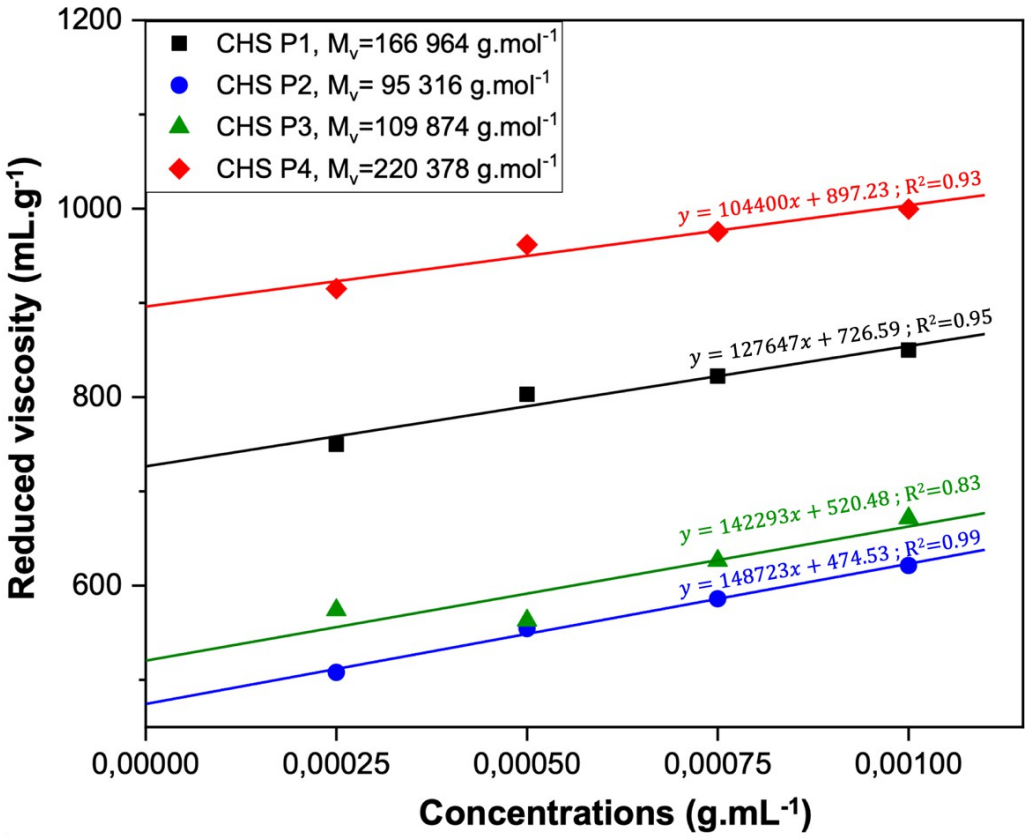

Figure 26. Examples of the viscosity curves of the chitosan samples CHS P1, P2, P3 and P4 prepared from pupal cases of BSF

Thermal stability, a critical property in assessing the potential applications of chitin and chitosan, can be evaluated through TGA techniques. Focusing on the thermal degradation of the backbone of chitin and chitosan, **figure 27** displays a mass loss after water removes, i.e. after 150°C. The thermal degradation is largely affected by the crystallinity, morphology and molecular weight [165]. Then, the TGA results could not be used alone for chitin configuration determination without the combined use of multiple instrumental analyses, i.e. FTIR, ^{1}H-NMR, XRD and SEM [166]. The thermal degradation of chitins occurs between 280°C and 450°C, primarily attributed to the

degradation of the chitin chain [167]. The DTG_{max} values for chitins are shown in **table 10**. CHT P1, P2, P3 and P4 exhibit DTG_{max} values of 384°C, 386°C, 411°C and 421°C, respectively. This confirms the α-chitin form, which is usually higher than 350°C [57]. The around 40°C shift of DTG_{max} between P1-P2 and P4, with the same onset behavior, can indirectly be attributed to a possible higher molecular weight but also to the crystalline structure being more homogeneous and the crystallinity rate (**figure 19** and **table 9**) obtained with P4 process. The TGA curves of different chitosan (CHS P1, P2, P3 and P4) **(figure 27)** display a mass loss between 290 °C and 450 °C, and it can be attributed to the decomposition of chitosan, especially the acetylated and deacetylated units [168].

Table 10. DTGmax of chitins and chitosans from P1, P2, P3 and P4 processes

	DTG_{max} (°C)	
	Chitin	**Chitosan**
P1	384	323
P2	386	338
P3	411	343
P4	421	345

Furthermore, the maximum degradation temperatures (DTG_{max}) are observed at peaks of 323°C, 338°C, 343°C, and 345°C, corresponding to CHS P1, CHS P2, CHS P3, and CHS P4, respectively **(Table 10)**. This variation in DTG_{max} among the four chitosan can be attributed to the distinct degrees of deacetylation associated with each process, the number of hydrogen bonds, and the influence of crystallinity on their thermal stability **[26]**. The results suggest that chitin CHT P4 and chitosan CHS P4 possess the highest thermal stability and longer chain lengths compared to the other three chitins and chitosans, as well as compared to chitins obtained through green preparation methods reported in the literature [62].

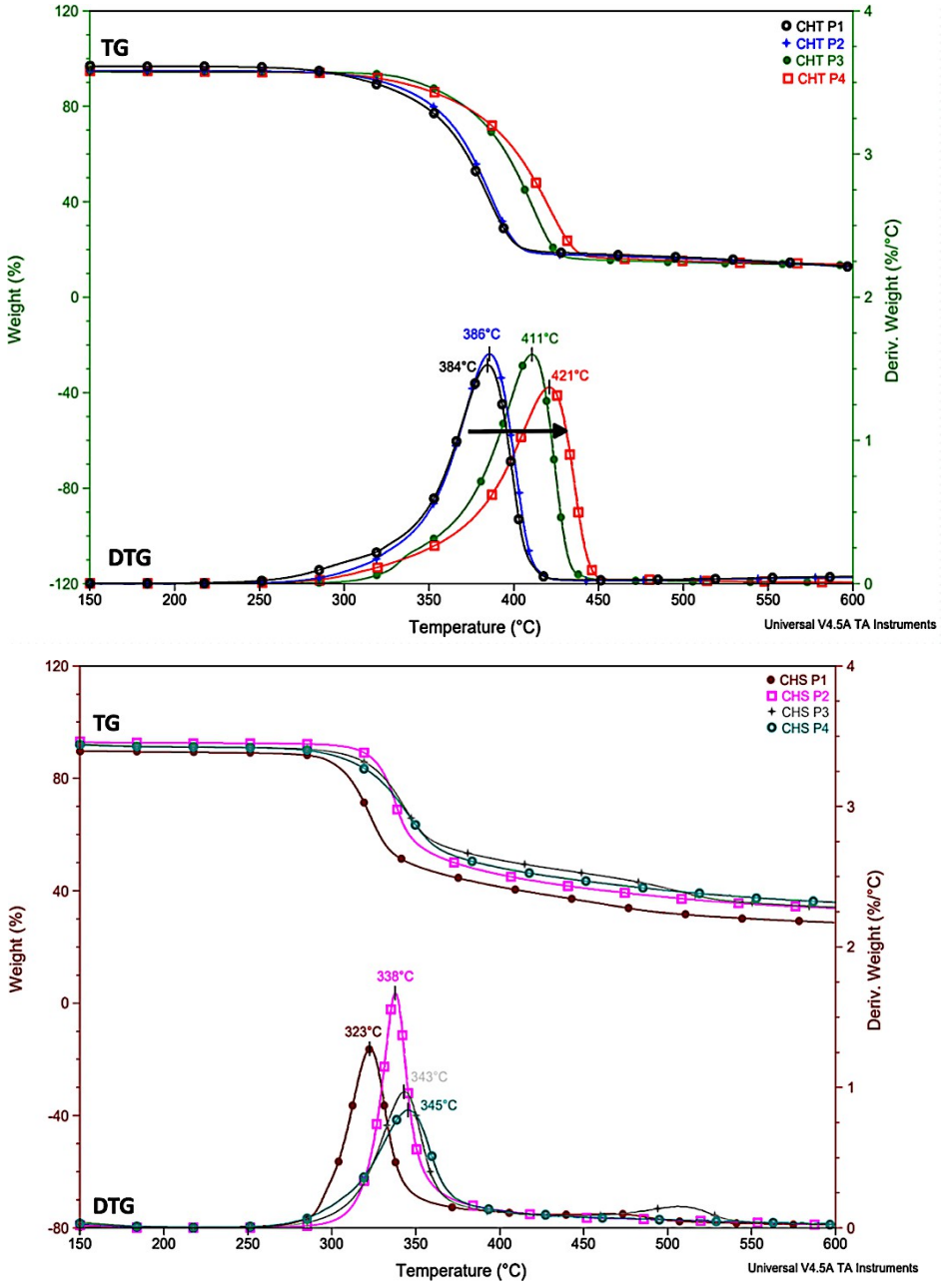

Figure 27. Thermograms (TG) and their derivatives (DTG) of chitins (CHT) and chitosans (CHS) P1, P2, P3 and P4

4. Influence of the process and role of deacetylation

Optimizing chitin and chitosan extraction from *Hermetia illucens* breeding waste offers a unique opportunity to enhance waste valorization through sustainable and efficient

processing. In insect waste valorization, the primary objective is to achieve high-purity chitin with structural integrity that closely resembles its native form, while also enabling efficient N-deacetylation to produce chitosan with desirable properties. Process 4 (P4), optimized in this study, demonstrates significant advantages in purity, yield, and efficiency, making it a promising candidate for industrial applications. This aligns with the fundamental requirements for sustainability and industrial scalability in chitin extraction processes, which rely heavily on maximizing yield, minimizing processing time, and ensuring operational simplicity.

This process allows the production of chitosan that is almost fully deacetylated with a high molecular weight, providing several options for environmental applications. The involvement of an autoclave-assisted process represents an environmentally friendly approach, minimizing processing time while achieving desirable physicochemical properties. When comparing chitin yields from BSF pupal cases across various studies **(Table 11)**, Process 4 stands out with a yield of 34.74±1.15%, which is significantly higher than those reported in other studies employing different extraction methods [135]. For instance, chemical methods have reported yields of 14.1%, 10.7%, and 9%, indicating a marked inefficiency compared to P4. Additionally, the microwave assisted process reported by Elouali et al., considered as an ecofriendly method for chitin extraction, yields a lower amount of chitin from prepupal cases of BSF compared to the optimized process P4, which achieves around 21.14% [79]. Although continuous fermentation technique, recognized as a biological method for chitin extraction, has yielded up to 59.9% [96], they often require longer processing times and more complex operational requirements, making them less practical for industrial production. In the study by Lin et al., microbial fermentation was applied to BSF pupal waste using *Bacillus licheniformis A6*, achieving a chitin yield of 12.4% after 10 days of fermentation [78]. While this method leverages a biological approach, its extended duration and lower efficiency highlight the trade-off in yield and operational complexity.

Additionally, it is important to note that the described biological approaches [78,96] are limited to the extraction of chitin. For subsequent deacetylation to produce chitosan, chemical methods remain indispensable. Specifically, the chemical protocols employed in related studies utilized 30% NaOH for 3 hours at a ratio of 1:50 [96] and 50% NaOH for 4 hours at the same ratio **[78]**. Moreover, the microbial method used in this study retained 7.51% protein content in the chitin, suggesting lower purity. In contrast, P4 achieved a deproteinization efficiency of 94.25 ± 0.6% within a markedly shorter duration (1.15 ± 0.08 hours), reinforcing its suitability for practical and scalable applications with minimal resource expenditure.

Regarding chitosan yields, Process 4 achieves a yield of 83.33±1.15%. This is notably higher than the yields obtained through chemical methods, with Elkadaoui et al. reporting only 74% from BSF pupal cases [134] and Hamdan et al. reporting 75.36% from *Akis granulifera* [130]. These results highlight the advantages of the autoclave technique, which combines the use of potassium hydroxide, ethanol and mono-ethylene glycol mixture under a pressure of 2.2 bar at 121°C in a total time of 1h. This approach facilitates obtaining the highest yield of chitosan by effectively removing proteins and acetyl groups without causing any degradation or yield loss of the chitosan.

Table 11. Comparison of chitin and chitosan properties obtained by Process 4 and other extraction methods across different sources

Study	Extraction method	Source	Yields (%)		DA (%)	Mv (kDa)	I_{Cr} (%)		DTG_{max} (°)	
			Chitin	Chitosan			Chitin	Chitosan	Chitin	Chitosan
This work	Process 4		34.74±1.15	83.33±1.15	2.92	220.38	73.38	47.7	421	345
[135]	Chemical		14.1	-	-	-	68.44	-	371	-
[151]	Chemical		9	-	-	-	25.20	-	371	-
[169]	Chemical		10.7	-	-	-	64	-	365	-

[96]	Biological	Pupal cases of BSF	59.9	-	18.52	-	68.44	-	373	-
[78]	Biological		12.4	-	-	-	52.8	55.4	-	-
[134]	Chemical		43±1.1	74	4	115	69	-	336	-
[150]	Chemical	Prepupal cases of BSF	17.97	-	3.15	62.24	47.11	30	328	307
[79]	Microwave-assisted process		21.14	65.89	4.1	155	-	51.26	-	326
[49]	Chemical	*Periplaneta americana L.*	-	-	15.3	75.05	55.08	40.28	-	-
[130]	Chemical	*Akis granulifera*	24.59±0.39	75.36±1.75	5.48	178	59.8	49	330	320

In terms of physicochemical properties, the chitin obtained by process 4 shows the highest crystallinity and thermal degradation compared to the other three processes conducted in this study. This indicates that these properties are also advantageous compared to studies that reported extraction from the same source, where the DTG_{max} did not exceed 373°C, and crystallinity did not surpass 69% **(Table 8)**. This confirms the successful extraction of chitin, which is close to its native form, primarily existing as a semi-crystalline polymer [170]. After N-deacetylation, the crystallinity and thermal stability of chitin decreased to 47.7% and 345°C, respectively, confirming its successful transformation into chitosan, which inherently has lower crystallinity and thermal stability due to the loss of acetyl groups and increased disorder in the polymer chains [171].

5. Multicriteria industrial assessment of chitin extraction processes

In order to evaluate the industrial relevance of the different extraction strategies investigated in this study, a multicriteria analysis was performed using the Industrial Feasibility Score (IFS), integrating process duration, extraction yield, scalability and product quality **(figure 28)**. This comparative framework provides a global assessment of the suitability of each method for large-scale implementation. The results clearly

demonstrate that the autoclave-assisted process exhibits the highest global performance, achieving an A score in terms of time efficiency, product quality and scalability, while maintaining high extraction yields. This performance is consistent with the experimental observations reported throughout this work, particularly the significant reduction in deproteinization time, the substantial decrease in water consumption and the preservation of chitin structural properties. In contrast, conventional chemical extraction, although widely used industrially, shows lower performance due to its long processing time, high chemical and water consumption, and partial degradation of the polymer structure.

Chitin Extraction Processes	Industrial Feasibility Score (IFS)				Category (based on the Global IFS)
	Time-score	Yield-score	Efficiency & product quality score	Scalability-score	
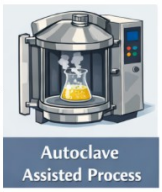 Autoclave Assisted Process	A	A-B	A	A	
 Microwave Assisted Process	A-B	A-B	B	A-B	
 Ultrasound Assisted Process	B	B	B-C	B	
 DES & Ionic Liquid Solvents	C	B	C	A	
 Traditional Chemical Method	D	C-D	C	C-D	
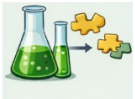 Enzymatic Extraction	E	C	D-E	A-B	

Figure 28. Multicriteria industrial benchmarking of chitin extraction technologies using the Industrial Feasibility Score (IFS), *integrating process duration (A: minutes–<2 h; B: 2–3 h; C: 3–8 h; D: 8–24 h; E: days), extraction yield (A: >20–25%; B: 15–20%; C: 10–15%; D: 5–10%; E: <5%), industrial scalability (A: industrial-scale ready; B: pilot-scale feasible; C: lab-scale with difficult scale-up; D: low scalability; E: non-scalable) and efficiency & product quality (A: high purity >90%, preserved crystallinity, controlled DA, minimal depolymerization; B: good purity 85–90%; C: medium purity 70–85%; D: low purity <70% with strong degradation; E: poor structural integrity, unsuitable for high-value applications).*

Similarly, emerging technologies such as microwave and ultrasound-assisted extraction exhibit intermediate performance, offering improvements in processing time but facing limitations in scalability and process control. Alternative green

approaches, including enzymatic extraction and DES/ionic liquid systems, remain limited by long processing times, lower yields or challenges related to industrial implementation. Overall, this multicriteria evaluation highlights the autoclave-assisted process as the most promising strategy for sustainable and industrial-scale chitin production, combining high efficiency, reduced resource consumption and good product quality.

6. Conclusion

Four extraction processes were developed to standardize and determine the best method for extracting chitin and producing chitosan from *Hermetia illucens* breeding waste (pupal cases). Among the processes studied, process P4 showed the highest efficiency in terms of polysaccharide purification, with a yield of 34.74% for chitin and 83.33% for chitosan, outperforming the other processes. This process also stands out for its environmentally friendly approach, reducing water use by 80%, chemical consumption by 83%, and reaction time by 95% during the deacetylation step. Additionally, the physicochemical and thermal properties of the chitosan obtained through this process are significantly better than those from the other methods, with a degree of acetylation (DA) of 2.92%, crystallinity of 47.7%, a molecular weight of 220 378 $g.mol^{-1}$, and a DTG_{max} of 345°C. A distinguishing aspect of this process is the incorporation of an autoclave technology, combined with a delipidation step, which preserves the structure and quality of the polysaccharides, unlike the other methods. Overall, the results demonstrate that the autoclave-assisted process (P4) constitutes a highly efficient, sustainable, and scalable approach for the extraction of chitin and chitosan from insect biomass, making it particularly suitable for industrial applications, as confirmed by its highest Industrial Feasibility Score (IFS = A). Furthermore, the application of this process to a wider range of bioresources is required to validate its robustness and general applicability, enabling its

standardization as a reliable method for the sustainable production of chitin and chitosan.

Chapter 2: Standardization of an Autoclave-Assisted Process for Sustainable Chitin and Chitosan Extraction from Moroccan Bioresources: Structural and Physicochemical Insights

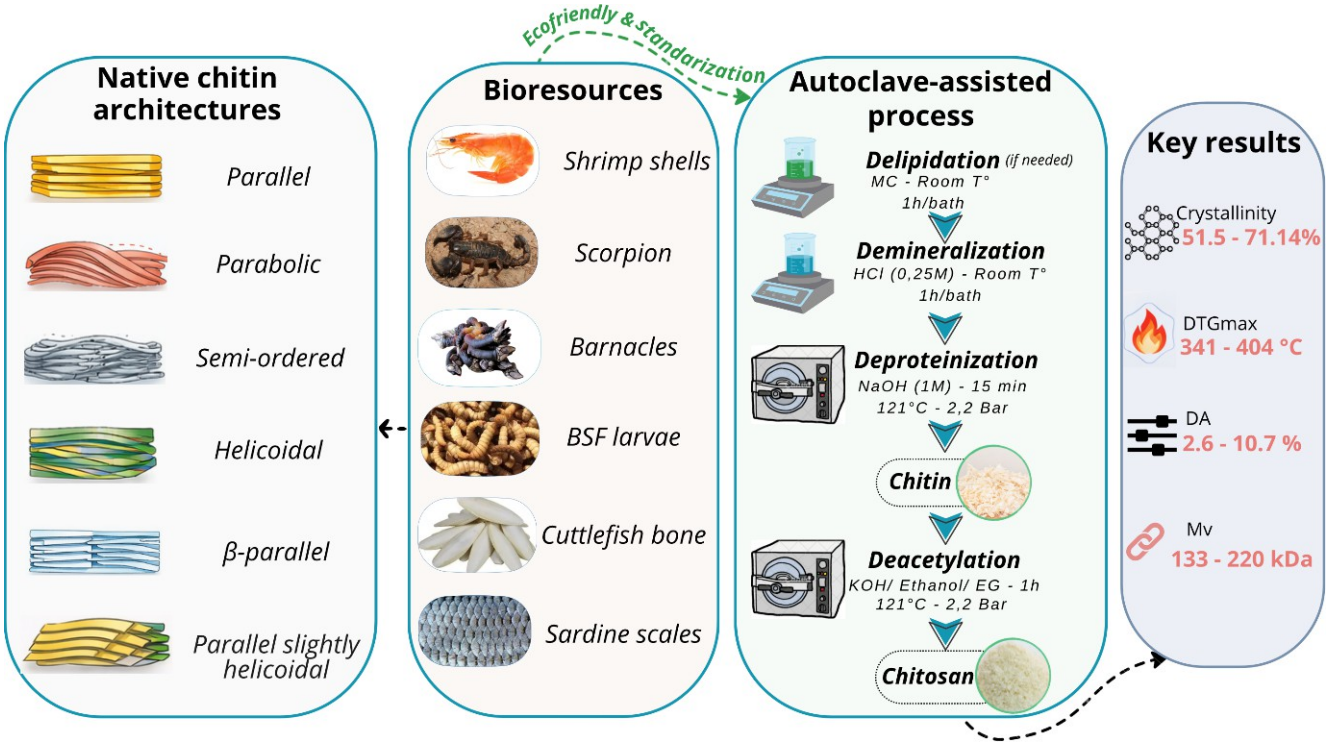

1. Introduction

As it was emphasized in the chapter 1, one of the most promising and scalable approaches validated for insect biomass is the autoclave-assisted extraction process. This method enables a substantial reduction in extraction time (by up to 95%), minimizes chemical consumption (reducing NaOH and HCl usage by 83%) and water use up to 80%, and increases chitin yield (up to 34.74%, i.e- BSF pupae) while maintaining high crystallinity and thermal stability. Nevertheless, to the best of our knowledge, the applicability and performance of this process have not yet been confirmed for other common industrial chitin sources, such as shrimp shells, cuttlefish bone and other abundant chitin-rich wastes found in Morocco. Therefore, the present work aims to standardize the autoclave-assisted extraction process across a representative range of arthropod and cephalopod sources: *Parapenaeus longirostris* shells (PL), *Pollicipes pollicipes* (PP), *Sepia officinalis* cuttlebone (SO), *Scorpio mogadorensis* exoskeleton (SM), *Hermetia illucens* larvae (HI) and *Sardina pilchardus* scales (SS). However, applying an identical extraction protocol to all these sources does not necessarily guarantee identical structural or functional properties in the recovered chitins and chitosans. This variability may arise from intrinsic biological and ecological factors, such as the organism's habitat, diet or developmental stage, that influence the microstructural organization of native chitin. Indeed, the fiber orientation within the chitin matrix differs among species, affecting both crystalline form and resulting material properties. Beyond the known α-, β- and γ-chitin allomorphs [171], several studies have revealed distinct microstructural organizations, including parallel, helicoidal, parabolic and lamellar arrangements [31,34], which govern mechanical performance, crystallinity index and accessibility to chemical treatments. In this context, the present chapter seeks to elucidate how these native structural orientations contribute to the observed physicochemical differences among chitins extracted from diverse biological origins under identical autoclave-assisted conditions.

2. Native chitin microfibril organization in biological cuticles

Polarized optical microscopy (POM) and ESEM revealed pronounced species-dependent variations in the hierarchical organization of chitin microfibrils across the investigated biological matrices. Such diversity in fibrillar orientation is a well-established feature of chitin-based biomaterials, where microfibrils are embedded within proteinaceous matrices and arranged in layered architectures that determine the mechanical performance of the cuticle [31,172]. In shrimp cuticle (PL), both POM and ESEM consistently showed highly parallel and densely packed lamellae, indicating a strongly ordered fibrillar organization across the cuticle thickness. Similar parallel lamellar stacking has been reported in several crustacean exoskeletons, where α-chitin nanofibrils form multilayered composites embedded in proteins and minerals. These structures typically exhibit high birefringence and well-defined lamellae when observed under polarized light, reflecting the strong orientation of chitin fibers within each layer [63,172,173]. Comparable lamellar arrangements have also been observed in decapod crustaceans using electron microscopy, where successive layers maintain nearly constant fibrillar orientation across micrometer-scale thicknesses [174]. Sardine scales (SS) exhibited closely parallel microlamellae, although ESEM imaging revealed slight undulations between adjacent layers **(figure 29)**. These deviations from perfect alignment correspond to the weak helicoidal modulation detected under polarized light. Similar undulated lamellar architectures have been described in biological fibrous composites where gradual angular changes between lamellae contribute to improved crack deflection and structural toughness [175,176]. In fish scales and other biological composites, such mild rotational transitions between layers are often interpreted as transitional states between purely parallel and helicoidal organizations.

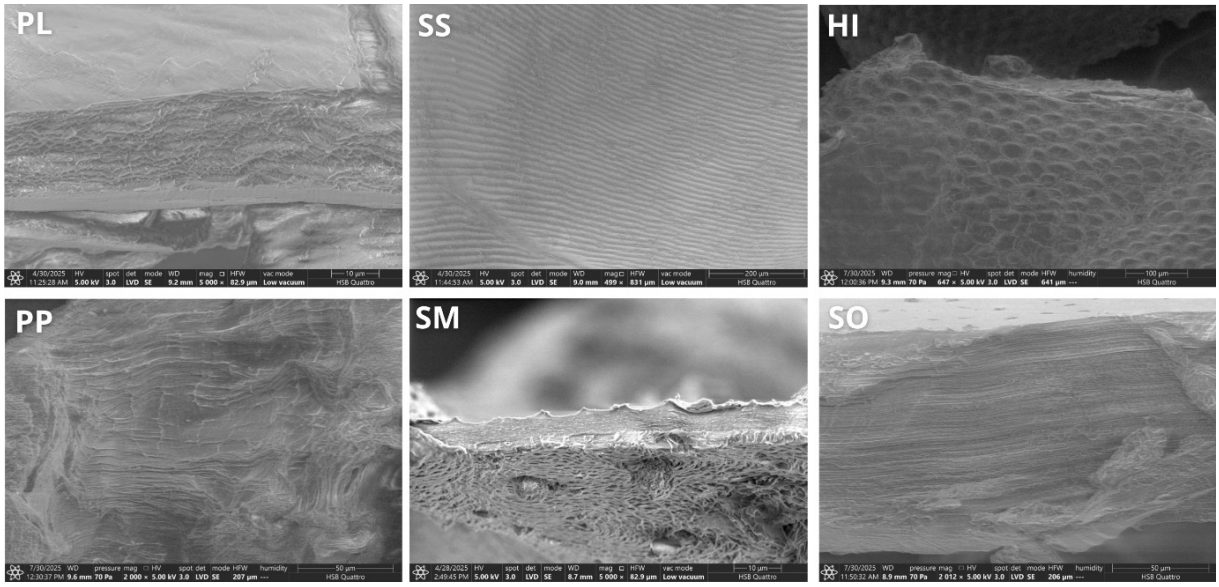

Figure 29. ESEM observation of bioresource cuticles of PL (*Parapenaeus longirostris*), SS (*Sardina pilchardus*), HI (*Hermetia illucens*), SM (*scorpio mogadorensis*), PP (*Pollicipes pollicipes*) and SO (*Sepia officinalis*)

A markedly different structural organization was observed in the cuticle of *Hermetia illucens* (HI), which displayed a helicoidally stacked lamellar architecture typical of Bouligand structures. In this configuration, the orientation of chitin microfibrils rotates gradually between successive lamellae, generating a twisted plywood arrangement clearly visible in both POM and ESEM observations **(figure 30 and 31)**. This hierarchical architecture represents one of the most characteristic structural motifs of insect cuticle and has been extensively documented in arthropods. Studies combining electron microscopy and diffraction techniques have shown that such helicoidal stacking arises from sequential deposition of chitin–protein fibers during cuticle formation [32,172].

Recent biomechanical investigations further emphasize that Bouligand architectures play a crucial role in improving resistance to crack propagation and mechanical damage in arthropod exoskeletons [177,178]. Similar helicoidal organizations have been reported in beetle cuticles and other insect exoskeletons, where nanoscale chitin fibrils rotate progressively between adjacent lamellae, forming multilayered chiral

composites [173,179]. In contrast to the helicoidal arrangement observed in insects, the scorpion cuticle (SM) displayed a parabolic lamellar organization characterized by curved fibrillar trajectories. Under polarized light, this organization produced anisotropic bands **(figure 31)**, while ESEM imaging provided clearer visualization of the curved arrangement of fibrillar bundles. Comparable curved or pseudo-helicoidal fibrillar architectures have been reported in several arthropod cuticles, where chitin bundles follow non-linear trajectories that vary across the cuticle thickness [174]. Such arrangements are thought to provide anisotropic reinforcement adapted to complex mechanical loading conditions experienced by arthropod exoskeletons [175,178].

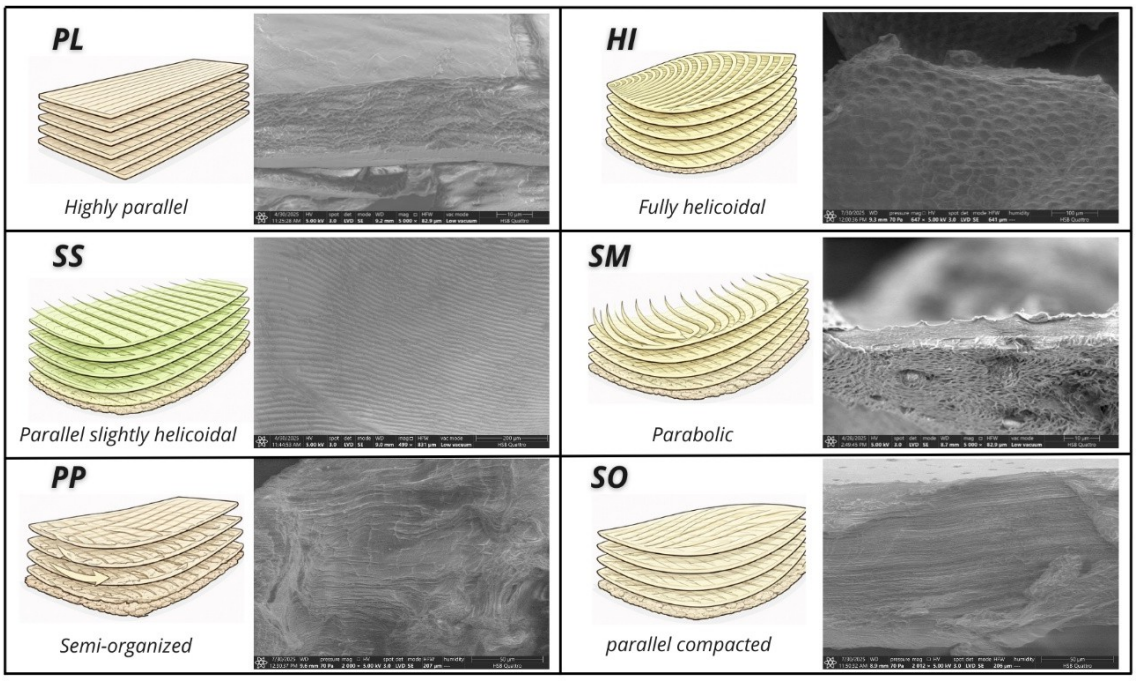

Figure 30. Schematic representation of chitin microfibril organization and matrix composition in different biological sources.

For *Pollicipes pollicipes* (PP), ESEM observations revealed parallel but less coherently oriented lamellae, where fibrillar alignment was locally interrupted by curvature and irregular stacking. Similar heterogeneous lamellar arrangements have been reported in barnacle cuticles and other marine arthropods, where structural irregularities may arise from variations in mineralization and organic matrix composition [173,174]. In such systems, the coexistence of aligned lamellae and locally disordered regions

contributes to a composite architecture capable of accommodating mechanical stress while maintaining structural integrity. In the dorsal region of *Sepia officinalis* (SO), ESEM observations revealed parallel but loosely packed lamellar layers, characterized by large spacing between adjacent fibrillar bundles. This organization is consistent with the structural characteristics of β-chitin matrices commonly found in cephalopod skeletal structures such as squid pens and cuttlebone. Compared with α-chitin, β-chitin exhibits weaker intermolecular hydrogen bonding and a more open crystalline arrangement, resulting in lower packing density and higher hydration capacity [63,64]. Similar loosely organized lamellae have been reported in cephalopod-derived chitin matrices where fibrils form broad parallel sheets with limited lateral cohesion [172]. T-These observations reveal a remarkable diversity of native chitin architectures across the investigated biological sources. The studied materials range from strictly parallel lamellar structures (shrimp), through weakly modulated or undulated arrangements (sardine scales), to helicoidal Bouligand architectures (insect cuticle), curved parabolic patterns (scorpion cuticle), semi-ordered lamellae (barnacle cuticle) and loosely packed β-chitin layers (cephalopod structures) **(figure 30)**. Such diversity highlights the exceptional versatility of chitin as a structural biopolymer and confirms that microfibril orientation and lamellar organization are strongly species-dependent, reflecting the distinct biological functions encoded within each cuticular design [32,172,177,178]. Understanding the native microstructural organization of chitin within these biological matrices is essential for interpreting the physicochemical characteristics of the extracted chitins and chitosans obtained through the standardized autoclave-assisted process

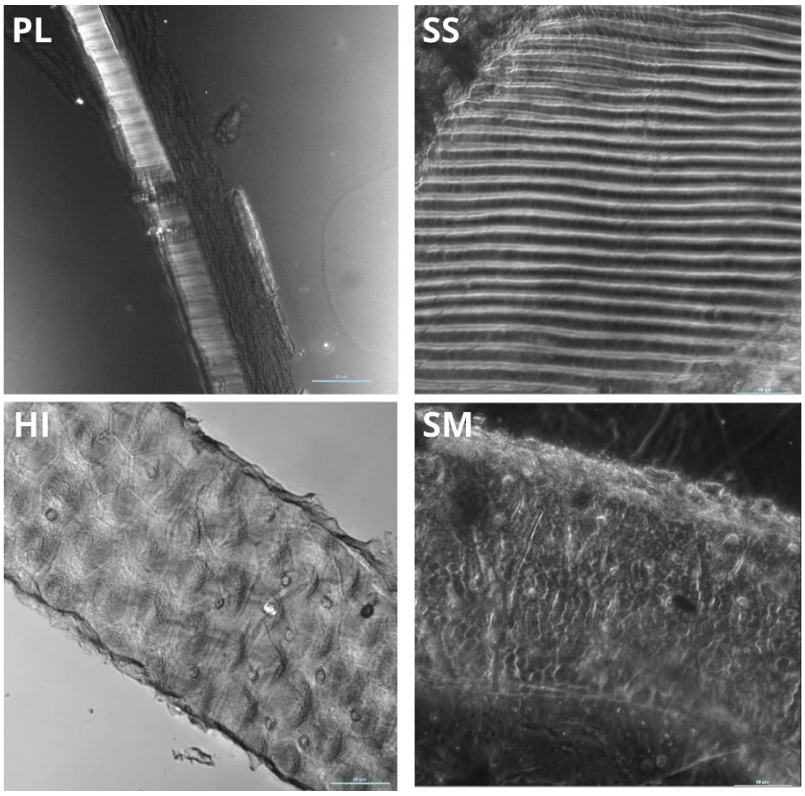

Figure 31. POM observation of bioresource cuticles of PL (*Parapenaeus longirostris*), SS (*Sardina pilchardus*), HI (*Hermetia illucens*) and SM (*scorpio mogadorensis)*

3. Autoclave-assisted process performance

The standardized autoclave-assisted extraction protocol was applied to six chitin-containing biomasses originating from marine and terrestrial environments, including *Parapenaeus longirostris* shells (PL), *Pollicipes pollicipes* (PP), *Sepia officinalis* cuttlebone (SO), *Scorpio mogadorensis* exoskeleton (SM), *Hermetia illucens* exuviae (HI) and *Sardina pilchardus* scales (SS). The process involved sequential demineralization using 0.25 M HCl, followed by autoclave-assisted deproteinization using 1 M NaOH at 121 °C and an optional delipidation step applied only when required (-i,e. HI and SS). The detailed extraction conditions and the number of treatment cycles for each biomass are summarized in Table 1. Demineralization was carried out under relatively mild acidic conditions compared with conventional protocols reported in the literature, which often employ 0.5 to 2 M. The use of 0.25 M HCl at room temperature for 1 h proved

sufficient to remove mineral phases such as calcium carbonate while minimizing hydrolysis of the polysaccharide matrix. Following this step, deproteinization was performed using 1 M NaOH in an autoclave at 121 °C for 15 min per cycle **(Table 12)**, repeated until the filtrate became clear.

Table 12. Chitin and chitosan extraction conditions

		Delipidation	Demineralization	Deproteinization	Deacetylation
Extraction conditions		Methanol-chloroform - 25°C 1h/bath 1:20 (w/v)	0,25M HCl - 25°C 1h/bath 1:40 (w/v)	1M NaOH 121°C-2.2 Bar 15 min/bath 1:40 (w/v)	50%KOH-25%EG-25%Eth 1h / 121°C-2.2 Bar 1:10(w/v)
Number of baths	**PL**	-	2×(2h)	2×15min	1×(1h)
	SO	-	3×(3h)		
	PP	-	1×(1h)		
	SM	-			
	HI	2×(1h)		6×15min	
	SS	1×(1h)		6×15min	

Compared with conventional alkaline treatments conducted at 80–100 °C for several hours, the autoclave treatment significantly reduced the extraction time while ensuring efficient removal of structural proteins. Similar autoclave-assisted approaches have recently been proposed as a promising strategy to accelerate chitin extraction while maintaining the structural integrity of the polymer [180]. The number of alkaline cycles required during deproteinization varied according to the biological origin of the biomass, reflecting differences in protein content and cuticular composition. Insect cuticles such as those of *Hermetia illucens* are known to contain a relatively high proportion of structural proteins tightly associated with chitin microfibrils, forming a rigid chitin–protein composite [28]. Consequently, HI samples required a greater number of alkaline treatments compared with marine shells, where proteins are generally less strongly bound to the mineralized matrix. Similar observations have been reported for insect-derived chitin, where the presence of cross-linked cuticular proteins often necessitates stronger or repeated alkaline treatments for complete deproteinization [19].

Delipidation was applied exclusively to *H. illucens* and *S. pilchardus* samples due to their relatively high lipid content. Black soldier fly larvae and exuviae may contain 15–35 % lipids depending on developmental stage and feeding substrate [181], while fish scales may retain lipophilic compounds associated with surface mucus and connective tissues. These lipids were removed using a methanol–chloroform mixture to ensure efficient purification of the chitin matrix without affecting its structural integrity [182,183]. The resulting chitin yields varied among the investigated sources, reflecting differences in the original biochemical composition of each biomass **(Table 13)**. The highest chitin yield was obtained from *Sardina pilchardus* scales (22.48 %), followed by *Scorpio mogadorensis* (21.23 %), values that are consistent with previously reported ranges for fish scales and arthropod cuticles, typically between 18 % and 25 % depending on species and extraction conditions [184,185]. Fish scales are composite structures composed mainly of collagen, minerals and chitinous polysaccharides and efficient removal of the protein and mineral fractions can therefore yield relatively high chitin recovery.

Intermediate yields were obtained for shrimp shells (PL), barnacles (PP) and black soldier fly larvae (HI). Crustacean shells are composed of a mineralized chitin–protein matrix containing significant amounts of calcium carbonate, while insect cuticles consist primarily of α-chitin embedded within a proteinaceous network. These compositional differences can influence extraction efficiency and the relative proportion of recoverable chitin [19,98]. In contrast, the lowest chitin yield was obtained from *Sepia officinalis* (10.31 %), which can be attributed to the extremely high mineral fraction of cuttlebone [92]. The internal structure of cuttlebone consists mainly of calcium carbonate arranged in a highly porous aragonite framework, representing more than 80–90 % of the total mass, while the organic matrix containing β-chitin represents only a small fraction of the material. Even though only the dorsal region known to contain a higher proportion of chitin was used in this study [141], the overall

mineral dominance of the structure inevitably limits the amount of recoverable chitin [141,186].

Table 13. Influence of different Bioresource on chitin and chitosan yields (%)

Bioresources	Chitin yield (%)	Chitosan yield (%) (from chitin)
PL	19.74±1.04	83.11±1.78
SO	10.31±0.92	87.04±2.11
PP	16.31±1.02	81.61±1.76
SM	21.23±1.23	79.15±0.23
HI	18.51±1.11	75.03±0.87
SS	22.48±1.40	88.13±1.05

Following alkaline deacetylation, the chitosan yields ranged from 75.03 % to 88.13 %, confirming efficient conversion of chitin into its deacetylated derivative **(Table 13)**. The highest chitosan yield was obtained for Sardina pilchardus (88.13 %), whereas *Hermetia illucens* exhibited slightly lower values (75.03 %), possibly reflecting differences in microfibril packing and accessibility of acetyl groups within the chitin crystalline structure. Variations in deacetylation efficiency depending on the biological source have been widely reported and are often associated with differences in crystallinity and structural organization of the chitin [64]. An additional advantage of the present protocol is the absence of a bleaching step, which is frequently used in conventional extraction methods to remove pigments and residual organic compounds. In the present work, the autoclave-assisted process produced visually clean chitin without requiring oxidative treatments.

To further evaluate the performance of the proposed process, the extraction conditions and yields obtained in this study were compared with previously reported methods for similar biomasses **(Table 14)**. Conventional chemical extraction procedures generally require strong acid and alkaline treatments applied for several hours, frequently combined with bleaching steps to improve purity. In contrast, the

autoclave-assisted approach employed here uses lower acid concentration and drastically shorter reaction times (15 min per cycle) while achieving chitin yields comparable to those reported in several studies. These results demonstrate the adaptability and efficiency of the standardized autoclave-assisted protocol for extracting both α-chitin and β-chitin from diverse biological sources while reducing chemical consumption and processing time.

Table 14. Comparison of chitin and chitosan yields from different sources and extraction methods

Source	Extraction method	Demineralization	Deproteinization	Time	Chitin yield (%)	Chitosan yield (%)	Ref
Shrimp shells (PL)	Conventional chemical	1 M HCl	1–2 M NaOH (90 °C)	12–24 h	20–30	65–85	[98]
	Microwave-assisted extraction	1 M HCl	1 M NaOH	2 h	22–28	70–88	[80]
	Autoclave-assisted	0.25 M HCl	1 M NaOH (121 °C)	15 min/ cycle	19.74	83.11	This study
Barnacles (PP)	Chemical extraction	1 M HCl	1 M NaOH	12–24 h	15–22	60–80	[187]
	Autoclave-assisted	0.25 M HCl	1 M NaOH (121 °C)	15 min/ cycle	16.31	81.61	This study
***Sepia officinalis* (SO)**	Conventional chemical	1–2 M HCl	1 M NaOH	12–24 h	10–20	60–75	[141]
	Autoclave-assisted	0.25 M HCl	1 M NaOH (121 °C)	15 min/ cycles	10.31	87.04	This study
BSF larvae	Chemical extraction	1 M HCl	1–2 M NaOH	6–12 h	15–25	60–80	[19]
	Autoclave-assisted	0.25 M HCl	1 M NaOH (121 °C)	15min/ cycle	18.51	75.03	This study
Fish scales	Chemical extraction	0.5–1 M HCl	1 M NaOH	6–12 h	18–25	65–85	[183]
Sardine scales (SS)	Autoclave-assisted	0.25 M HCl	1 M NaOH (121 °C)	15 min/ cycle	22.48	88.13	This study
Arthropod cuticles	Chemical extraction	1 M HCl	1–2 M NaOH	6–24 h	15–25	60–80	[188]
Scorpion cuticle (SM)	Autoclave-assisted	0.25 M HCl	1 M NaOH (121 °C)	15 min/ cycle	21.23	79.15	This study

4. Chitins and chitosans characterization

4.1. Assessment of deacetylation and functional groups

The FTIR spectra of the extracted chitins CHT (SS), CHT (SM), CHT (PL), CHT (HI), CHT (SO) and CHT (PP) and their corresponding chitosans CHS (SS), CHS (SM), CHS (PL), CHS (HI), CHS (SO) and CHS (PP) confirmed the successful recovery of chitin from the different biomasses and chitosan (**Figs. 32 and 33**).

All chitin samples exhibited a broad absorption band in the 3700–3000 cm^{-1} region, corresponding to overlapping O–H and N–H stretching vibrations associated with the hydrogen-bonding network within the chitin structure [37]. This band appeared broader and more intense for α-chitin samples (CH (SM), CH (PL), CH (HI) and CH (PP)), reflecting the stronger intermolecular hydrogen bonding characteristic of the antiparallel chain arrangement in α-chitin [189]. In contrast, the β-chitin samples (CH (SS) and CH (SO)) displayed comparatively narrower bands, consistent with the more open crystalline structure and weaker hydrogen-bonding interactions typically reported for β-chitin [190,191]. In the amide region, the characteristic Amide I band (1650–1620 cm^{-1}) associated with C=O stretching and the Amide II band (around 1550 cm^{-1}) corresponding to N–H bending were clearly visible in all chitin spectra [192]. These bands were generally sharper for α-chitin samples, indicating a higher degree of structural organization and stronger intermolecular interactions compared with β-chitin sources. Additional peaks corresponding to the polysaccharide backbone were also observed, including C–H stretching vibrations around 2920 and 2870 cm^{-1}, CH bending at 1380 cm^{-1} and glycosidic C–O–C vibrations between 1150 and 1030 cm^{-1}, confirming the preservation of the chitin molecular structure after extraction [193].

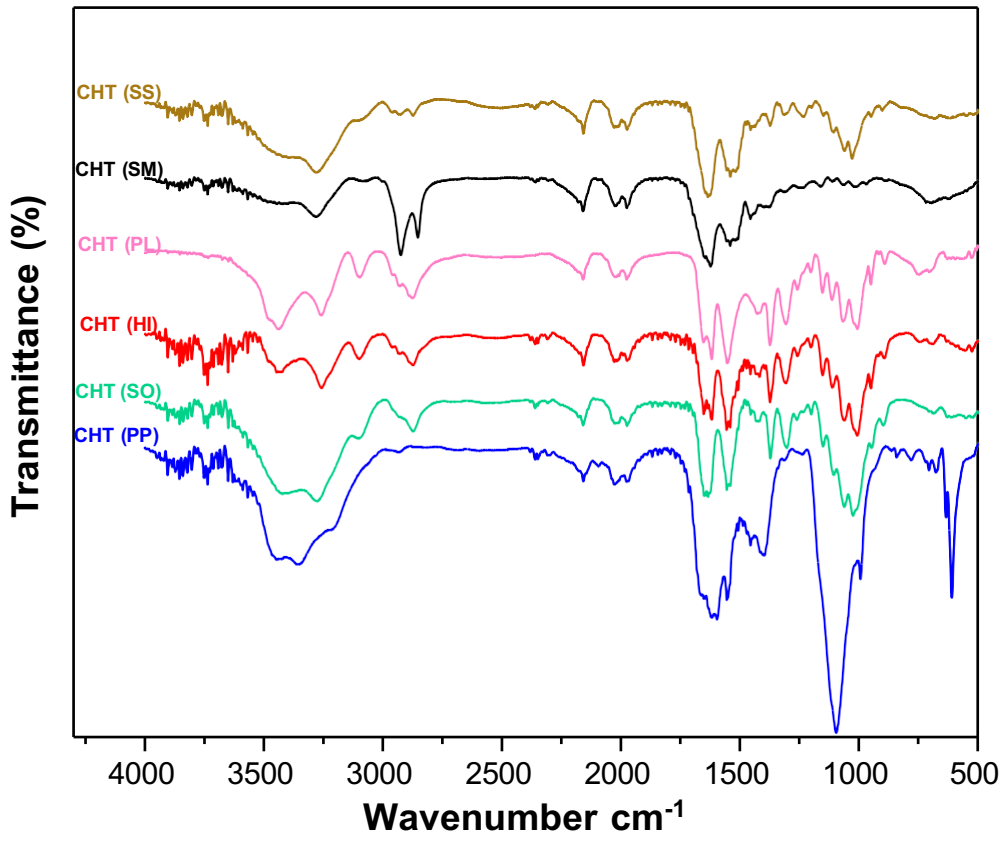

Figure 32. FTIR spectra of chitins (CHT)

Following alkaline treatment, the FTIR spectra of the resulting chitosans showed the expected spectral modifications associated with deacetylation of chitin. In particular, a decrease in the intensity of the Amide I and Amide II bands was observed, accompanied by the appearance of a band around 1590–1560 cm^{-1}, attributed to N–H bending vibrations of protonated amino groups characteristic of chitosan. Meanwhile, the persistence of glycosidic bands in the 1150–1000 cm^{-1} region indicates that the polysaccharide backbone remained intact during the deacetylation process. These spectral changes are widely reported as indicators of successful transformation of chitin into chitosan [194,195]. Although the overall spectral profiles were similar across all samples, minor differences in band sharpness and intensity were observed depending on the biological source. These variations may reflect differences in crystalline organization and hydrogen-bonding density inherited from the original cuticular structures, as previously observed in arthropod and marine-derived chitins

[196]. Such structural differences are expected to influence the degree of crystalline ordering within the polymer.

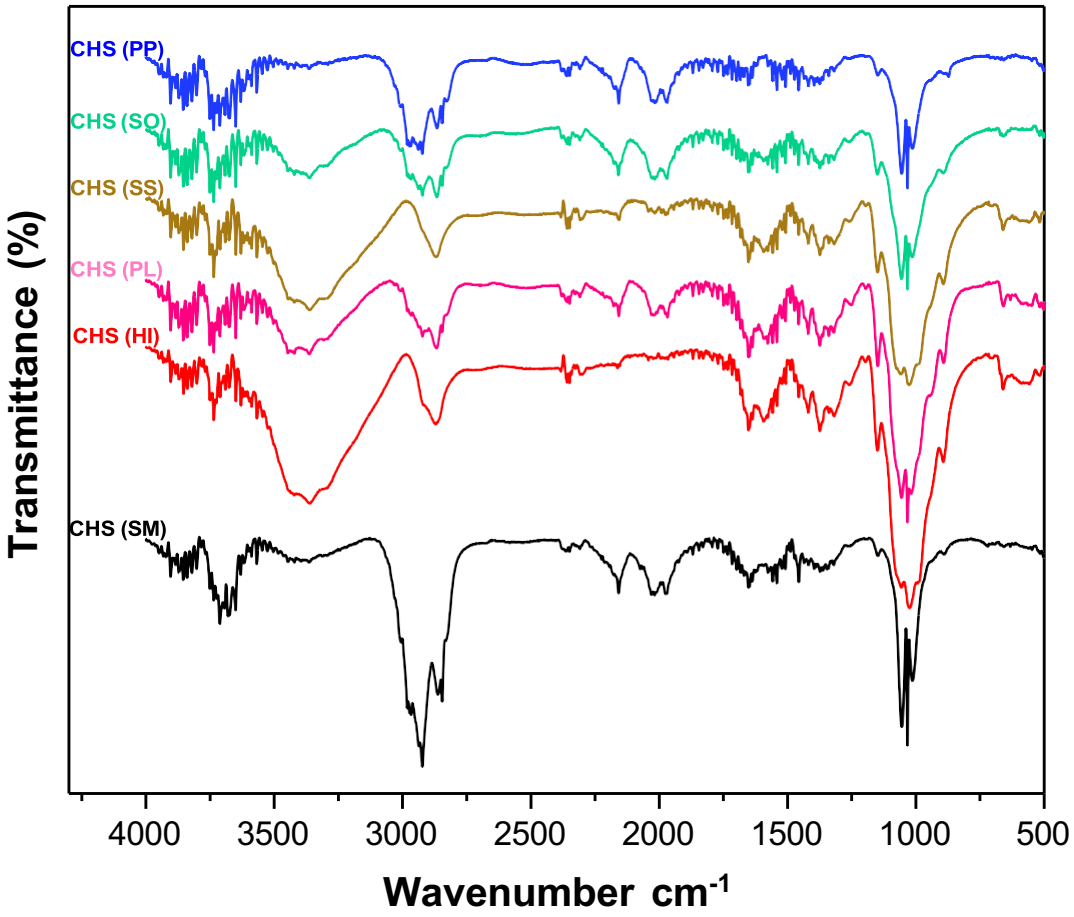

Figure 33. FTIR spectra of chitosans (CHS)

4.2. Crystalline structure and morphology of extracted chitins and chitosans

The XRD patterns of the chitin samples exhibited diffraction peaks characteristic of α- and β-chitin crystalline structures **(Figure 34)**. The detailed diffraction angles and crystallinity indices are summarized in **Table 15**. The α-chitin samples CHT (PL), CHT (SM), CHT (HI) and CHT (PP) showed the typical reflections associated with the orthorhombic crystalline structure of α-chitin. In particular, the main diffraction peaks were observed at approximately $2\theta \approx 9$–$10°$ and 19–20°, corresponding to the (020) and (110) crystallographic planes of α-chitin, which confirms the presence of the antiparallel chain arrangement characteristic of this polymorph [197]. In contrast, the

β-chitin samples CHT (SO) and CHT (SS) displayed broader reflections centered near 2θ ≈ 8–9° and 19–20°, which are commonly reported for the more open crystalline lattice of β-chitin found in cephalopods and certain marine organisms [198,199].

The calculated crystallinity indices (I_{Cr}) revealed noticeable differences among the investigated sources. The highest crystallinity was obtained for CHT (HI) (71.14%), followed by CHT (SM) (65.56%), indicating a highly ordered crystalline structure in these arthropod cuticles [78]. Intermediate crystallinity values were observed for CHT (SO) (57.33%) and CHT (SS) (56.37%), which correspond to β-chitin matrices generally characterized by a less densely packed crystalline arrangement. Lower crystallinity indices were obtained for CHT (PP) (51.63%) and CHT (PL) (51.48%), reflecting the heterogeneous composition of crustacean shells where chitin microfibrils are embedded within a mineralized matrix. Comparable crystallinity ranges have been reported for chitin extracted from crustaceans and insects using chemical extraction methods [85].

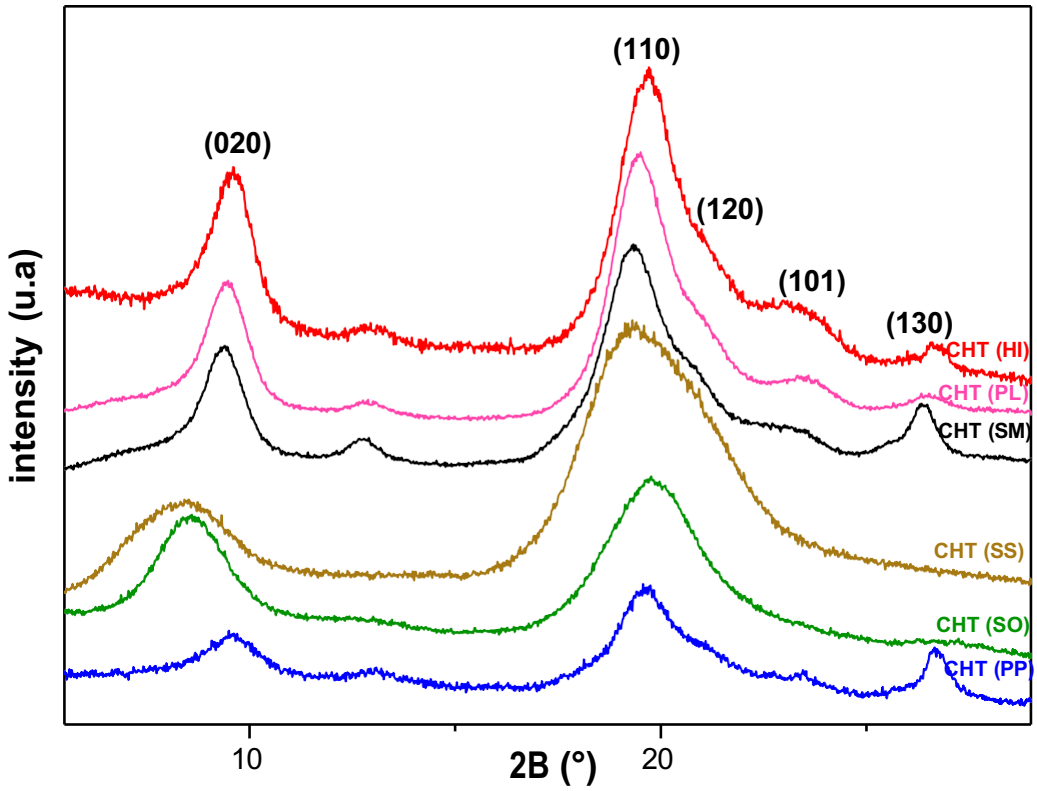

Figure 34. XRD spectra of chitin (CHT)

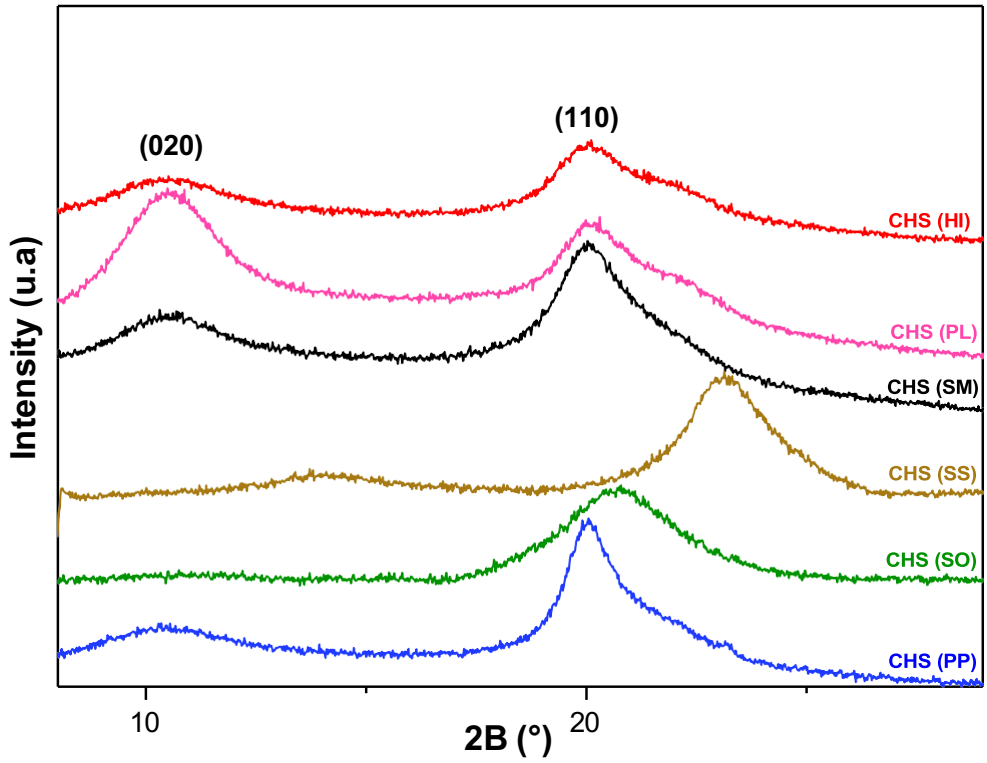

Figure 35. XRD spectra of chitosan (CHS)

After alkaline deacetylation, the XRD patterns of the resulting chitosans showed a reduction in crystallinity compared with the corresponding chitins **(Figure 35)**. The crystallinity indices ranged from 39.10% to 51.63% (Table 4). The highest crystallinity among chitosans was observed for CHS (HI) (51.63%), whereas CHS (SS) exhibited the lowest value (39.10%). This decrease in crystallinity is attributed to the disruption of the hydrogen-bonding network of chitin during alkaline deacetylation, which leads to partial loss of crystalline ordering and formation of a more amorphous chitosan structure [200].

Table 15. Diffraction peak positions (2θ) and crystallinity indices (ICr) of chitin and chitosan extracted from the different biological sources

Source	Chitin		Chitosan	
	2θ (°)	**I_{Cr} (%)**	**2θ (°)**	**I_{Cr} (%)**
PL	9.46 12.88 19.5 20.8 23.54 26.5	51.48	10.54 20.08	47.51
SO	8.6 19.76	57.33	10.88 20.84	47.79
PP	9.6 19.64	51.63	10.4 20.02	48.05
SM	9.4 12.78 19.32	65.56	10.62	46.9

	20.54 23.18 26.34		20	
HI	9.6 12.94 19.7 22.98 26.7	71.14	10.32 20.02	51.63
SS	8.42 19.3	56.37	14.08 23.12	39.10

The SEM micrographs of the chitin samples revealed distinct morphological patterns that reflect their biological origin and intrinsic structural organization **(Figure 36)**. The samples CHT (PL) and CHT (PP) exhibited relatively compact lamellar surfaces, typical of crustacean-derived chitin where microfibrils are embedded within a mineralized matrix [100,201]. In contrast, CHT (SM) and CHT (HI) displayed more porous and entangled fibrillar networks, reflecting the hierarchical organization of chitin–protein complexes commonly found in arthropod cuticles [33].

The β-chitin sample CHT (SO) showed layered sheet-like structures with folded morphologies, consistent with the more loosely packed crystalline organization characteristic of cephalopod-derived chitin [141]. Meanwhile, CHT (SS) exhibited heterogeneous and rough surface, typical of sardine scales chitin [202]. These morphological features are consistent with the crystallinity results obtained by XRD, where samples with higher crystallinity such as CHT (HI) and CHT (SM) exhibited more clearly defined fibrillar organizations.

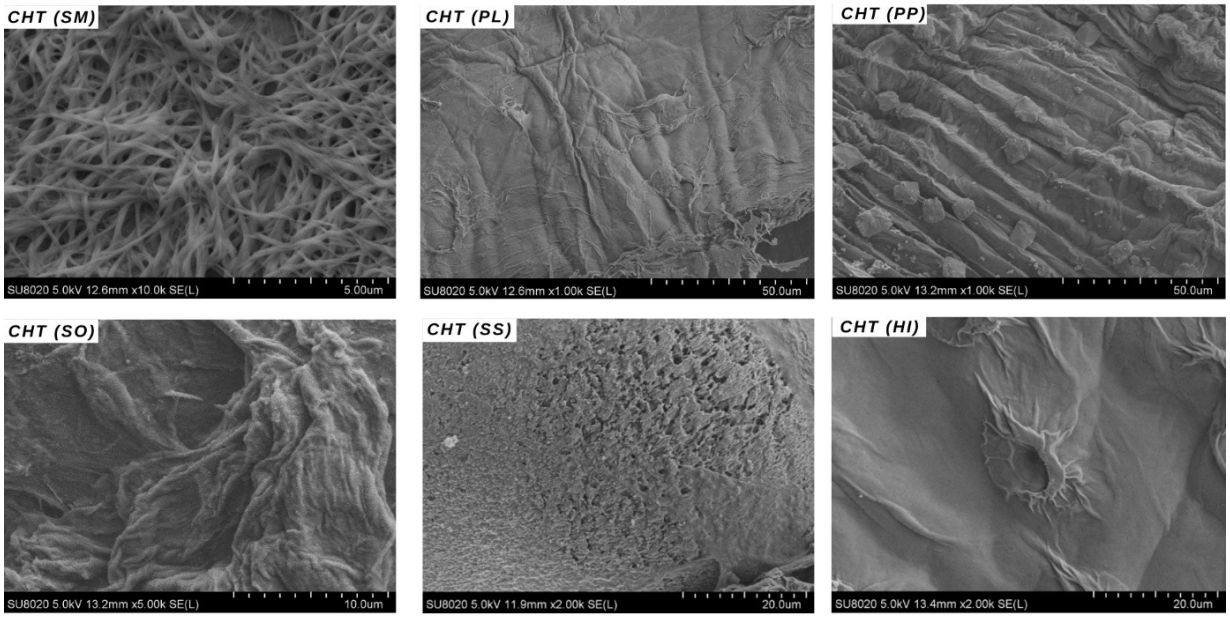

Figure 36. SEM images of chitins (CHT)

After deacetylation, the SEM micrographs of the corresponding chitosans revealed structural rearrangements compared with the original chitins **(Figure 37)**. In most cases, the fibrillar networks collapsed into denser lamellar or sheet like morphologies, reflecting the structural reorganization associated with the reduction in crystallinity observed by XRD. Similar morphological transitions during chitin to chitosan conversion have been reported in previous studies [79,130].

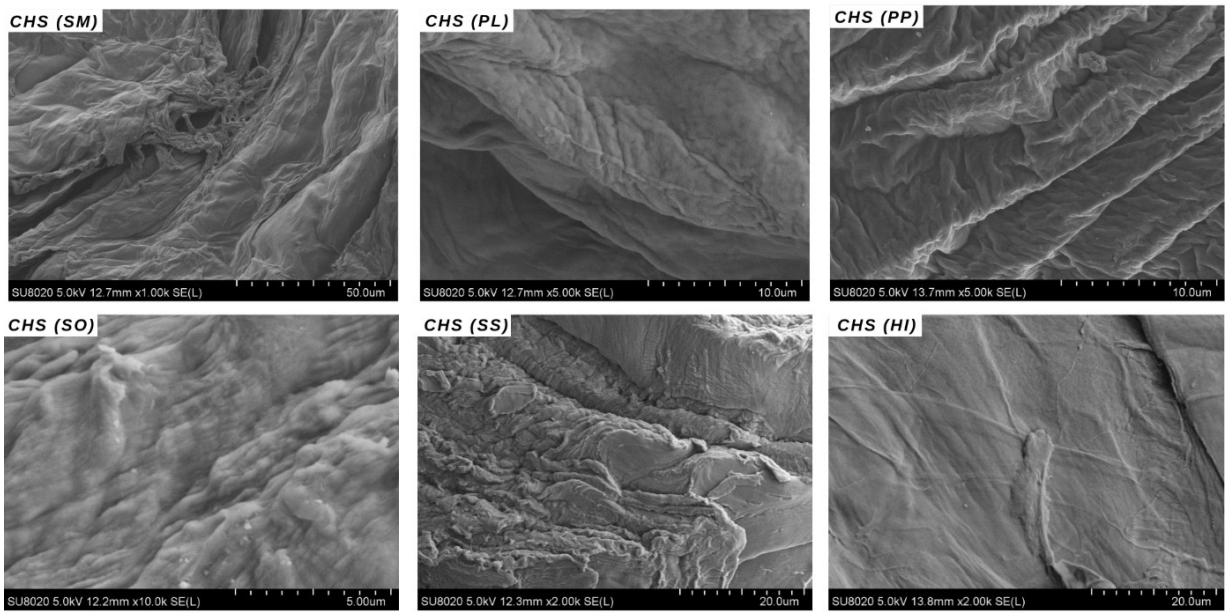

Figure 37. SEM images of chitosans (CHS)

4.3. Thermal properties of chitins and chitosans

The TGA and DTG profiles of the chitin samples exhibited the typical two-stage thermal degradation behavior characteristic of chitin **(Figure 38)**. The initial mass loss below 150 °C corresponds to moisture release [165], with slightly higher losses observed for the β-chitin samples (CHT (SS) and CHT (SO)), consistent with their more hydrated and loosely packed crystalline structure. The major degradation step occurred between 280 and 420 °C, associated with depolymerization and cleavage of the glycosidic and acetamide linkages [167,197]. The DTG curves showed distinct maximum decomposition temperatures (DTG_{max}), which varied according to the structural organization of each sample. α-chitins displayed higher thermal stability, with CHT (HI) and CHT (PL) showing DTG_{max} values at 404 °C and 397 °C, respectively, indicating stronger intermolecular interactions and higher crystallinity [153,180]. CHT (SM) and CHT (PP) exhibited intermediate degradation peaks around 386–395 °C, reflecting moderately ordered structures. In contrast, the β-chitin samples presented lower DTG_{max} values, particularly CHT (SS) (352 °C) and CHT (SO) (341 °C), confirming the reduced thermal resistance associated with the weaker hydrogen-bond network of β-chitin. Beyond 450 °C, all samples showed gradual carbonization, with

slight differences in residual char depending on biological origin. Overall, the thermal behavior correlates well with the allomorphic form and structural compactness revealed by FTIR, XRD and SEM analyses.

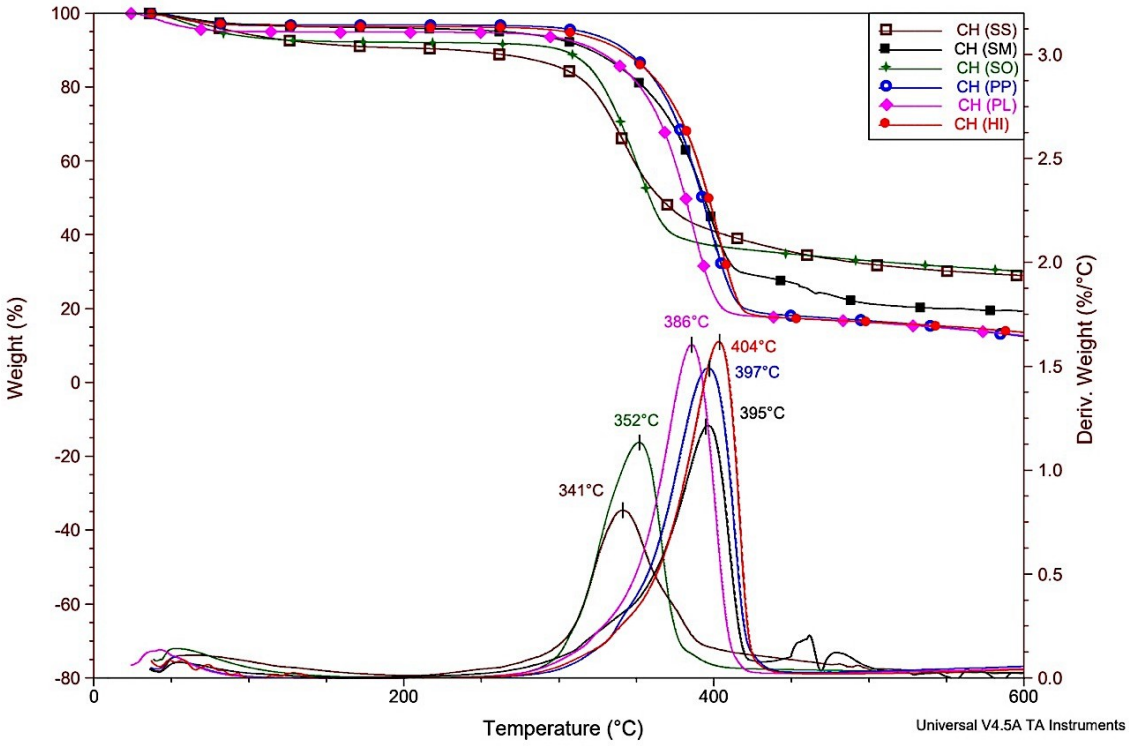

Figure 38. Thermograms and their derivatives of chitins (CHT)

The TGA and DTG curves of the chitosans (CHS) exhibited the characteristic thermal profile associated with deacetylated polysaccharides **(Figure 39)**. All samples showed an initial minor mass loss below 150 °C due to adsorbed moisture [203]. The principal thermal degradation occurred between 250 and 380 °C, corresponding to depolymerization and breakdown of amino-rich glucosamine chains [26]. The DTG peaks revealed clear differences in thermal resistance among samples, with DTG_{max} values ranging from 310 to 345 °C. CHS(SO) and CHS(SM) recorded the lowest DTG_{max} values (310–317 °C), indicating a more amorphous organization and reduced structural cohesion following deacetylation. CHS(PL), CHS(HI) and CHS(PP), in contrast, exhibited higher DTG_{max} values (between 335 and 345 °C), reflecting improved chain packing and a more ordered molecular arrangement. Peak broadening

across all samples further supports the decrease in structural regularity relative to their chitin precursors. At temperatures above 450 °C, all materials underwent gradual carbonization, with slight differences in char residue depending on source-related compositional factors. Overall, the DTG_{max} values confirm a general decrease in thermal stability after deacetylation, while also highlighting persistent microstructural differences among chitosans from different biological origins.

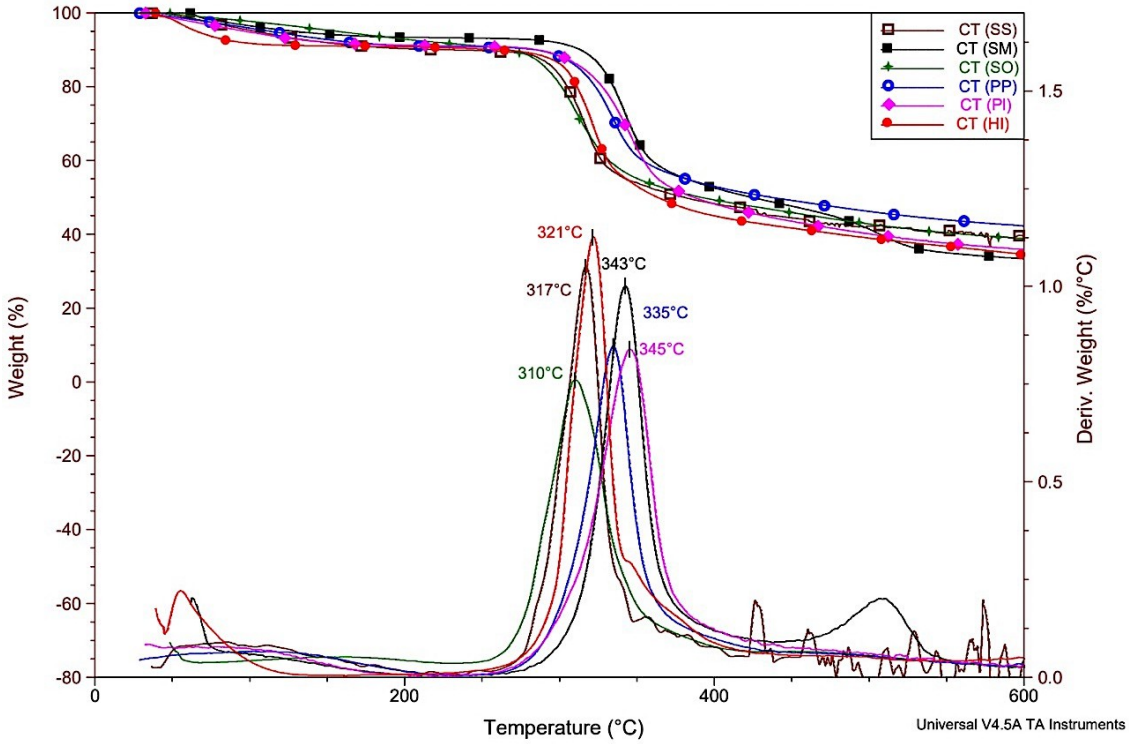

Figure 39. Thermograms and their derivatives of chitosans (CHS)

4.4. Molecular structure analysis and degree of acetylation determination

The chemical structure and degree of acetylation (DA) of the produced chitosans CHS (PL), (PP), (SO), (SM), (HI) and (SS) were analyzed using ^{1}H-NMR and the spectra are presented in **Figure 40**. All spectra exhibited the characteristic proton signals of chitosan, confirming the successful deacetylation of the extracted chitins. The resonance signal observed around 2.3 ppm corresponds to the methyl protons of the residual N-acetyl groups (–$COCH_3$) and is commonly used as the reference signal for determining the degree of acetylation (position a) [204]. The proton signals associated

with the glucosamine ring (H2–H6) appeared as multiplets in the region between around 3.0 and 4.0 ppm (proton b,c,d,e,f,g), while the anomeric proton (H1) was detected around 5.4 ppm (position a)[205]. These chemical shift assignments are consistent with those typically reported for chitosan derived from marine and insect sources [80,206]. The degree of acetylation (DA) was determined from the ratio between the integrated area of the methyl proton signal of the acetyl group (i) and the proton signals of the glucosamine backbone. The calculated DA values ranged from 2.6% to 10.7%, indicating a high degree of deacetylation for all produced samples deacetylated only in 1hour.

Among the investigated materials, CHS (SS) exhibited the lowest DA value, suggesting more extensive deacetylation compared with the other sources. In contrast, slightly higher DA values were observed for CHS (HI) and CHS (PL). These variations may be related to differences in the crystalline organization and structural compactness of the chitin matrices, which can influence the accessibility of acetyl groups during alkaline treatment. Highly ordered crystalline regions may hinder reagent penetration and therefore reduce deacetylation efficiency [206]. The obtained DA values fall within the typical range reported for chemically produced chitosans. Previous studies have reported DA values generally between 5% and 20%, depending on the biological source of chitin and the deacetylation conditions applied [71,194]. The relatively low DA values obtained in the present study therefore demonstrate the high efficiency of the autoclave-assisted deacetylation process, which allowed the production of highly deacetylated chitosan from diverse biological sources.

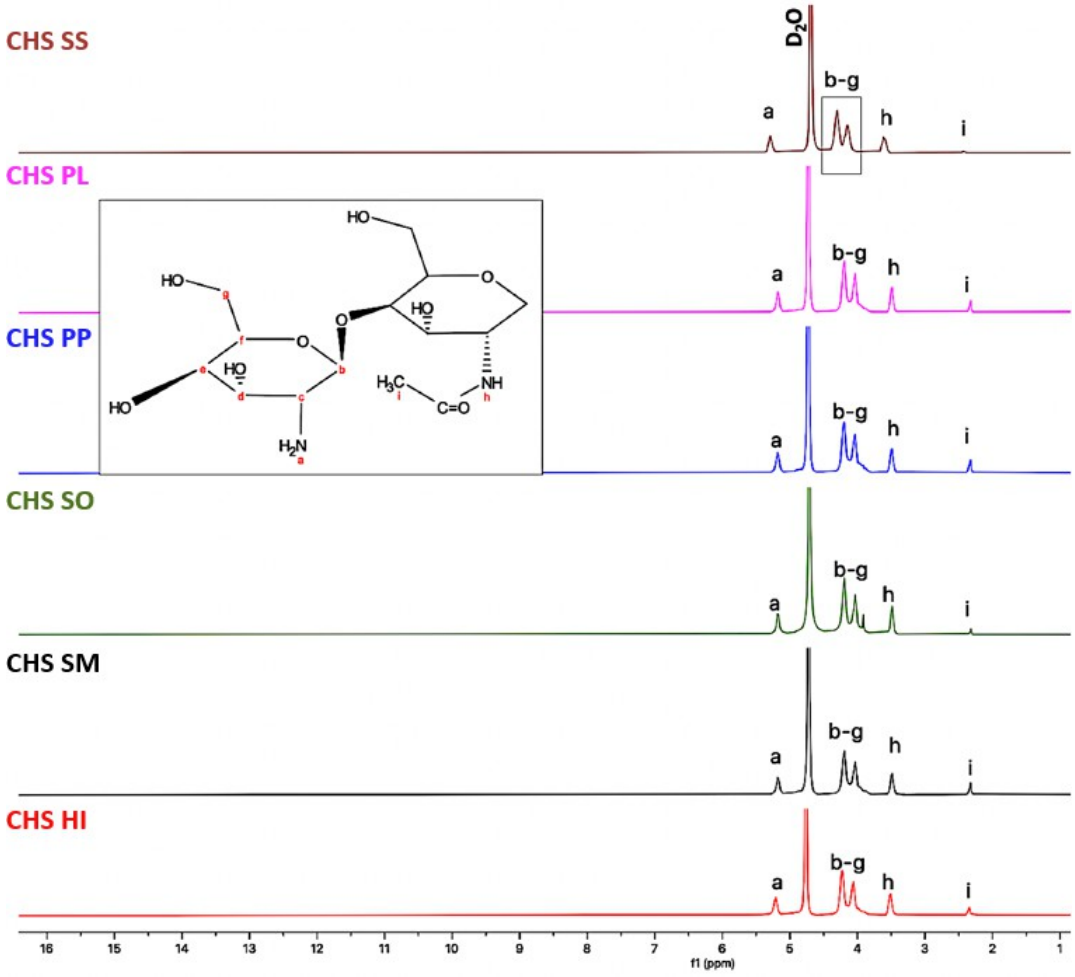

Figure 40. 1H-NMR spectra of chitosans

4.5. Viscosimetric molecular weight determination

The viscometric molecular weight (Mv) of the produced chitosans was determined **(Figure 41)**. The obtained molecular weights ranged between 133 and 220 kDa, indicating that the produced chitosans belong to the medium molecular weight range. The preservation of relatively long polymer chains confirms as previously proved that the autoclave-assisted process did not induce significant depolymerization of the chitin backbone during extraction and deacetylation [180]. In conventional chemical extraction methods, prolonged alkaline treatments at high temperatures may lead to cleavage of glycosidic bonds and reduction of molecular weight. In contrast, the short

reaction time associated with autoclave-assisted treatments can limit chain scission while maintaining efficient deproteinization and deacetylation [78,98,207].

Variations in molecular weight among the samples can also be associated with differences in the biological origin and composition of the starting materials. For instance, chitosan derived from *Hermetia illucens* exhibited medium molecular weight, which may be related to the highly organized chitin–protein matrix typical of insect cuticles that can protect polymer chains from excessive degradation during alkaline treatment. Similar observations have been reported for insect-derived chitin, where the hierarchical organization of the cuticle contributes to maintaining longer polymer chains after extraction [19,208]. Conversely, slightly lower molecular weights were obtained for samples requiring additional purification steps, such as delipidation or multiple deproteinization cycles. Lipid-rich biomasses, including insect and fish-derived materials, often require solvent extraction prior to alkaline treatment, and repeated chemical steps may promote partial depolymerization of the polysaccharide chains [145]. Likewise, the number of alkaline treatments applied during deproteinization may influence the final molecular weight, as repeated exposure to strong bases can induce hydrolytic cleavage of the polymer backbone [209,210]. These observations highlight the combined influence of process parameters and biomass composition on the final molecular weight of the produced chitosans. The relatively narrow molecular weight range obtained in this study indicates that the standardized autoclave-assisted process provides a controlled extraction environment, enabling efficient purification while preserving the integrity of the chitin polymer chains.

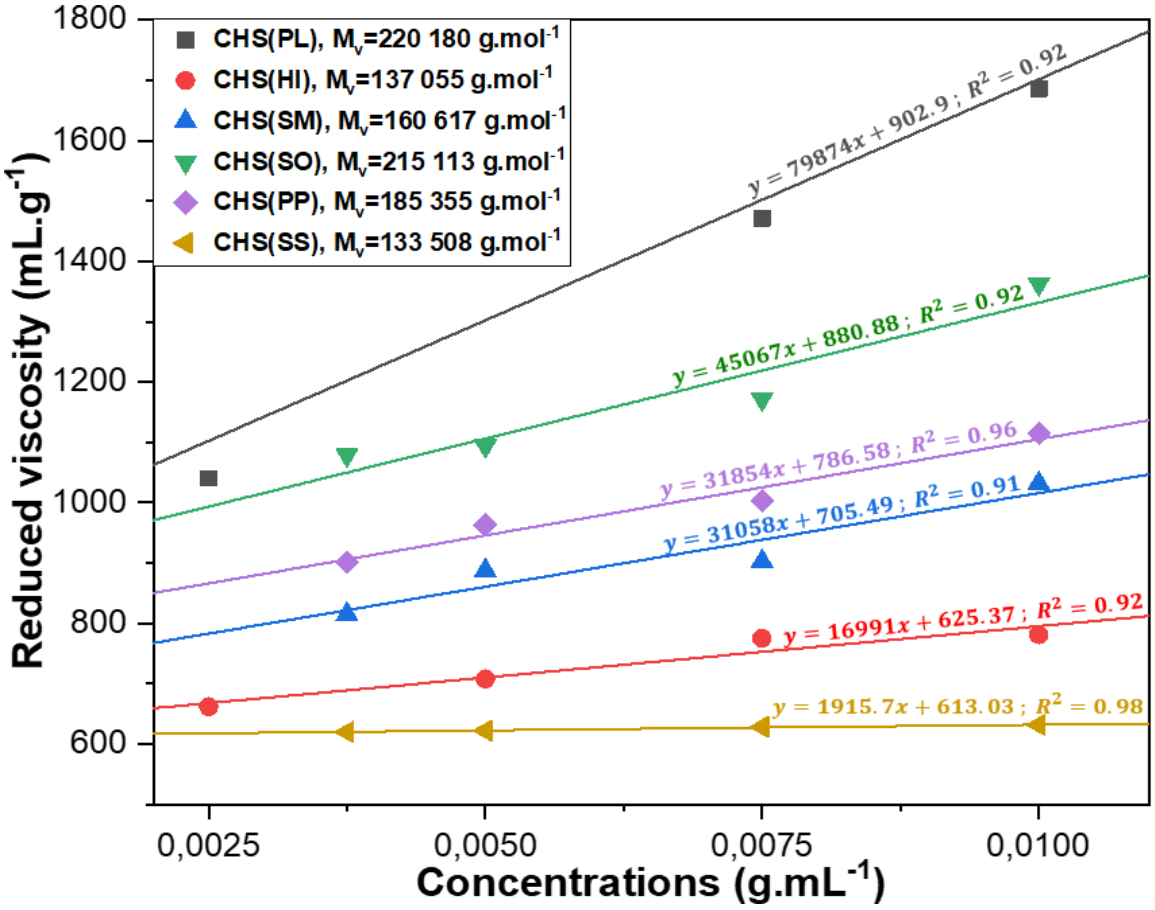

Figure 41. Examples of the viscosity curves of the chitosan samples (CHS)

5. Conclusion

In this study, a standardized autoclave-assisted process was successfully applied for the extraction of chitin and chitosan from six Moroccan biological resources, including marine and terrestrial organisms (*Parapenaeus longirostris, Pollicipes pollicipes, Sepia officinalis, Scorpio mogadorensis, Hermetia illucens and Sardina pilchardus*). The approach allowed efficient removal of mineral and protein fractions using relatively mild chemical conditions and significantly reduced processing time compared with conventional extraction protocols. Microscopic observations of the native cuticles revealed diverse chitin microfibril architectures, including parallel, helicoidal, parabolic and semi-ordered lamellar arrangements depending on the species. These structural differences were reflected in the physicochemical characteristics of the extracted chitins. FTIR analysis confirmed the successful extraction of both α-chitin

and β-chitin, while XRD revealed crystallinity indices ranging from approximately 51% to 71%, depending on the biological source. SEM observations showed distinct fibrillar and lamellar morphologies consistent with the crystalline organization of the materials. Thermogravimetric analysis demonstrated typical two-step thermal degradation profiles, with degradation temperatures influenced by the crystalline organization and biological origin of the chitin. Subsequent alkaline deacetylation produced chitosans with low degrees of acetylation (2.6–10.7%). Viscometric measurements indicated medium molecular weight chitosans ranging from 133 to 220 kDa, suggesting that the autoclave-assisted process effectively preserved polymer chain length while enabling efficient deacetylation. Overall, the results highlight the strong influence of both extraction conditions and source specific structural organization on the final properties of chitin and chitosan. The autoclave-assisted method provides an efficient and scalable strategy for producing structurally preserved chitin and highly deacetylated chitosan from diverse bioresources. This approach offers promising perspectives for the sustainable valorization of marine and insect biomass within emerging biorefinery and biomaterials applications.

Chapter 3: Hierarchical Chitosan Scaffolds From Bio-sourced Feedstocks For High-performance Heavy Metal Adsorption

1. Introduction

In the previous chapter, chitin was extracted from various biological sources, including marine organisms, insects and arachnids. Particular attention was given to the influence of the biological origin on the physicochemical properties of the extracted chitin and the resulting chitosan. This approach provided a diversified set of raw materials suitable for subsequent material development. In continuation of this work, the present chapter is devoted to the elaboration and evaluation of chitosan-based materials for water treatment applications. More specifically, a three-dimensional (3D) scaffold structure was developed in this study. This approach constitutes an original contribution of the present thesis, aiming to improve the adsorption performance of chitosan through structural organization.

Previous studies have reported chitosan-based adsorbents in various physical forms, including beads [58], membranes [211], films, fibers, hydrogels and nanochitosan [212], each offering distinct advantages in terms of surface area, diffusion pathways and mechanical stability. Nevertheless, the adsorption efficiency of chitosan-based materials remains strongly dependent on their structural organization, porosity and biological origin, highlighting the need for advanced material architectures and diversified chitin sources to enhance performance and sustainability. Three-dimensional (3D) porous scaffolds represent an advanced class of chitosan-based materials characterized by interconnected pore networks, high porosity and large accessible surface areas, which collectively favor mass transfer and adsorption kinetics. To date, chitosan scaffolds have been predominantly explored in biomedical applications [213–216], such as tissue engineering [74], wound healing and drug delivery [217], where their porous morphology supports cell adhesion, proliferation and nutrient transport. In contrast, their potential for environmental applications, particularly in the removal of dissolved salts and heavy metal ions from water, remains insufficiently investigated, despite their structural suitability for such processes.

In the present work, 3D chitosan scaffolds derived from multiple biological sources, including shrimp shells (commercial chitosan), *Hermetia illucens* (black soldier fly) pupal and prepupal cases, scorpion (*Buthus atlantis*) exoskeletons and *Pollicipes pollicipes*, were prepared and evaluated as bioadsorbents for water purification. The scaffolds were assessed for their capacity to remove a representative set of inorganic contaminants, namely NaCl, $MgCl_2$, KCl, $CaCl_2$, $CdCl_2$, $PbCl_2$, $CrCl_3$ and $CuCl_2$. Chloride salts were selected due to their chemical stability, high solubility and widespread occurrence in natural and contaminated aquatic environments. By combining structural engineering with the valorization of diverse and underexplored chitin-rich resources, this study aims to demonstrate the potential of chitosan-based 3D scaffolds as efficient, sustainable and multifunctional materials for advanced removal of salts and heavy metals from aqueous systems.

2. Autoclave-assisted extraction of chitosan from *Buthus atlantis*: preliminary EDX analysis and process optimization

Prior to initiating the extraction process, energy-dispersive X-ray (EDX) analysis was conducted to determine the mineral composition of the *Buthus atlantis* exoskeleton **(Fig. 42)**. The total mineral content was quantified at 3.22%, comprising Cl (0.21%), Si (0.23%), Al (0.33%), Ca (0.35%), Mg (0.38%), Na (0.81%), and K (0.91%). This mineral content is lower than that previously reported by *Elouali et al. (2026)* for *Tityus tenuimanus*, which exhibited a total mineral fraction of approximately 3.22%, highlighting species-dependent variations in exoskeletal composition. Upon this preliminary assessment, a single demineralization bath was performed for 1 h, followed by two consecutive autoclave-assisted deproteinization treatments (15 min per bath) and a final deacetylation step of 1 h. Remarkably, a total processing time of only 2 h 30 min was sufficient to obtain a highly purified chitosan, characterized by its white coloration and complete solubility in 1% (v/v) acetic acid, indicating effective removal of minerals, proteins and endogenous pigments throughout the extraction process.

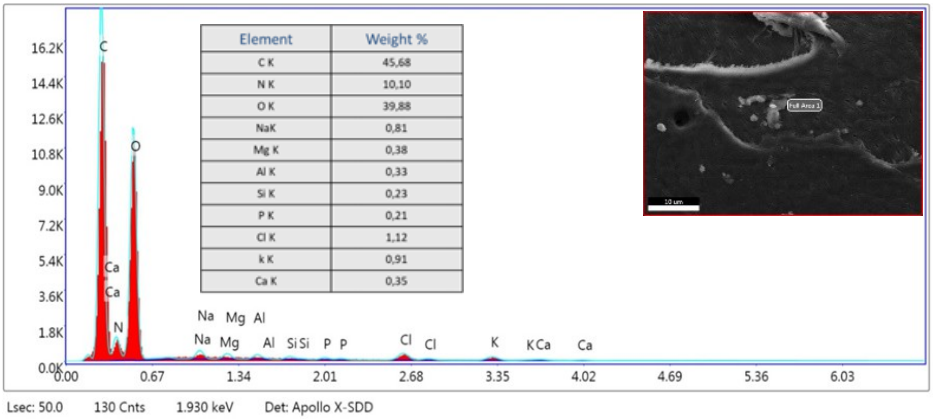

Figure 42. EDX analysis of *Buthus atlantis* exoskeleton

The adoption of the autoclave-assisted extraction process in this study was motivated by our previous investigation [180]. We demonstrated that this approach constitutes a sustainable and environmentally benign alternative to conventional chitin and chitosan extraction methods. Specifically, the autoclave-assisted protocol enabled a substantial reduction in processing time, water consumption, and overall energy demand, while significantly limiting the quantities of chemical reagents required. These improvements stem primarily from the enhanced mass and heat transfer under pressurized conditions, which accelerate deproteinization and deacetylation reactions [218], thereby increasing process efficiency. Consequently, this method aligns with the principles of green chemistry and sustainable process engineering, offering a scalable and resource-efficient strategy for the valorization of another arthropod-derived biopolymers.

3. Chitin and chitosan characterization

3.1. Functional group analysis

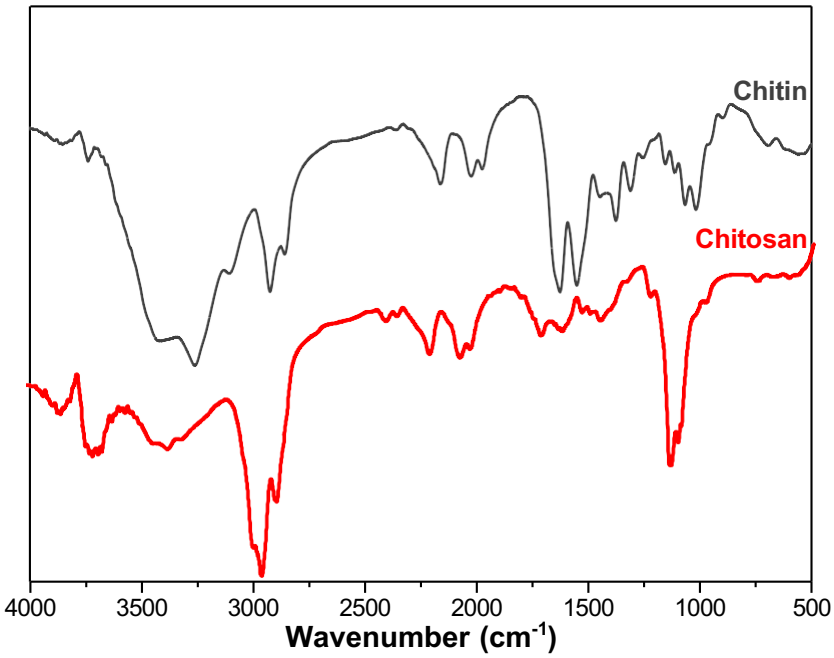

Figure 43. FTIR spectra of chitin and chitosan

The FTIR spectra of chitin and chitosan exhibit the characteristic vibrational features of amino-polysaccharides, while clearly reflecting the structural modifications associated with deacetylation **(Figure 43)**. In the region between 3600 and 3000 cm^{-1}, both materials show a broad absorption assigned to overlapped O–H and N–H stretching vibrations. This band becomes broader and more intense in chitosan, consistent with the increased hydrogen-bonding capacity and reduced crystallinity generally observed for deacetylated chitin derivatives, whereas the corresponding band in chitin remains comparatively sharper due to its more ordered structure.

Significant differences are observed in the amide region. Chitin presents the typical amide-I band at ~1650–1660 cm^{-1} (C=O stretching) and amide-II band at ~1550 cm^{-1} (N–H bending coupled with C–N stretching), confirming the presence of N-acetyl groups [125]. In contrast, these two bands show a marked reduction in intensity in the chitosan spectrum, reflecting the removal of acetyl moieties during alkaline deacetylation [219]. Concurrently, chitosan exhibits a more intense band at 1590–1600 cm^{-1}, attributed to N–H bending of protonated amino groups ($–NH_3^+$) [92], which is widely recognized as a key indicator of chitin to chitosan conversion.

Both spectra display the characteristic polysaccharide fingerprint region between 1200 and 900 cm^{-1}, including C–O–C and C–O stretching vibrations and the band at ~895 cm^{-1} associated with β-glycosidic linkages [85]. However, these bands are broader in chitosan, which is consistent with its lower crystallinity. Altogether, the attenuation of amide I–II absorption bands, the emergence of the amino-related signal around 1590 cm^{-1} and the increased band broadness throughout the spectrum collectively confirm the chemical transformation from the highly acetylated to chitosan.

3.2. Molecular weight determination

The reduced viscosity of chitosan solutions exhibited a linear increase with rising polymer concentration, as illustrated in Figure 44. The extrapolation of the fitted line according to the Huggins model yielded an intrinsic viscosity [η] of approximately 587 $mL \cdot g^{-1}$. This value reflects the hydrodynamic volume and chain expansion of the extracted biopolymer in the solvent system used. Using the Mark–Houwink equation, the calculated viscosity-average molecular weight (M_v) of the chitosan obtained through the autoclave-assisted extraction from *Buthus atlantis* exoskeleton was estimated to be 126.2 kDa. This molecular weight sets the produced chitosan within the medium–high molecular weight category. This is consistent with the values reported for chitosan derived from arthropod exoskeletons using mild or moderate deproteinization and demineralization conditions [98,220]. The strong linear correlation ($R^2 = 0.9$) further confirms the reliability of the viscosity measurements and suggests good solubility and homogeneous polymer chain distribution in the tested concentration range.

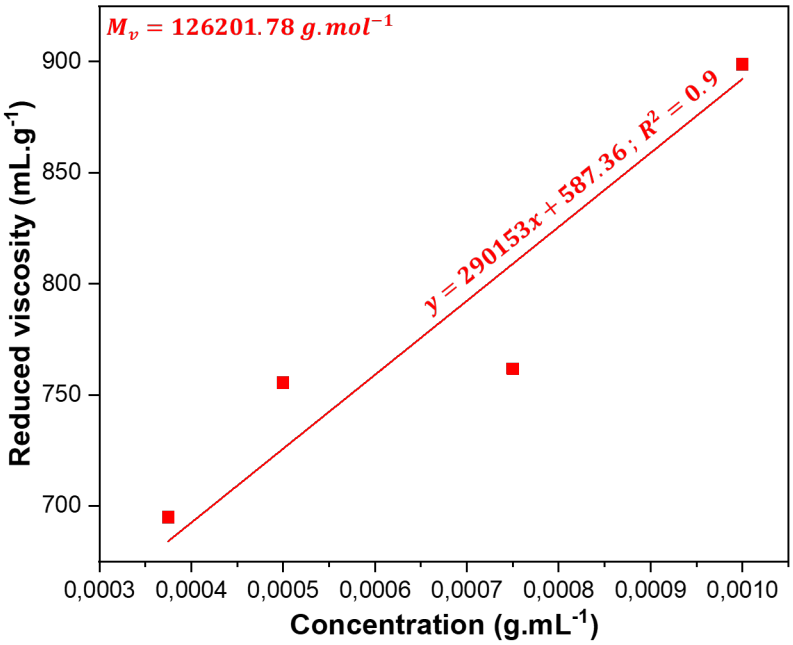

Figure 44. Examples of the viscosity curve of the chitosan

3.3. Crystalline properties

The crystalline structure and phase evolution of chitin and chitosan were investigated by X-ray diffraction (XRD), and the corresponding diffractograms are presented in **Figure 45**. The XRD pattern of chitin exhibits several well-defined diffraction peaks located at 2θ = 9.3°, 12.6°, 19.2°, 20.7°, 23.7° and 26.3°, which can be indexed to the (020), (021), (110), (120), (101) and (130) crystallographic planes, respectively [146,209]. The characteristic reflections observed at 2θ ≈ 9.3° and 19.2° are widely recognized as the fingerprint peaks of chitin, confirming the successful extraction of this biopolymer. Moreover, the presence of additional diffraction peaks at 12.6°, 20.7°, 23.7° and 26.3° is consistent with the typical diffraction profile of α-chitin [147], indicating that the native crystalline allomorph was preserved during the extraction process [33].

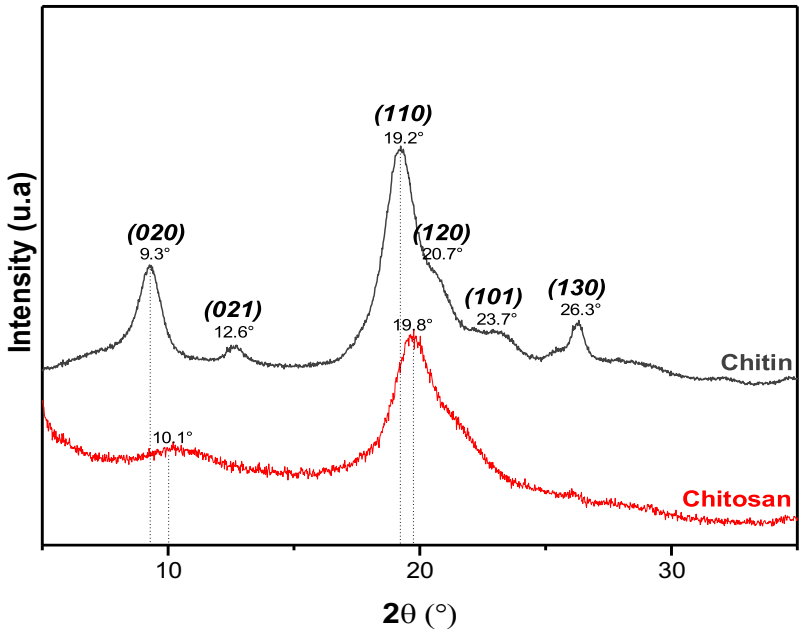

Figure 45. XRD spectra of chitin and chitosan

After deacetylation, the XRD pattern of chitosan shows a significant structural transformation, characterized by the appearance of two broad diffraction peaks centered at 2θ = 10.1° and 19.8°, corresponding to the (020) and (110) planes, respectively. The disappearance of the characteristic α-chitin reflections and the retention of only these two peaks confirm the effective deacetylation and the conversion of chitin into chitosan. The absence of any additional diffraction peaks further indicates the high purity of the obtained chitosan, with no detectable crystalline impurities or residual inorganic phases [180,221].

Furthermore, the broad diffraction band at approximately 2θ ≈ 10.1° is attributed to the amorphous domains of chitosan, while the peak at 2θ ≈ 19.8° corresponds to its crystalline regions.

3.4. Morphological characterization

SEM micrographs revealed clear morphological differences between chitin and its deacetylated derivative **(Figure 46)**, i.e., chitosan. Native chitin exhibited a compact and highly ordered surface composed of polygonal microdomains arranged in a continuous, tightly packed network [28]. These polygonal units displayed smooth

interiors and sharply defined boundaries, reflecting the dense microfibrillar organization and high crystallinity characteristic of α-chitin, where extensive intra- and intermolecular hydrogen bonding maintains the integrity of the hierarchical structure [134]. In contrast, chitosan showed a markedly altered morphology following deacetylation, with the disappearance of the polygonal arrangement and the emergence of an irregular, layered and less cohesive surface. The chitosan samples displayed elongated fibrillar structures, discontinuous domains and localized grooves and cracks, indicating structural loosening and partial disruption of the original chitin microfibrils.

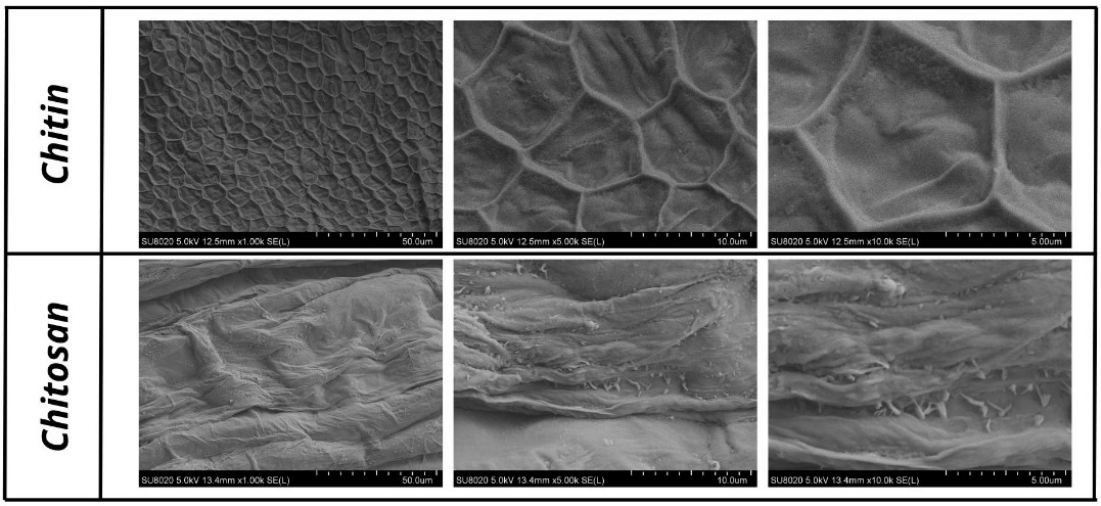

Figure 46. SEM images of chitin and chitosan

This morphological transition is consistent with the reduction in crystallinity and increased amorphous character typically reported after deacetylation, as the removal of acetyl groups weakens intermolecular interactions and promotes fibrillation. Overall, the observed evolution from a dense and organized chitin matrix to a more heterogeneous and fibrillated chitosan surface supports the known structural effect of alkaline deacetylation and aligns with the previous reports describing the morphological degradation and increased surface roughness associated with chitosan formation [141].

3.5. Thermal properties of chtiin and chitosan

The thermogravimetric analysis (TGA) of chitin shows a typical two stage degradation profile **(Figure 47)**. A slight initial mass loss of approximately 3% between room temperature and 100 °C is observed, which corresponds to the evaporation of physically adsorbed and bound water within the polymer structure [222]. Following this minor dehydration step, the material remains thermally stable up to around 300 °C, after which a major decomposition event occurs. The primary degradation stage begins sharply and reaches its maximum rate at 395 °C, as indicated by the peak in the derivative thermogravimetric (DTG) curve. This DTG_{max} reflects the main pyrolytic decomposition associated with the breakdown of the chitin polymer backbone, including cleavage of glycosidic linkages and the deacetylation process typically reported for chitin [189].

Beyond this major step, the mass decreases progressively until ~800°C, at which point the total weight loss reaches approximately 88%. The remaining residue (≈12%) is consistent with the formation of a carbonaceous char, characteristic of nitrogen containing polysaccharides such as chitin. Overall, the thermogram reflects the known high thermal stability of chitin and its characteristic decomposition behavior, with a dominant degradation stage centered near 395°C.

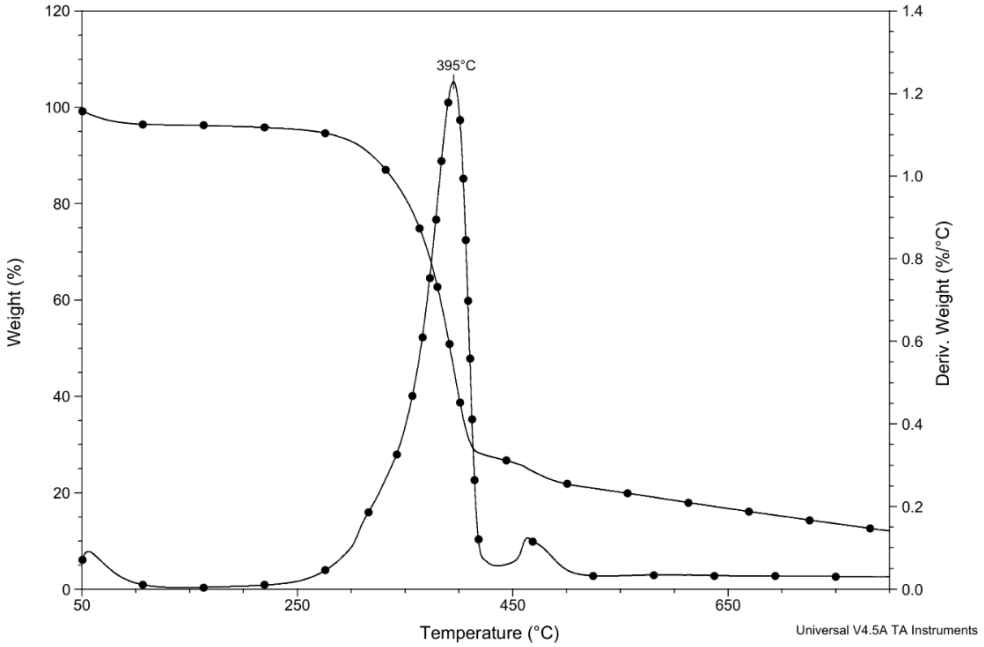

Figure 47. Thermogram (TG) and its derivative (DTG) of chitin from *Buthus atlantis*

The thermogravimetric analysis of chitosan shows a two-step thermal degradation profile characteristic of partially deacetylated chitin derivatives **(Figure 48)**. An initial mass loss of approximately 4% occurring between room temperature and 100 °C corresponds to the evaporation of residual moisture and weakly bound water molecules, which are typically retained due to the hydrophilic nature of chitosan [35]. Beyond this dehydration region, the material remains relatively stable until roughly 250–280 °C, after which a pronounced decomposition event takes place. The main degradation stage reaches its maximum rate at 343 °C, as evidenced by the peak in the DTG curve. This DTG_{max} is lower than that of chitin, reflecting the reduced crystallinity and weaker hydrogen-bonding network of chitosan resulting from deacetylation [180]. After the principal pyrolytic event, the mass continues to decrease gradually up to ~800 °C, leading to a total mass loss of approximately 69%. The remaining 31% residue at 800 °C can be attributed to the formation of a carbonaceous char typical of nitrogen-rich biopolymers such as chitosan [26,188]. Overall, the TGA and DTG profiles illustrate the expected reduction in thermal stability upon deacetylation of

chitin to chitosan, manifested by the lower DTG_{max} and lower overall mass loss compared to the chitin.

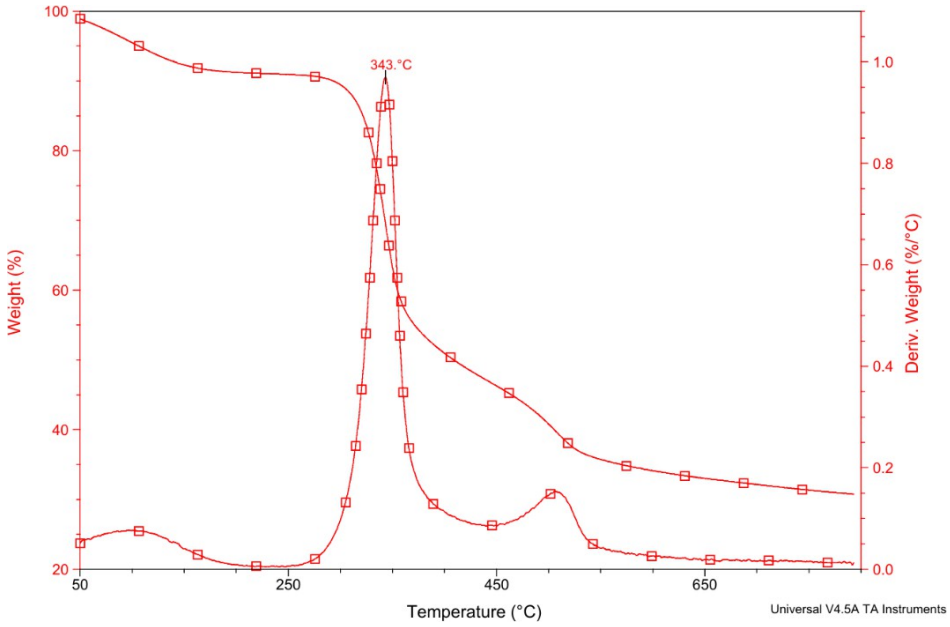

Figure 48. Thermogram (TG) and its derivative (DTG) of chitosan from *Buthus atlantis*

3.6. Chemical structure analysis and DA determination

The ^{1}H-NMR spectrum of chitosan **(Figure 49)** shows the characteristic resonances of the glucosamine backbone and the integration values confirm its very low degree of acetylation (DA = 2.5%). The anomeric proton (H-1) appears as a distinct peak at 5.15 ppm (signal *a*) [150], which was used as the reference and normalized to an integral of 1.00. The solvent peak corresponding to D_2O is clearly observed at 4.75 ppm and does not participate in the integration used for DA determination. The ring protons H-2 to H-6 (signals *b*–*g*) form a cluster of overlapping multiplets between 4.00 and 4.16 ppm [141], as typically observed for chitosan dissolved in D_2O or mildly acidic aqueous media. Their chemical shifts are consistent with those expected for the glucopyranose ring protons in highly deacetylated chitosan [204]. A well-defined resonance attributed to the H-2 proton of deacetylated glucosamine units appears between 3.45 and 3.42 ppm (signal *h*), with an integral of 0.57 [157]. The position and relative intensity of this

resonance reflect the presence of free amino groups (–NH_2/–NH_3^+), which dominate in chitosan with a low acetylation level. A small but clearly distinguishable peak is observed at 2.28 ppm (signal *i*), with an integral of 0.08. This resonance corresponds to the methyl group (–$COCH_3$) of the *N*-acetylated units. Its very low intensity relative to the anomeric proton directly reflects the small fraction of acetylated residues present along the polymer chain. Using the ratio of the methyl integral (0.08) to the anomeric proton integral (1.00), and applying the formula described previously, the calculated degree of acetylation (DA) is of 2.5%, confirming that the material is highly deacetylated chitosan. This is consistent with the low intensity of the acetyl methyl peak and the clear prominence of the H-2 signal for the deacetylated units. Overall, the chemical shifts, peak patterns and integral ratios observed in the ^{1}H-NMR spectrum confirm the expected structure of chitosan and validate the successful deacetylation of the parent chitin to a material with very low residual acetyl content.

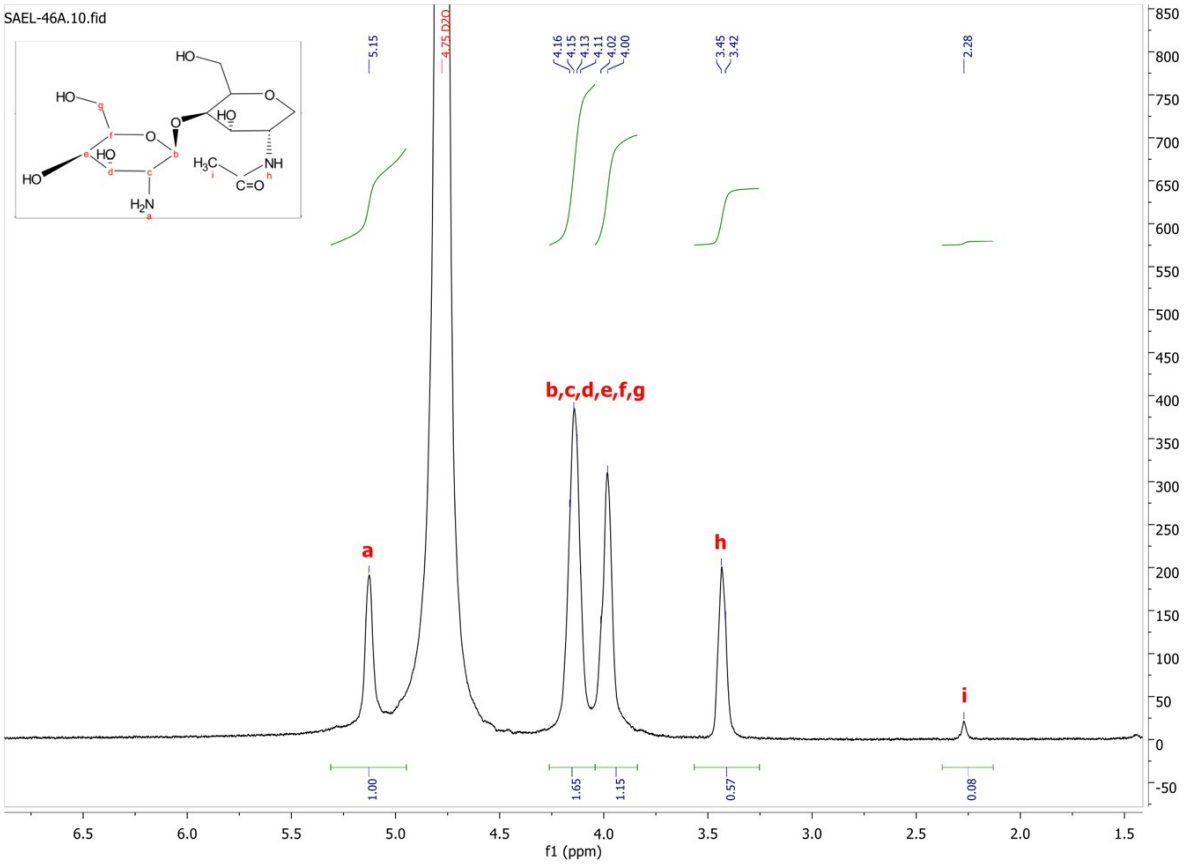

Figure 49. ^{1}H NMR spectrum of chitosan recorded in D_2O

3.7. Efficiency of extraction and its impact on the physicochemical properties of chitin and chitosan

The efficiency of the autoclave-assisted process (AAP) developed in this study is reflected not only in the high extraction yield but also in the fine control achieved over the structural and physicochemical properties of the resulting chitin and chitosan, which are critical determinants of their adsorption performance in water purification applications. By tailoring the number of purification baths to the intrinsically lower mineral and protein content of *Buthus atlantis* exoskeletons, we obtained a highly purified chitin exhibiting a crystallinity index (I_{Cr}) of 52.21% and a maximum thermal degradation temperature (DTG_{max}) of approximately 395 °C, alongside a chitosan characterized by low degree of acetylation equal to 2.5%, moderate viscosity average molecular weight (Mv = 126.2 kDa), I_{Cr} of 48.42%, and DTG_{max} of 343 °C. Importantly, SEM observations confirmed the preservation of a compact, organized and native-like

microarchitecture, typical of terrestrial arthropod cuticles, indicating minimal disruption of the hierarchical fibrillar assembly during extraction.

When benchmarked against our previous AAP-based extraction from black soldier fly (BSF) residues [180], which yielded chitin with higher crystallinity (I_{Cr} = 73.38%) and superior thermal stability (DTG_{max} = 421 °C), as well as chitosan with comparable DA (2.92%) but higher Mv (≈ 220 kDa), the *Buthus*-derived materials display moderately lower crystallinity and molecular weight. These differences can be primarily ascribed to feedstock-dependent factors, including taxon-specific cuticular architecture [33], mineral distribution and initial protein content, which collectively govern polymer packing, hydrogen-bonding density and crystalline perfection. In addition, the reduced number of purification baths applied here, while sufficient for effective demineralization and deproteinization, likely resulted in slight attenuation of crystalline order and thermal resistance, yet effectively limited excessive chain scission, yielding chitosan with balanced molecular weight and low DA two parameters critically influencing adsorption efficiency [49].

Compared with our previously reported microwave-assisted extraction of BSF chitin and chitosan [79], which produced materials with comparable DA (2.3%) but lower thermal stability (DTG_{max} ≈ 326 °C) and more disordered morphology, the present AAP protocol demonstrates superior preservation of mesostructural organization and enhanced thermal resistance. These improvements highlight the milder and more homogeneous thermal and chemical environment provided by autoclave processing, which mitigates localized overheating and uncontrolled depolymerization commonly associated with microwave irradiation. The better-defined porous and fibrillar architecture observed here is particularly advantageous for adsorption processes, as it promotes increased surface accessibility, enhanced diffusion pathways, and improved interaction between functional amino groups and aqueous contaminants.

Furthermore, relative to thermal-pretreatment optimization reported for blue crab shells [223], which yielded chitin with substantially lower crystallinity (≈ 35%) and altered polymorphic features, the present AAP applied to *Buthus* exoskeletons achieves markedly higher crystalline order at comparable thermal stability. This observation further underscores the combined influence of biological origin and processing modality in dictating the supramolecular structure and, consequently, the functional performance of chitin-based materials.

In a broader methodological comparison, previous multi-route extraction studies on shrimp shells employing chemical, microwave and autoclave treatments with concentrated NaOH (50%, 1 h) reported chitosan with relatively high DA (≈ 7%), low Mv (≈ 55 kDa), reduced thermal stability and severely disrupted morphology [81]. In contrast, our use of a moderated mixed alkaline system (50% KOH, 25% ethanol, 25% monoethylene glycol) under identical autoclave conditions enabled a significant reduction in DA to 2.5% while maintaining a substantially higher molecular weight and preserving structural integrity. This optimized balance between deacetylation efficiency and polymer chain preservation is particularly beneficial for adsorption applications, as low DA enhances amino group density and metal-binding affinity, whereas moderate Mv ensures adequate mechanical stability and reusability of the adsorbent. Collectively, these results demonstrate that extraction efficiency and functional performance of chitin and chitosan are maximized when autoclave parameters are carefully matched to feedstock composition and alkaline chemistry is strategically moderated. The resulting materials exhibit a favorable combination of low DA, adequate molecular weight, enhanced thermal stability and preserved hierarchical structure, all of which are essential for high-performance adsorption in water purification systems. Notably, the tailored *Buthus*-derived chitosan produced in this study presents physicochemical attributes particularly suited for heavy-metal

binding and organic pollutant removal, supporting its strong potential as a sustainable, high-value bioadsorbent for advanced water treatment applications.

4. Scaffold characterization

The X-ray diffractogram of the scaffold prepared from the previously characterized chitosan reveals a clear structural reorganization induced during scaffold formation. In the parent chitosan, two diffraction features were observed: a broad reflection around 10° (2θ) corresponding to the amorphous domain, and a more intense peak at 19.8° (2θ) assigned to the (110) crystallographic plane typically associated with the semi-crystalline regions of chitosan. In the scaffold, the 10° amorphous peak completely disappears (**Figure 50**), indicating a significant reduction in disordered domains and suggesting that the lyophilization and gelation steps favored polymer chain rearrangement and intermolecular alignment. Concurrently, the main crystalline peak is retained but appears slightly shifted from 19.8° to 20.2° (2θ), still corresponding to the (110) plane, which reflects the presence of ordered crystalline domains within the scaffold matrix. This shift may be attributed to changes in interchain spacing and variations in hydrogen-bonding patterns resulting from the scaffold preparation process.

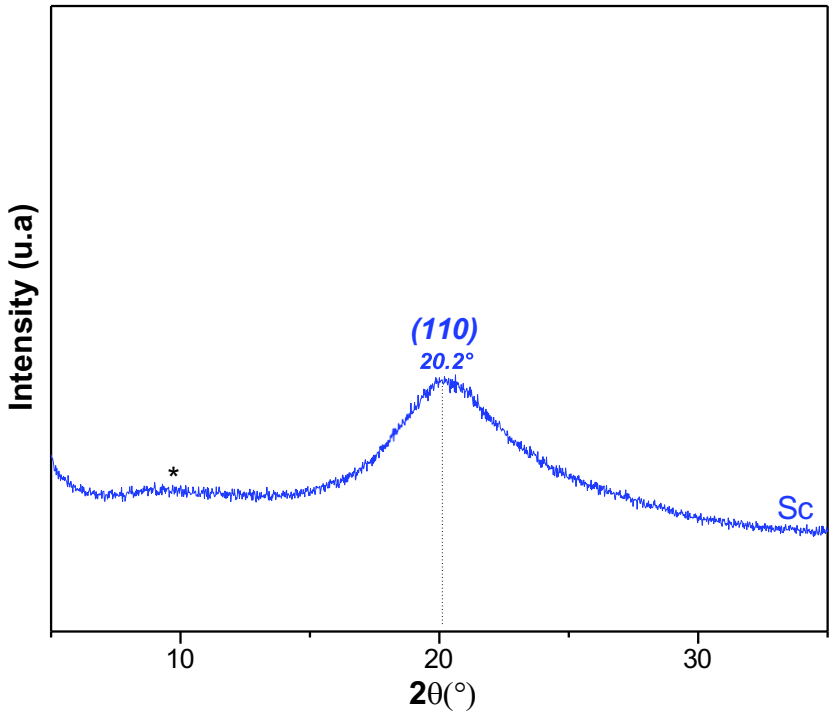

Figure 50. XRD spectrum of chitosan scaffold (Sc)

The XRD findings are in strong agreement with the SEM observations (**Figure 51**). While the chitin precursor presents a well-organized, polygonal, native-type cuticular morphology and chitosan exhibits **a** flattened, smoother and partially collapsed structure typical of deacetylated chitin, the scaffold displays a highly porous, interconnected architecture**.** The pores appear uniformly distributed, with well-defined walls and continuous channels, demonstrating that the scaffold fabrication process promoted three-dimensional structural organization rather than collapse of the polymer chains. The hierarchical porosity observed in SEM corroborates the disappearance of the amorphous XRD peak, indicating that the scaffold's structural assembly favored a more organized arrangement of chitosan chains, in line with the enhanced (110) reflection. Together, these results confirm that the scaffold maintains structural integrity, exhibits improved internal organization, and possesses a porous network suitable for applications requiring high surface area

and interconnected geometry, such as biomedical, adsorption or tissue engineering uses.

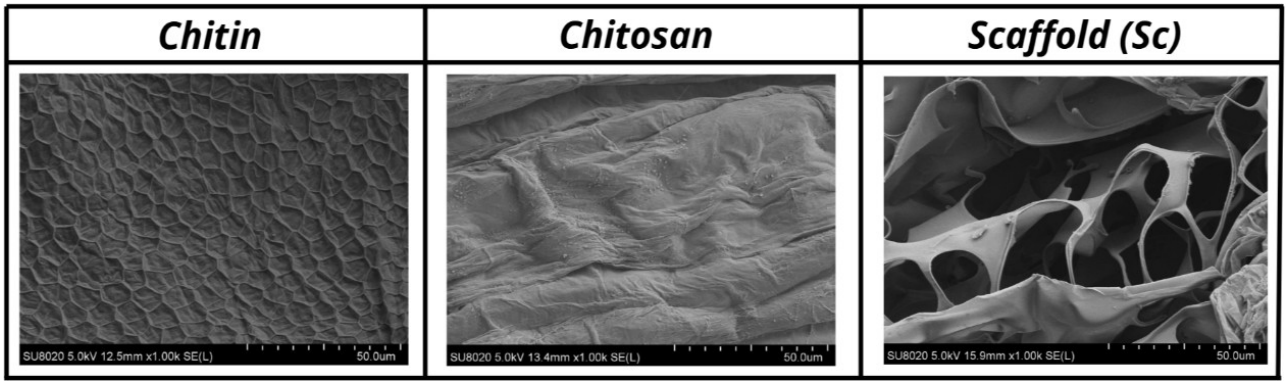

Figure 51. SEM images of chitin, chitosan and pure chitosan scaffold (Sc) from *Buthus Atlantis*

5. Efficiency of chitosan scaffold in heavy metals and salts removal

5.1. Evaluation of Ion Removal Efficiency Based on TDS Measurements

To evaluate the ion removal efficiency of the material/system according to the present work, a series of aqueous solutions containing various chloride salts were prepared. The initial total dissolved solids (TDS) values were measured using a calibrated TDS meter. Each solution was then subjected to contact with the proposed treatment medium under identical conditions for a duration over one hour. After this contact time, the TDS values were measured again. The following table summarizes the results:

Table 16. TDS measurements after adsorption tests

Elements	Initial TDS (ppm)	Final TDS (after 1h) (ppm)	TDS reduction (ppm)	% Reduction
$MgCl_2$	572	526	46	8.04
KCl	970	775	195	20.10
NaCl	970	950	20	2.06
$CdCl_2$	469	302	167	35.61

$CuCl_2$	630	96	534	84.76
$CaCl_2$	816	379	437	53.55
$PbCl_2$	409	206	203	49.63
$CrCl_3$	547	168	379	69.29

These results demonstrate that the material or process according to the invention exhibits a preferential removal of transition metal ions such as Cu^{2+}, Cr^{3+}, Pb^{2+} and Cd^{2+}, with removal efficiencies reaching up to 84.76% in the case of copper. The material shows moderate efficiency for calcium and magnesium ions and limited effectiveness for monovalent alkali metal ions such as sodium (Na^+) and potassium (K^+), which is consistent with their lower charge density and binding affinity. A trend that has been widely reported in recent studies on chitosan-based and other polymeric adsorbents [224,225]. This behavior is primarily related to the charge carried by the cations, as well as their hydration characteristics and interaction affinity with functional groups present on the adsorbent surface [226]. Divalent cations such as Ca^{2+} and Mg^{2+} exhibit stronger adsorption compared to monovalent ions due to their higher charge density, which enhances electrostatic attraction and facilitates complexation with amino and hydroxyl groups of chitosan. However, the adsorption of Mg^{2+} remains lower than that of Ca^{2+}, which can be attributed to its higher hydration energy and smaller ionic radius, leading to a more stable hydration shell that limits its interaction with active sites [227].

5.2. Evaluation of Ionic Conductivity Reduction as an Indicator of Ion Removal Efficiency

In another set of experiments, the removal efficiency of the treatment system was evaluated by measuring the electrical conductivity of aqueous solutions of various chloride salts before and after 1 hour in contact with the adsorbent material. Conductivity is a function of the ionic strength of the solution and is used here as an indirect measurement of ion removal. The decrease in conductivity indicates the extent of ion uptake by the treatment system.

The results are summarized in the table 17:

Table 17. Conductivity parameters after before and after adsorption tests

Chloride salt	Initial conductivity (μS/cm)	Conductivity after 1h (μS/cm)	Reduction (μS/cm)	% Reduction
$MgCl_2$	1152	982	170	14.76
KCl	1950	1557	393	20.15
NaCl	1940	1900	40	2.06
$CdCl_2$	931	606	325	34.90
$CuCl_2$	1295	192	1103	85.21
$CaCl_2$	1602	758	844	52.68
$PbCl_2$	801	413	388	48.44
$CrCl_3$	1101	337	764	69.39

The highest conductivity reduction was observed for $CuCl_2$ (85.21%), followed by $CrCl_3$ (69.39%), $CaCl_2$ (52.68%) and $PbCl_2$ (48.44%), confirming a high selectivity of the treatment system for multivalent and toxic transition metal ions. $CdCl_2$ also showed a significant conductivity drop (34.90%), indicating good but lower adsorption compared to Cu^{2+} and Cr^{3+}. KCl and $MgCl_2$ showed moderate reductions (20.15% and 14.76%, respectively), while NaCl exhibited minimal conductivity change (2.06%), demonstrating low affinity toward monovalent ions.

The conductivity results further corroborate the selectivity of the adsorbent material for divalent and trivalent metal ions over monovalent ions. The observed selectivity agrees with the TDS-based findings and reflects the material's suitability for applications targeting the removal of environmentally hazardous metal ions such as Cu^{2+}, Cr^{3+}, Pb^{2+} and Cd^{2+}.

The uptake capacity of the bioadsorbent material was evaluated for various chloride salts, demonstrating selective affinity in the following ascending order: sodium chloride (NaCl) at approximately 3%, magnesium chloride ($MgCl_2$) at 15%, potassium chloride (KCl) at 21%, cadmium chloride ($CdCl_2$) at 35%, lead(II) chloride ($PbCl_2$) at

49%, calcium chloride ($CaCl_2$) at 54%, chromium(III) chloride ($CrCl_2$) at 70% and copper(II) chloride ($CuCl_2$) exhibiting the highest uptake rate of 86% (**Figure 52**).

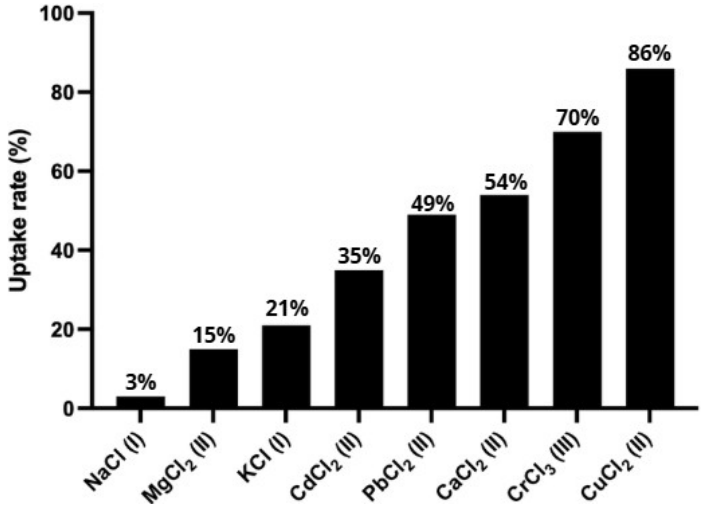

Figure 52. Uptake rate (%) of scaffold chitosan (Sc)

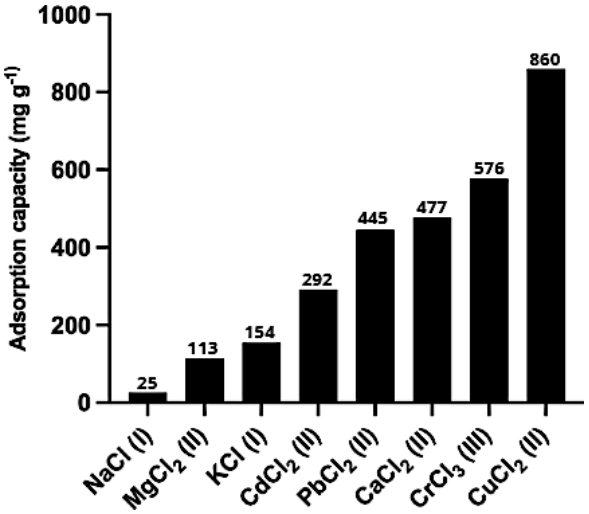

Figure 53. Adsorption capacity ($mg \cdot g^{-1}$) of scaffold (Sc) for selected metal salts

The resulting adsorption capacities, expressed in milligrams of adsorbate per gram of adsorbent ($mg \cdot g^{-1}$), were as follows: sodium chloride (NaCl), 25 $mg \cdot g^{-1}$; magnesium chloride ($MgCl_2$), 113 $mg \cdot g^{-1}$; potassium chloride (KCl), 154 $mg \cdot g^{-1}$; cadmium chloride ($CdCl_2$), 292 $mg \cdot g^{-1}$; lead(II) chloride ($PbCl_2$), 445 $mg \cdot g^{-1}$; calcium chloride ($CaCl_2$), 477

$mg \cdot g^{-1}$; chromium(III) chloride ($CrCl_3$), 576 $mg \cdot g^{-1}$ and copper(II) chloride ($CuCl_2$), exhibiting the highest adsorption capacity at 860 $mg \cdot g^{-1}$ (**Figure 53**). The combination of high-performance selectivity with low affinity toward essential, non-toxic monovalent ions (Na^+, K^+) makes the system ideal for selective water purification and environmental remediation strategies.

For instance, *Humelnicu et al. (2020)* reported maximum adsorption capacities of approximately 120–180 $mg \cdot g^{-1}$ for Cu^{2+} and 90–150 $mg \cdot g^{-1}$ for Cr^{3+} using chitosan-based cryogels [225]. Similarly, *EL Messaoudi et al. (2022)* obtained adsorption capacities of around 210 $mg \cdot g^{-1}$ for Cu^{2+} and 150 $mg \cdot g^{-1}$ for Cd^{2+} using modified chitosan materials [224]. More recently, *Liu et al. (2025)* reported maximum adsorption capacities of 259.4 $mg \cdot g^{-1}$ for Cu^{2+}, 291.5 $mg \cdot g^{-1}$ for Pb^{2+}, 278.7 $mg \cdot g^{-1}$ for Cd^{2+} and 171.4 $mg \cdot g^{-1}$ for Cr^{3+} using a bioinspired hydrogel system (PSSC) [228]. In comparison, the adsorption capacity obtained in the present work for Cu^{2+} (860 $mg \cdot g^{-1}$) is more than three times higher than that reported by [228], while Cr^{3+} adsorption (576 $mg \cdot g^{-1}$) exceeds literature values by a factor of approximately 3.4. Similarly, Pb^{2+} adsorption (445 $mg \cdot g^{-1}$) remains significantly higher than most reported values, while Cd^{2+} adsorption is comparable to or higher than the upper range of recent studies.

In addition to high adsorption capacity, the material exhibits a pronounced selectivity toward multivalent and transition metal ions. Based on the experimental results, the selectivity follows the order:

$$\mathbf{Cu^{2+} > Cr^{3+} > Ca^{2+} > Pb^{2+} > Cd^{2+} > K^{+} > Mg^{2+} > Na^{+}}$$

5.3. Microscopic observation after adsorption tests

Microscopic observation conducted following the adsorption tests revealed significant morphological changes in the porous scaffold structure (Sc). Specifically, for chromium (Cr), lead (Pb) and copper (Cu), the characteristic porous architecture defined by a major pore diameter "D" and a minor diameter "d", was no longer discernible, indicating substantial structural collapse or occlusion. In contrast, for

calcium (Ca), cadmium (Cd), potassium (K) and magnesium (Mg), although the porous network remained partially intact, the initially smooth surface topology was visibly disrupted, and a marked reduction in both diameters "D" and "d" was observed, as illustrated in **the figure 54**.

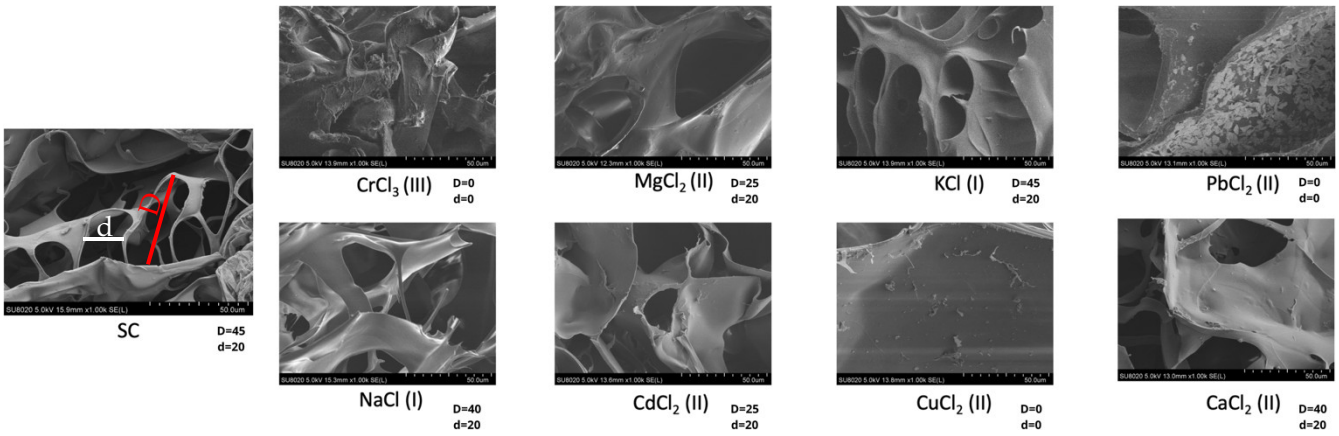

Figure 54. Microscopic comparison of the scaffold porous structure (Sc) after adsorption tests

6. Comparative tests

In a subsequent series of experiments, scaffold forms were prepared using alternative chitosan sources, namely: (i) commercial chitosan derived from shrimp shells (Sigma-Aldrich, high molecular weight), (ii) chitosan extracted from *Buthus atlantis*, chitosan obtained from *Hermetia illucens* (Black Soldier Fly, BSF) pupal (iii) and prepupal exuviae (iv), and (v) chitosan extracted from *Pollicipes pollicipes (***Figure 55***)*. The scaffold fabrication procedure was identical to that employed for the initial scaffold (Sc).

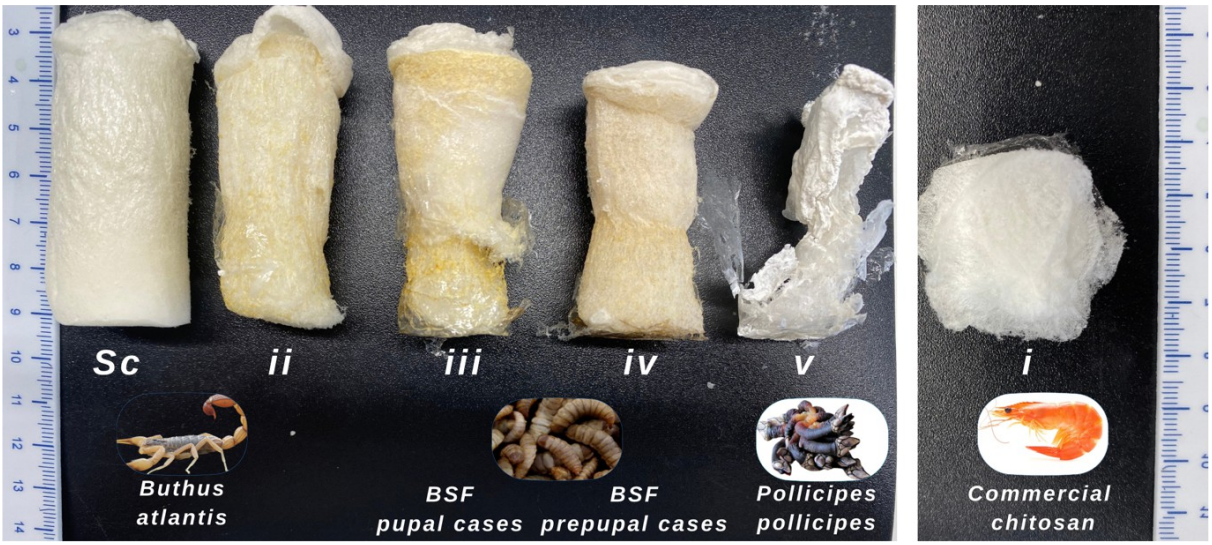

Figure 55. Visual comparison of scaffold morphology derived from different chitosan sources

Morphological analysis revealed distinct structural differences among the scaffolds. In particular, the scaffold derived from BSF chitosan exhibited a visibly lower density and lighter coloration. In the case of the commercial chitosan, the scaffold dimensions deviated significantly from those of the reference, and the resulting structure displayed poor mechanical integrity, appearing fragile and prone to disintegration upon contact with water. It is important to note that, although a fixed initial mass of chitosan (1 g) was used, incomplete solubilization, insufficient deacetylation, or the presence of residual impurities may lead to a discrepancy between the initial mass and the effectively dissolved polymer fraction. As a result, the real polymer concentration in solution is lower than expected, which affects solution viscosity, intermolecular interactions, and gelation behavior. This, in turn, influences the density, homogeneity, and structural integrity of the resulting scaffold. Additionally, chitosan powder and cast films derived from *Buthus atlantis* chitosan were tested in parallel to evaluate their adsorption efficiency in comparison to the scaffold form. Activated carbon, a commercially available filtration adsorbent, was also included as a benchmark reference material for performance comparison.

Based on TDS values, a notable reduction was observed particularly for divalent and trivalent metal salts, indicating effective adsorption. For $CuCl_2$ and $CrCl_3$ solutions, the strongest reductions were observed with adsorbent Sc, where TDS dropped from 630 ppm to 96 ppm and from 547 ppm to 168 ppm, respectively, highlighting significant affinity toward copper and chromium ions (**Table 18**). Similarly, Cd^{2+} and Pb^{2+} removal was efficiently achieved by scaffold Sc, with TDS decreasing to 302 ppm and 206 ppm, respectively. Chitosan films (Chitosan BA and BA film) showed moderate to high adsorption efficiency, especially for Mg^{2+}, Na^{+} and K^{+} ions. Importantly, during the adsorption tests, it was visually observed that certain adsorbents underwent physical degradation in aqueous media. Specifically, the scaffold forms fabricated from adsorbents (i), (ii), (iii), (iv) and (v) exhibited partial disintegration, with visible fragments of the scaffold present in solution, indicating a lack of mechanical stability in prolonged contact with metal-containing solutions, which is the reason of the absence of scaffold v that was completely dissociated in the metal solution. This behavior was not observed with the original scaffold (Sc), which maintained its structural integrity and did not disintegrate during testing, demonstrating superior stability and usability under the same experimental conditions. For comparison, activated carbon was evaluated under identical experimental conditions. While activated carbon benefits from a highly developed surface area and direct accessibility of adsorption sites, it differs significantly from the scaffold in terms of physical form and structure. In contrast, the 3D scaffold provides a continuous porous network, where adsorption occurs not only at the surface but also within the internal structure. Therefore, although the comparison remains relevant as a reference, the differences in morphology and mass transfer pathways should be taken into account.

Table 18. TDS values (in ppm) measured after 1hour contact between different adsorbents and solutions containing individual metal salts

Elements	TDS (ppm)

	T_0	iii	iv	i	Sc	Chitosan BA	BA film	Activated carbon
$MgCl_2$	572	604	576	560	526	542	504	565
KCl	970	881	839	877	775	841	844	960
NaCl	970	970	1010	890	950	745	970	966
$CdCl_2$	469	401	408	408	302	396	419	421
$CuCl_2$	630	557	622	614	96	607	600	514
$CaCl_2$	816	728	408	697	379	699	696	801
$PbCl_2$	409	377	369	376	206	317	313	340
$CrCl_3$	547	443	421	549	168	493	514	441

The observed changes in conductivity values correlate with those in TDS, reflecting the ionic strength remaining in solution post-treatment. Notably, the scaffold form (Sc) led to significant reductions in conductivity across all tested salts, especially for divalent and trivalent metal ions (Cd^{2+}, Cu^{2+}, Ca^{2+}, Pb^{2+}, Cr^{3+}) (**Table 19**), suggesting high adsorption capacity.

Table 19. Conductivity values (in µS/cm) measured after 1-hour contact between different adsorbents and solutions containing individual metal salts

Elements	Conductivity (µS/cm)							
	T_0	iii	iv	i	Sc	Chitosan BA	BA film	Activated carbon
$MgCl_2$	1147	1196	1155	1117	982	1090	975	1135
KCl	1950	1773	1700	1740	1557	1679	1707	1940
NaCl	1940	1970	2040	1729	1900	1489	1920	1920
$CdCl_2$	931	801	819	801	606	794	806	881
$CuCl_2$	1295	1109	1244	1226	192	1213	1205	1023
$CaCl_2$	1602	1540	1483	1384	758	1394	1375	1571
$PbCl_2$	810	751	756	750	413	631	641	715
$CrCl_3$	1101	882	859	1226	337	986	1262	891

The data presented in the table below illustrate the adsorption performance of several chitosan-based materials and a commercial activated carbon when exposed to solutions of different metallic salts. The adsorption capacities were determined after 1-hour contact under standardized test conditions. The results demonstrate a markedly superior adsorption efficiency for the scaffold form (Sc), notably in the case of divalent and trivalent cations such as Cu^{2+} (860 $mg \cdot g^{-1}$), Cr^{3+} (576 $mg \cdot g^{-1}$), Ca^{2+} (477 $mg \cdot g^{-1}$), and Pb^{2+} (445 $mg \cdot g^{-1}$) (**Table 20**). The scaffold's porosity and structural integrity likely contribute to its enhanced uptake performance. In contrast, traditional forms such as chitosan powders or films, while still active (e.g., Chitosan BA: 451 $mg \cdot g^{-1}$ for Na^{+}), show limitations due to either disintegration or lower surface reactivity. Activated carbon, used as a commercial benchmark, showed inferior adsorption across all tested elements.

Table 20. Adsorption capacity ($mg \cdot g^{-1}$) of various adsorbents for selected metal salts

Elements	Adsorption capacity ($mg.g^{-1}$)						
	iii	**iv**	**i**	**Sc**	**Chitosan BA**	**BA film**	**Activated carbon**
$MgCl_2$	0	0	30	113	57	132	8
KCl	175	250	210	154	271	243	11
NaCl	0	0	211	25	451	20	5
$CdCl_2$	130	112	130	292	137	125	51
$CuCl_2$	186	51	69	860	82	90	131
$CaCl_2$	62	119	218	477	208	227	14
$PbCl_2$	59	54	60	445	179	169	72
$CrCl_3$	219	242	0	576	115	0	120

To achieve a comprehensive understanding of the adsorption behavior of the chitin-derived materials obtained from *Buthus atlantis* exoskeleton, a systematic comparison was performed between the different structural forms, namely chitosan BA, BA film and BA scaffold and benchmarked against representative adsorbents reported in the literature **(Table 21)**. This comparative approach reveals a clear structure–function relationship, where the material architecture, porosity and functional group accessibility govern ion capture efficiency and highlights the exceptional potential of these materials for hazardous water remediation.

For Mg^{2+} adsorption, the BA film exhibited the highest uptake capacity (132 $mg \cdot g^{-1}$), significantly surpassing conventional chitosan-based and mineral adsorbents. In comparison, magnetic chitosan/Fe3O4 composites typically exhibit capacities below 100 mg·g-1 [229], while modified bentonite and zeolite display much lower values of 14.63 and 26.2 $mg \cdot g^{-1}$ [230], respectively and alginate–citrate composite aerogels rarely exceed 30 $mg \cdot g^{-1}$ [231]. The enhanced performance of the BA film is attributed to its compact yet permeable polymeric network, homogeneous functional group distribution and increased surface reactivity, which together facilitate rapid Mg^{2+} diffusion and strong electrostatic interactions with protonated amino groups ($–NH_3^+$) [232]. Moreover, the film configuration limits structural collapse during adsorption, preserving pore accessibility and maintaining high adsorption efficiency. This behavior highlights the relevance of polymer film engineering for effective alkaline-earth metal removal, particularly in water softening and mineral regulation processes [211].

In contrast, chitosan BA in powder form displayed superior affinity toward monovalent ions, achieving 271 $mg \cdot g^{-1}$ for K^+ and 451 $mg \cdot g^{-1}$ for Na^+, values that largely exceed those reported for EDTA-functionalized chitosan (10–20 $mg \cdot g^{-1}$) [229] and biochar hybrids (<5 $mg \cdot g^{-1}$) [233]. This remarkable performance can be explained by the high availability of protonated amino groups and flexible polymer chains [49],

which promote efficient ion exchange and electrostatic attraction mechanisms [234]. The strong Na^+ and K^+ uptake suggests that BA chitosan possesses intrinsic desalination potential, making it particularly attractive for salinity reduction, brackish water treatment and pretreatment of seawater desalination systems.

Table 21. Reported adsorption capacity ($mg.g^{-1}$) of ions by different adsorbents

Ion	Adsorbent	Capacity ($mg.g^{-1}$)	Reference
Mg^{2+}	BA film	132	This study
	Magnetic chitosan/Fe_3O_4	50 to 100	[229]
	Mesoporous MgO	Limited	[235]
	Modified bentonite	14.63	[230]
	Modified zeolite	26.2	[236]
	Alginate-citrate composite	28	[231]
K^+/Na^+	Chitosan BA	271 (K+)/451 (Na+)	This study
	EDTA chitosan	10 to 20	[229]
	Biochar hybrids	<5	[233]
Ca^{2+}	Scaffold (Sc)	477	This study
	Functionalized chitosan	20 to 50	[229]
	Modified bentonite	14.63	[230]
	Alginate citrate composite	18	[231]
Pb^{2+}	Scaffold (Sc)	445	This study
	Magnetic chitosan	121.95	[117]
	Magnetized activated carbon	253.2	[237]
Cd^{2+}	Scaffold (Sc)	292	This study
	Magnetized activated carbon	73.3	[237]
	Zeolite	84.3	[238]
	Chitosan BSF	131.1	[79]
Cr^{3+}	Scaffold (Sc)	576	This study
	NaOH/Fe(III) modified Clinoptilolite zeolite	31.47	[239]
	Chitosan microfiber immobilized with bayberry tannin	20.90	[240]
Cu^{2+}	Scaffold (Sc)	860	This study
	Olivine loaded with magnesium oxide micro rods	225.82	[241]
	ZnAI-LDH	213	[242]
	CuS-PVDF electrodes	551.49	[243]

For hazardous heavy metal ions, including Cd^{2+}, Pb^{2+}, Ca^{2+}, Cr^{3+} and Cu^{2+}, the scaffold configuration consistently exhibited the highest adsorption capacities, reaching 292, 445, 477, 576 and 860 $mg \cdot g^{-1}$, respectively **(Table 21)**. These values surpass not only the other BA derived forms but also the most reported adsorbents, including magnetized activated carbon [237], modified zeolites [238], layered double hydroxides and functionalized polymer composites [242]. The outstanding performance of the scaffold is primarily governed by its three-dimensional interconnected porous architecture, which provides large accessible surface area, reduced diffusion resistance, and homogeneous distribution of active binding sites [244].

At the molecular level, adsorption proceeds through a synergistic mechanism involving electrostatic attraction, chelation and surface complexation [245]. The amino and hydroxyl groups of chitosan act as primary coordination sites, enabling the formation of stable inner-sphere complexes with heavy metal ions, particularly for Cu^{2+} and Cr^{3+} [246,247], which exhibit strong affinity toward nitrogen- and oxygen-donor ligands. Additionally, hydrogen bonding and physical entrapment within the hierarchical pore network further contribute to the high adsorption capacities [47]. The macroporous channels ensure rapid ion transport, while mesoporous domains enhance contact probability between metal ions and active functional groups, collectively leading to exceptionally fast kinetics and high uptake efficiency.

Importantly, the observed trend in adsorption performance (scaffold > film > powder for heavy metals) directly reflects the increasing degree of structural organization and porosity, confirming that morphological engineering plays a decisive role in controlling adsorption mechanisms and efficiency. The exceptional Cu^{2+} uptake (860 $mg \cdot g^{-1}$) is particularly noteworthy and positions the BA scaffold among the highest performing bio-based adsorbents reported to date, highlighting its strong potential for industrial effluent treatment, electroplating wastewater remediation and mining wastewater purification.

7. Conclusion

The efficiency of the autoclave-assisted process developed is reflected in the high extraction yield and the fine control achieved over the structural and physicochemical properties of chitin and chitosan, which are critical determinants of their adsorption performance in water purification applications. By tailoring the number of purification baths to the intrinsically lower mineral and protein content of *Buthus atlantis* exoskeletons, chitin exhibits a crystallinity index (I_{Cr}) of 52.21% and a maximum thermal degradation temperature (DTG_{max}) of approximately 395 °C, alongside a chitosan characterized by a low degree of acetylation (2.5%), moderate viscosity average molecular weight (Mv = 126.2 kDa), I_{Cr} of 48.42% and DTG_{max} of 343 °C. SEM observations confirmed the preservation of a compact, organized and native-like microarchitecture, typical of terrestrial arthropod cuticles, indicating minimal disruption of the hierarchical fibrillar assembly during extraction.

The chitosan was subsequently engineered into a three-dimensional porous scaffold, characterized by an interconnected network of macro and mesopores, which ensures maximal exposure of reactive amino and hydroxyl groups and provides a robust architecture for metal ion adsorption. Adsorption experiments demonstrated that this scaffold achieved the highest performance among all chitosan-derived materials from BA, significantly outperforming the BA powder and BA film forms for heavy metal removal. The scaffold exhibited exceptional uptake capacities for Cd^{2+}, Pb^{2+}, Cr^{3+} and Cu^{2+}, exceeding other bio-based 3D scaffolds reported in the literature as well as conventional commercial adsorbents such as activated carbon. The superior performance is attributed to the synergistic effect of hierarchical porosity and a large accessible surface, which collectively facilitate strong chelation, electrostatic interactions and surface complexation with metal ions. These results highlight the unique potential of BA derived chitosan scaffolds as high-performance, sustainable bioadsorbents, combining renewable origin, structural tunability and broad-spectrum heavy metal removal efficiency.

General Discussion

General Discussion

This work demonstrates the successful development of an integrated strategy for the valorization of chitin-rich biomass through the combination of process innovation, material design and application performance. The autoclave-assisted process (AAP) developed in this thesis represents a significant advancement over conventional extraction methods, enabling substantial improvements in process efficiency and industrial feasibility. The optimized AAP protocol allows a drastic reduction in processing time for key extraction steps. In particular, the deproteinization step was reduced from approximately 18 hours to 75 minutes, while the deacetylation step decreased from 24 hours to 1 hour, corresponding to reductions greater than 90%. These results clearly demonstrate the efficiency of hydrothermal-assisted extraction conditions in accelerating reaction kinetics, in agreement with previous studies reporting enhanced mass transfer and reaction rates under elevated temperature and pressure [77,81].

In addition to time reduction, the process enables a significant decrease in chemical reagent consumption, with an estimated reduction of 83%, as well as a substantial 80% reduction in water usage, due to the simplification of washing and treatment steps [180]. These improvements contribute directly to the high Industrial Feasibility Score (IFS) obtained for the process, confirming its strong potential for industrial implementation. The extraction efficiency is further supported by a protein removal efficiency of 94%, indicating effective purification of the chitin matrix.

Beyond process efficiency, the extracted chitin exhibits high purity, well-preserved crystallinity and favorable thermal stability, which are essential for subsequent valorization. The preservation of crystalline structure under optimized conditions is consistent with findings reported in the literature, where controlled extraction parameters contribute to maintaining the structural integrity of chitin [81]. These

characteristics are critical for ensuring the performance of derived materials and confirm the quality of the extraction process.

The influence of biomass origin on the physicochemical properties of chitin and chitosan was clearly demonstrated, with variations in degree of deacetylation, molecular weight and structural organization. These differences directly impact material behavior and were successfully exploited in the design of functional materials. In this context, the development of a three-dimensional chitosan scaffold represents a major contribution of this work. The scaffold exhibited outstanding adsorption capacities toward inorganic pollutants, reaching 860 $mg \cdot g^{-1}$ for Cu^{2+}, 576 $mg \cdot g^{-1}$ for Cr^{3+}, 477 $mg \cdot g^{-1}$ for Ca^{2+} and 445 $mg \cdot g^{-1}$ for Pb^{2+}, which significantly exceed most values reported for conventional chitosan-based adsorbents, typically ranging between 100 and 400 $mg \cdot g^{-1}$ depending on material structure [115,225,227,248]. The adsorption behavior further revealed a pronounced selectivity toward multivalent ions, driven by coordination interactions with amino functional groups and electrostatic effects [249]. This selectivity enhances the relevance of the developed material for targeted water treatment applications, particularly for the removal of toxic heavy metals. The combination of high adsorption capacity and selectivity positions the developed scaffold among the most efficient chitosan-based adsorbents reported to date.

An important outcome of this work is the successful transition from laboratory-scale validation to pilot-scale implementation. The application of the AAP process within the Moroccan startup SGW–ShrimpGreenWater, involving the processing of approximately 600 kg of shrimp shell waste, confirms the scalability and robustness of the process under real operating conditions. This progression from TRL 3 to TRL 5 represents a critical step toward industrial deployment and demonstrates the transferability of the developed technology beyond laboratory conditions [250].

Overall, this thesis establishes a coherent and scalable approach to chitin valorization, combining efficient extraction, advanced material design and high-performance applications. The significant improvements achieved in processing efficiency, resource consumption and adsorption performance highlight the potential of the proposed strategy for the development of sustainable and economically viable chitin-based technologies. These results provide a solid foundation for the implementation of future biorefinery systems, particularly in regions such as Morocco, where abundant biomass resources and favorable conditions support the emergence of bio-based industries [210].

Conclusion & Outlooks & Perspectives

Conclusion & Outlooks & Perspectives

General Conclusion

This thesis demonstrates the feasibility of an integrated approach for the valorization of chitin-rich biomass, combining process intensification, material engineering and application-oriented design. The development of the autoclave-assisted process (AAP) represents a major advancement in chitin extraction, enabling a significant reduction in processing time, chemical consumption and water usage. The reduction of deproteinization time from 18 hours to 75 minutes and deacetylation from 24 hours to 1 hour illustrates the efficiency of the process, while the decrease of 83% in chemical use and 80% in water consumption confirms its relevance from an industrial perspective. These improvements are reflected in the high Industrial Feasibility Score (IFS), highlighting the strong potential of the process for large-scale implementation (IFS=A). The extracted chitins exhibited high purity, preserved crystallinity and favorable thermal properties, confirming the quality of the developed extraction protocol. The influence of biomass origin was shown to play a key role in determining the physicochemical properties of chitin and chitosan, opening opportunities for tailoring material performance according to targeted applications. In this context, the development of a three-dimensional chitosan scaffold constitutes a major contribution, demonstrating outstanding adsorption capacities for heavy metal ions, with values reaching 860 $mg \cdot g^{-1}$ for Cu^{2+} and 576 $mg \cdot g^{-1}$ for Cr^{3+}. These performances place the developed material among the most efficient chitosan-based adsorbents reported in recent literature.

A key achievement of this work is the successful transition from laboratory-scale validation to pilot-scale implementation. The application of the AAP process within the Moroccan startup SGW–ShrimpGreenWater, involving the treatment of 600 kg of shrimp shell waste, confirms the robustness and transferability of the process under real conditions. This advancement corresponds to a progression from TRL 3 to TRL 5,

marking a critical step toward industrial deployment. Taken together, these results demonstrate that the combination of an efficient extraction process, adaptable feedstock strategy and high-value material development provides a solid foundation for the emergence of sustainable chitin-based technologies.

Scientific perspectives

The results obtained in this work open several directions for future research. A first perspective concerns the optimization of the AAP process through fine control of operating parameters, with the objective of further improving extraction selectivity and reproducibility across different biomass sources. The adaptation of the process to continuous or semi-continuous systems represents an important step toward higher technological maturity levels, particularly in view of reaching TRL 6–7.

Another important direction relates to the control of structure–property relationships in chitosan-based materials. The ability to tune degree of deacetylation, molecular weight and crystallinity offers opportunities for designing materials with targeted functionalities. Future work may focus on advanced functionalization strategies, including chemical modification or hybridization with inorganic phases, in order to enhance selectivity, stability, multifunctionality and diversify the potential applications.

Economical perspectives

The results of this thesis strongly support the development of a chitin-based biorefinery in Morocco, based on a multi-feedstock strategy. The concept of an Adaptive Multi-Feedstock Biorefinery Hub (AMFBH) **(Figure 56)**, introduced in this work, provides a relevant framework for such an implementation. By integrating diverse biomass sources, including shrimp shell waste, insect-derived materials and marine organisms, this approach ensures resource availability, flexibility and resilience against supply fluctuations.

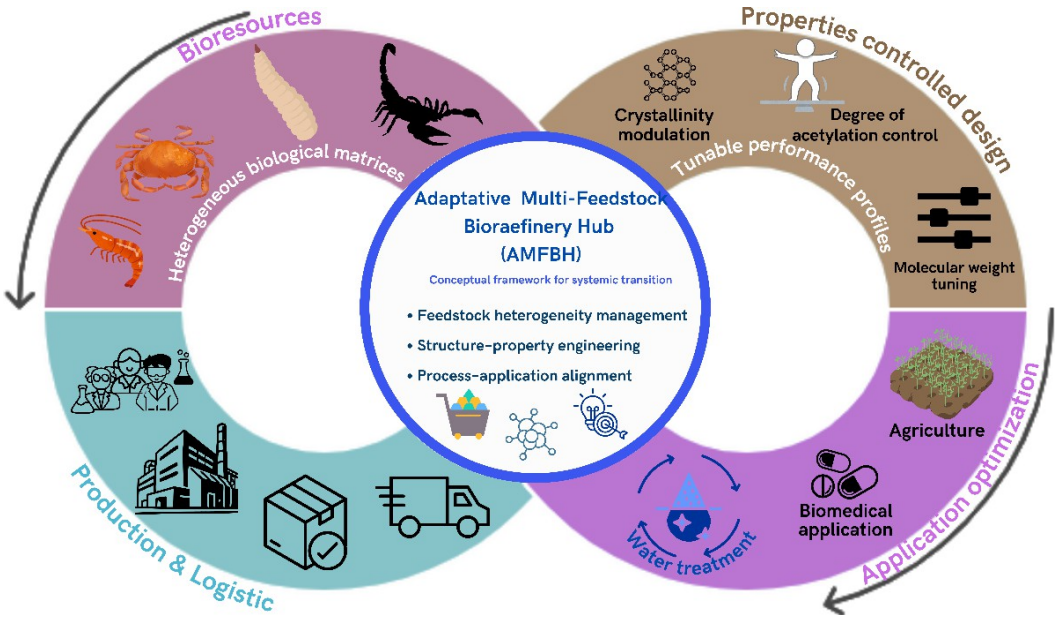

Figure 56. Conceptual representation of an adaptive multi-feedstock chitin biorefinery architecture

Morocco presents a particularly favorable environment for the deployment of such a system. The presence of a well-established seafood processing industry generates significant quantities of chitin-rich by-products, while the emergence of insect farming and the availability of diverse marine resources further expand the biomass base. In addition, favorable climatic conditions and strategic geographical positioning facilitate the development of integrated and sustainable industrial infrastructures.

From an economic perspective, the transformation of low-value biological residues into high-value functional materials represents a key driver for industrial viability. The development of advanced applications, such as high-performance adsorbents for water treatment, creates opportunities for market integration and value creation. The successful implementation of the AAP process within SGW–ShrimpGreenWater demonstrates that this transition is already underway and can be further expanded. Looking forward, the combination of technological readiness (TRL 5), process efficiency and resource availability provides the necessary conditions to progress toward higher maturity levels (TRL 6–7), involving pilot-scale optimization and pre-

industrial demonstration. In this context, the development of a Moroccan chitin biorefinery based on a multi-feedstock strategy appears not only feasible but strategically relevant for supporting the transition toward a circular and sustainable bioeconomy.

References

[1] M. İvgin, T. Demirel, Advancing Sustainable Energy Security in Türkiye: Geopolitical and Policy Perspectives, Sustainability 17 (2025) 9264. https://doi.org/10.3390/su17209264.

[2] I. Renewable Energy Agency, Geopolitics of the energy transition: Energy security, 2024. www.irena.org.

[3] P.G.C. Nayanathara Thathsarani Pilapitiya, A.S. Ratnayake, The world of plastic waste: A review, Cleaner Materials 11 (2024) 100220. https://doi.org/10.1016/j.clema.2024.100220.

[4] M. Khanna, D. Zilberman, G. Hochman, B. Basso, An economic perspective of the circular bioeconomy in the food and agricultural sector, Commun. Earth Environ. 5 (2024) 507. https://doi.org/10.1038/s43247-024-01663-6.

[5] A. Abba, S. Sabarinath, R.A. Mustapha, Advancing circular bioeconomy through systematic review of multi-product biorefinery approaches for water hyacinth based renewable energy, IScience 28 (2025) 112807. https://doi.org/10.1016/j.isci.2025.112807.

[6] United Nations, Transforming our world: the 2030 Agenda for Sustainable Development. Resolution adopted by the General Assembly on 25 September 2015, A/RES/70/1. New York: United Nations; 2015., Https://Unctad.Org/Node/7351 (n.d.).

[7] M. Rinaudo, Chitin and chitosan: Properties and applications, Prog. Polym. Sci. 31 (2006) 603–632. https://doi.org/10.1016/J.PROGPOLYMSCI.2006.06.001.

[8] Global Chitosan Market by Product (Food Grade, Industrial Grade, Pharmaceutical Grade), Source (Crab, Krill, Shrimp), Packaging Material, Application - Forecast 2024-2030, (n.d.). https://www.researchandmarkets.com/report/chitosan#rela0-338576 (accessed May 2, 2024).

[9] F. Arrouze, J. Desbrieres, M. Rhazi, M. Essahli, A. Tolaimate, Valorization of chitins extracted from North Morocco shrimps: Comparison of chitin reactivity and characteristics, J. Appl. Polym. Sci. 136 (2019). https://doi.org/10.1002/app.47804.

[10] J. Hou, B.E. Aydemir, A.G. Dumanli, Understanding the structural diversity of chitins as a versatile biomaterial, Philosophical Transactions of the Royal Society A: Mathematical, Physical and Engineering Sciences 379 (2021). https://doi.org/10.1098/rsta.2020.0331.

[11] Z. Mei, P. Kuzhir, G. Godeau, Update on Chitin and Chitosan from Insects: Sources, Production, Characterization, and Biomedical Applications, Biomimetics 9 (2024). https://doi.org/10.3390/biomimetics9050297.

[12] G. Galassi, C. Jucker, P. Parma, D. Lupi, G.M. Crovetto, S. Savoldelli, S. Colombini, Impact of Agro-industrial Byproducts on Bioconversion, Chemical Composition, in vitro Digestibility, and Microbiota of the Black Soldier Fly (Diptera: Stratiomyidae) Larvae, Journal of Insect Science 21 (2021). https://doi.org/10.1093/jisesa/ieaa148.

[13] H. González-Lara, B. Parra-Pacheco, E. Rico-García, H. Aguirre-Becerra, A.A. Feregrino-Pérez, J.F. García-Trejo, Black Soldier Fly Culture as a Source of Chitin and Chitosan for Its Potential Use in Concrete: An Overview, Polymers (Basel). 17 (2025) 717. https://doi.org/10.3390/polym17060717.

[14] G.I. Guangorena Zarzosa, T. Kobayashi, Properties of Chitin and Its Regenerated Hydrogels from the Insect Zophobas morio Fed Citrus Biomass or Polystyrene, Gels 10 (2024) 433. https://doi.org/10.3390/gels10070433.

[15] C.K.S. Pillai, W. Paul, C.P. Sharma, Chitin and chitosan polymers: Chemistry, solubility and fiber formation, Prog. Polym. Sci. 34 (2009) 641–678. https://doi.org/10.1016/j.progpolymsci.2009.04.001.

[16] G. Crini, Historical Landmarks in the Discovery of Chitin, in: 2019: pp. 1–47. https://doi.org/10.1007/978-3-030-16538-3_1.

[17] N. Morin-Crini, E. Lichtfouse, G. Torri, G. Crini, Applications of chitosan in food, pharmaceuticals, medicine, cosmetics, agriculture, textiles, pulp and paper, biotechnology, and environmental chemistry, Environ. Chem. Lett. 17 (2019) 1667–1692. https://doi.org/10.1007/s10311-019-00904-x.

[18] B.E. Teixeira-Costa, C.T. Andrade, Chitosan as a Valuable Biomolecule from Seafood Industry Waste in the Design of Green Food Packaging, Biomolecules 11 (2021) 1599. https://doi.org/10.3390/biom11111599.

[19] T. Hahn, E. Tafi, A. Paul, R. Salvia, P. Falabella, S. Zibek, Current state of chitin purification and chitosan production from insects, Journal of Chemical

Technology & Biotechnology 95 (2020) 2775–2795. https://doi.org/10.1002/jctb.6533.

[20] A. Bouanga, S. El Assri, R. Bouharroud, A. Asehraou, V.L. Balázs, A. Széchenyi, V. Hock, R. Sabbahi, Chitosan at the crossroads: Engineering sustainable biofunctional materials for health, food, and environmental resilience, Int. J. Biol. Macromol. 353 (2026) 151305. https://doi.org/10.1016/j.ijbiomac.2026.151305.

[21] Y. Rohyami, N.A. Sari, Simple method on determination of deacetyllation degree for chitosan, in: 2021: p. 030003. https://doi.org/10.1063/5.0062473.

[22] M. Rinaudo, M. Milas, P. Le Dung, Characterization of chitosan. Influence of ionic strength and degree of acetylation on chain expansion, Int. J. Biol. Macromol. 15 (1993) 281–285. https://doi.org/10.1016/0141-8130(93)90027-J.

[23] C.Y. Soon, Y.B. Tee, C.H. Tan, A.T. Rosnita, A. Khalina, Extraction and physicochemical characterization of chitin and chitosan from Zophobas morio larvae in varying sodium hydroxide concentration, Int. J. Biol. Macromol. 108 (2018) 135–142. https://doi.org/10.1016/j.ijbiomac.2017.11.138.

[24] H. Tomida, T. Fujii, N. Furutani, A. Michihara, T. Yasufuku, K. Akasaki, T. Maruyama, M. Otagiri, J.M. Gebicki, M. Anraku, Antioxidant properties of some different molecular weight chitosans, Carbohydr. Res. 344 (2009) 1690–1696. https://doi.org/10.1016/j.carres.2009.05.006.

[25] E. Vafa, R. Bazargan-Lari, M.E. Bahrololoom, Electrophoretic deposition of polyvinyl alcohol/natural chitosan/bioactive glass composite coatings on 316L stainless steel for biomedical application, Prog. Org. Coat. 151 (2021) 106059. https://doi.org/10.1016/j.porgcoat.2020.106059.

[26] M. Kaya, M. Asan-Ozusaglam, S. Erdogan, Comparison of antimicrobial activities of newly obtained low molecular weight scorpion chitosan and medium molecular weight commercial chitosan, J. Biosci. Bioeng. 121 (2016) 678–684. https://doi.org/10.1016/J.JBIOSC.2015.11.005.

[27] S. Olza, N.M. Hadj Bouzidi, L. Rubatat, V. Pellerin, U. Montejo, A. Alonso-Varona, S.C.M. Fernandes, Mineralized chitin nanocrystals enhance osteoinductive ability of chitosan 3D porous biohybrid scaffolds for bone tissue regeneration, Carbohydr. Polym. 366 (2025) 123911. https://doi.org/10.1016/j.carbpol.2025.123911.

[28] M. Triunfo, E. Tafi, A. Guarnieri, R. Salvia, C. Scieuzo, T. Hahn, S. Zibek, A. Gagliardini, L. Panariello, M.B. Coltelli, A. De Bonis, P. Falabella,

Characterization of chitin and chitosan derived from Hermetia illucens, a further step in a circular economy process, Sci. Rep. 12 (2022). https://doi.org/10.1038/s41598-022-10423-5.

[29] M. Rhazi, J. Desbrières, A. Tolaimate, A. Alagui, P. Vottero, Investigation of different natural sources of chitin: influence of the source and deacetylation process on the physicochemical characteristics of chitosan, Polym Int 49 (2000) 337–344.

[30] A.I. Saenz-Mendoza, P.B. Zamudio-Flores, M.C. García-Anaya, C.R. Velasco, C.H. Acosta-Muñiz, M. Espino-Díaz, J.M. Tirado-Gallegos, M. Hernández-González, G. Vela-Gutiérrez, R. Salgado-Delgado, J.R. Rendón-Villalobos, A. Ortega-Ortega, Insects as a potential source of chitin and chitosan: Physicochemical, morphological and structural characterization. -A review, Emir. J. Food Agric. (2023). https://doi.org/10.9755/ejfa.2023.v35.i5.3095.

[31] A.C. Neville, Chitin Orientation in Cuticle and its Control, in: 1967: pp. 213–286. https://doi.org/10.1016/S0065-2806(08)60209-X.

[32] A.C. Neville, Biology of the Arthropod Cuticle, Springer Berlin Heidelberg, Berlin, Heidelberg, 1975. https://doi.org/10.1007/978-3-642-80910-1.

[33] S. Sviben, O. Spaeker, M. Bennet, M. Albéric, J.-H. Dirks, B. Moussian, P. Fra£l, L. Bertinetti, Y. Politi, Epidermal Cell Surface Structure and Chitin–Protein Co-assembly Determine Fiber Architecture in the Locust Cuticle, ACS Appl. Mater. Interfaces 12 (2020) 25581–25590. https://doi.org/10.1021/acsami.0c04572.

[34] J.-H. Dirks, A dermal light sensor controls anisotropic biomechanical properties in insect cuticle, J. Mech. Behav. Biomed. Mater. 169 (2025) 107076. https://doi.org/10.1016/j.jmbbm.2025.107076.

[35] M.A. Diab, A.Z. El-Sonbati, M.M. Al-Halawany, D.M.D. Bader, Thermal Stability and Degradation of Chitosan Modified by Cinnamic Acid, Open Journal of Polymer Chemistry 02 (2012) 14–20. https://doi.org/10.4236/ojpchem.2012.21003.

[36] H. Moussout, H. Ahlafi, M. Aazza, M. Bourakhouadar, Kinetics and mechanism of the thermal degradation of biopolymers chitin and chitosan using thermogravimetric analysis, Polym. Degrad. Stab. 130 (2016) 1–9. https://doi.org/10.1016/j.polymdegradstab.2016.05.016.

[37] A. Pawlak, M. Mucha, Thermogravimetric and FTIR studies of chitosan blends, Thermochim. Acta 396 (2003) 153–166. https://doi.org/10.1016/S0040-6031(02)00523-3.

[38] B. Focher, P.L. Beltrame, A. Naggi, G. Torri, Alkaline N-deacetylation of chitin enhanced by flash treatments. Reaction kinetics and structure modifications, Carbohydr. Polym. 12 (1990) 405–418. https://doi.org/10.1016/0144-8617(90)90090-F.

[39] M. Râpaˇ, C. Vasile, Processing and Properties of Chitosan and/or Chitin Biocomposites for Food Packaging, in: Food Packaging, CRC Press, First edition. | Boca Raton, FL : CRC Press, 2020., 2020: pp. 291–326. https://doi.org/10.1201/9780429322129-11.

[40] M.B. Coltelli, V. Gigante, L. Panariello, L. Aliotta, C. Scieuzo, P. Falabella, A. Lazzeri, Chitin and chitosan materials from black soldier fly (Hermetia illucens): An insight onto their thermal degradation and mechanical behavior linked to their copolymeric structure, Polym. Test. 150 (2025) 108922. https://doi.org/10.1016/j.polymertesting.2025.108922.

[41] H. Hemmami, S. Zeghoud, I. Ben Amor, S. Ahmed, Chitin and Chitosan Characterization: Spectroscopic Methods, in: Chitin and Chitosan, Jenny Stanford Publishing, New York, 2024: pp. 221–254. https://doi.org/10.1201/9781003589778-8.

[42] H. Moussout, M. Aazza, H. Ahlafi, Thermal degradation characteristics of chitin, chitosan, Al2O3/chitosan, and benonite/chitosan nanocomposites, Handbook of Chitin and Chitosan: Volume 2: Composites and Nanocomposites from Chitin and Chitosan, Manufacturing and Characterisations (2020) 139–174. https://doi.org/10.1016/B978-0-12-817968-0.00005-6.

[43] S. Ramachandran, M. Rajinipriya, J. Soulestin, M. Nagalakshmaiah, Recent Developments in Chitosan-Based Nanocomposites, in: Bio-Based Polymers and Nanocomposites, Springer International Publishing, Cham, 2019: pp. 183–215. https://doi.org/10.1007/978-3-030-05825-8_9.

[44] M. Yanat, K. Schroën, Advances in chitin-based nanoparticle use in biodegradable polymers: A review, Carbohydr. Polym. 312 (2023) 120789. https://doi.org/10.1016/J.CARBPOL.2023.120789.

[45] J. Vinsova, E. Vavrikova, Chitosan Derivatives with Antimicrobial, Antitumour and Antioxidant Activities - a Review, Curr. Pharm. Des. 17 (2011) 3596–3607. https://doi.org/10.2174/138161211798194468.

[46] Samira Jebahi, Repair of bone defect using bioglass-chitosan as a pharmaceutical drug: An experimental study in an ovariectomised rat model, Afr. J. Pharm. Pharmacol. 6 (2012). https://doi.org/10.5897/AJPP12.214.

[47] E. Ablouh, A. Essaghraoui, N. Eladlani, M. Rhazi, M. Taourirte, Uptake of Pb(II) onto nanochitosan/sodium alginate hybrid beads: Mechanism and kinetics study, Water Environment Research 91 (2019) 239–249. https://doi.org/10.1002/wer.1050.

[48] M. Rhazi, A. Tolaimate, Y. Habibi, INTERACTIONS OF CHITOSAN WITH METALS FOR WATER PURIFICATION, in: 2012. https://doi.org/10.1002/9781118229484.ch4 (accessed August 5, 2024).

[49] S. Elouali, H. Ait Ali Ouydir, Y. Ait Hamdan, N. Eladlani, M. Rhazi, Chitosan from Periplaneta americana L.: a sustainable solution for heavy metals removal, EuroMediterr J Environ Integr (2024). https://doi.org/10.1007/s41207-024-00645-6.

[50] N. Eladlani, E. Montassir Dahmane, M. Rhazi, M. Taourirte, Y. Habibi, H. Tudor, COMPLEXATION OF CHROMIUM (III) IONS WITH CHITOSAN AND ITS DERIVATIVES, NANOPARTICLES AND WHISKERS, Fresenius Environ. Bull. 23 (2014) 3278–3285.

[51] P.M.C. Matias, J.F.M. Sousa, E.F. Bernardino, J.P. Vareda, L. Durães, P.E. Abreu, J.M.C. Marques, D. Murtinho, A.J.M. Valente, Reduced Chitosan as a Strategy for Removing Copper Ions from Water, Molecules 28 (2023) 4110. https://doi.org/10.3390/molecules28104110.

[52] M. Monier, Adsorption of Hg2+, Cu2+ and Zn2+ ions from aqueous solution using formaldehyde cross-linked modified chitosan–thioglyceraldehyde Schiff's base, Int. J. Biol. Macromol. 50 (2012) 773–781. https://doi.org/10.1016/j.ijbiomac.2011.11.026.

[53] X. Zhang, R. Bai, Mechanisms and kinetics of humic acid adsorption onto chitosan-coated granules, J. Colloid Interface Sci. 264 (2003) 30–38. https://doi.org/10.1016/S0021-9797(03)00393-X.

[54] Y. Chen, Y. Chen, D. Lu, Y. Qiu, Synthesis of a Novel Water-Soluble Polymer Complexant Phosphorylated Chitosan for Rare Earth Complexation, Polymers (Basel). 14 (2022) 419. https://doi.org/10.3390/polym14030419.

[55] F. El Amerany, M. Rhazi, G. Balcke, S. Wahbi, A. Meddich, M. Taourirte, B. Hause, The Effect of Chitosan on Plant Physiology, Wound Response, and Fruit Quality of Tomato, Polymers (Basel). 14 (2022) 5006. https://doi.org/10.3390/polym14225006.

[56] S. Boulila, H. Oudadesse, R. Kallel, F. Ghrab, B. Lefeuvre, T. Boudawara, A. Elfeki, H. Elfeki, The performance of a scaffold bioglass–chitosan in the treatment of bone defect, Polymer Bulletin 75 (2018) 5567–5586. https://doi.org/10.1007/s00289-018-2342-x.

[57] Q. Wu, E. Jungstedt, M. Šoltésová, N.E. Mushi, L.A. Berglund, High strength nanostructured films based on well-preserved β-chitin nanofibrils †, (2019). https://doi.org/10.1039/c9nr02870f.

[58] C. Zheng, K. Sun, Q. Wu, Y. Sun, B. Xu, Adsorption of ionic contaminants from complex water matrices by versatile chitosan-based beads, Bioresour. Technol. 411 (2024) 131332. https://doi.org/10.1016/J.BIORTECH.2024.131332.

[59] H. Abdollahi, S. Amiri, F. Amiri, S. Moradi, P. Zarrintaj, Antibacterial Biocomposite Based on Chitosan/Pluronic/Agarose Noncovalent Hydrogel: Controlled Drug Delivery by Alginate/Tetracycline Beads System, J. Funct. Biomater. 15 (2024) 286. https://doi.org/10.3390/j™15100286.

[60] S. Bensalem, B. Hamdi, S. Del Confetto, R. Calvet, Characterization of surface properties of chitosan/bentonite composites beads by inverse gas chromatography, Int. J. Biol. Macromol. 166 (2021) 1448–1459. https://doi.org/10.1016/j.ijbiomac.2020.11.024.

[61] I. Arzate-Vázquez, J.J. Chanona-Pérez, G. Calderón-Domínguez, E. Terres-Rojas, V. Garibay-Febles, A. Martínez-Rivas, G.F. Gutiérrez-López, Microstructural characterization of chitosan and alginate films by microscopy techniques and texture image analysis, Carbohydr. Polym. 87 (2012) 289–299. https://doi.org/10.1016/j.carbpol.2011.07.044.

[62] T.M. Le, C.L. Tran, T.X. Nguyen, Y.H.P. Duong, P.K. Le, V.T. Tran, Green Preparation of Chitin and Nanochitin from Black Soldier Fly for Production of Biodegradable Packaging Material, J. Polym. Environ. 31 (2023) 3094–3105. https://doi.org/10.1007/s10924-023-02793-2.

[63] M.A. Islam, M.N. Hasan, M.S.H. Evan, M.J. Uddin, W.S. Tulin, M.S. Islam, M.U. Khandaker, I.M.M. Rahman, F.I. Chowdhury, Chitin nanofibers: recent advances in preparation and applications in biomedical and beyond, RSC Adv. 15 (2025) 14655–14690. https://doi.org/10.1039/D4RA06937D.

[64] S. Ifuku, H. Kaminaka, Md.I. Shams, Nanochitin From Crab Shells: Production, Chemical Modification, Composite Materials, and Physiological Functions, Macromol. Rapid Commun. 46 (2025). https://doi.org/10.1002/marc.202400765.

[65] N. Petelinšek, S. Mommer, Tough Hydrogels for Load-Bearing Applications, Advanced Science 11 (2024). https://doi.org/10.1002/advs.202307404.

[66] C.D. Díaz-Marín, L. Masetti, M.A. Roper, K.E. Hector, Y. Zhong, Z. Lu, O.R. Caylan, G. Graeber, J.C. Grossman, Physics-based prediction of moisture-capture properties of hydrogels, Nat. Commun. 15 (2024) 8948. https://doi.org/10.1038/s41467-024-53291-5.

[67] M.C.G. Pellá, M.K. Lima-Tenório, E.T. Tenório-Neto, M.R. Guilherme, E.C. Muniz, A.F. Rubira, Chitosan-based hydrogels: From preparation to biomedical applications, Carbohydr. Polym. 196 (2018) 233–245. https://doi.org/10.1016/j.carbpol.2018.05.033.

[68] X.Y. Godeau, F.J. Andrianandrasana, O. Volkova, C.R. Szczepanski, A. Zenerino, O. Montreuil, R.P. Godeau, P. Kuzhir, G. Godeau, Investigation on dung beetle's (Heliocopris Hope, 1838) chitosan valorisation for hydrogel 3D printing, Int. J. Biol. Macromol. 199 (2022) 172–180. https://doi.org/10.1016/J.IJBIOMAC.2021.12.077.

[69] S. Van Vlierberghe, P. Dubruel, E. Schacht, Biopolymer-based hydrogels as scaffolds for tissue engineering applications: A review, Biomacromolecules 12 (2011) 1387–1408. https://doi.org/10.1021/bm200083n.

[70] A.A. Al-esnawy, K.T. Ereiba, A.M. Bakr, A.S. Abdraboh, Characterization and antibacterial activity of Streptomycin Sulfate loaded Bioglass/Chitosan beads for bone tissue engineering, J. Mol. Struct. 1227 (2021) 129715. https://doi.org/10.1016/J.MOLSTRUC.2020.129715.

[71] M. Dash, F. Chiellini, R.M. Ottenbrite, E. Chiellini, Chitosan—A versatile semi-synthetic polymer in biomedical applications, Prog. Polym. Sci. 36 (2011) 981–1014. https://doi.org/10.1016/j.progpolymsci.2011.02.001.

[72] F. Croisier, C. Jérôme, Chitosan-based biomaterials for tissue engineering, Eur. Polym. J. 49 (2013) 780–792. https://doi.org/10.1016/j.eurpolymj.2012.12.009.

[73] J. Refifi, H. Oudadesse, O. Merdrignac-Conanec, H. El Feki, B. Lefeuvre, Salt leaching using powder (SLUP) process for glass/chitosan scaffold elaboration for biomaterial applications, Journal of the Australian Ceramic Society 56 (2020) 1167–1178. https://doi.org/10.1007/s41779-020-00460-6.

[74] H. Oudadesse, S. Najem, S. Mosbahi, N. Rocton, J. Refifi, H. El Feki, B. Lefeuvre, Development of hybrid scaffold: Bioactive glass nanoparticles/chitosan for tissue

engineering applications, J. Biomed. Mater. Res. A 109 (2021) 590–599. https://doi.org/10.1002/jbm.a.37043.

[75] S.I. Ahmad, R. Ahmad, M.S. Khan, R. Kant, S. Shahid, L. Gautam, G.M. Hasan, M.I. Hassan, Chitin and its derivatives: Structural properties and biomedical applications, Int. J. Biol. Macromol. 164 (2020) 526–539. https://doi.org/10.1016/j.ijbiomac.2020.07.098.

[76] N.I.W. Azelee, D. Dahiya, S. Ayothiraman, N.M. Noor, Z.I.A. Rasid, A.N.M. Ramli, B. Ravindran, F.U. Iwuchukwu, R. Selvasembian, Sustainable valorization approaches on crustacean wastes for the extraction of chitin, bioactive compounds and their applications - A review, Int. J. Biol. Macromol. 253 (2023) 126492. https://doi.org/10.1016/j.ijbiomac.2023.126492.

[77] I. Younes, S. Hajji, V. Frachet, M. Rinaudo, K. Jellouli, M. Nasri, Chitin extraction from shrimp shell using enzymatic treatment. Antitumor, antioxidant and antimicrobial activities of chitosan, Int. J. Biol. Macromol. 69 (2014) 489–498. https://doi.org/10.1016/J.IJBIOMAC.2014.06.013.

[78] Y.-S. Lin, S.-H. Liang, W.-L. Lai, J.-X. Lee, Y.-P. Wang, Y.-T. Liu, S.-H. Wang, M.-H. Lee, Sustainable Extraction of Chitin from Spent Pupal Shell of Black Soldier Fly, Processes 9 (2021) 976. https://doi.org/10.3390/pr9060976.

[79] S. Elouali, Y. Ait Hamdan, M. Belmajdoub, M. Rhazi, Green chitosan extraction from Hermetia illucens breeding waste (prepupal cases): Characterization and bioadsorption activity, Int. J. Biol. Macromol. 281 (2024) 136449. https://doi.org/10.1016/j.ijbiomac.2024.136449.

[80] H. El Knidri, R. El Khalfaouy, A. Laajeb, A. Addaou, A. Lahsini, Eco-friendly extraction and characterization of chitin and chitosan from the shrimp shell waste via microwave irradiation, Process Safety and Environmental Protection 104 (2016) 395–405. https://doi.org/10.1016/J.PSEP.2016.09.020.

[81] M. Çelebi, A. Tav, M.A. Kaya, Z.Ö. Özdemir, Scalable Production of Low-Molecular-Weight Chitosan: Comparative Study of Conventional, Microwave, and Autoclave-Assisted Methods, Polymers (Basel). 18 (2026) 213. https://doi.org/10.3390/polym18020213.

[82] Q. Zhang, L. Duan, Y. Li, Positive effects and mechanism of ultrasound on chitin preparation from shrimp shells by co-fermentation, Ultrason. Sonochem. 88 (2022) 106066. https://doi.org/10.1016/j.ultsonch.2022.106066.

[83] X. Mao, J. Zhang, F. Kan, Y. Gao, J. Lan, X. Zhang, Z. Hu, Y. Li, H. Lin, Antioxidant production and chitin recovery from shrimp head fermentation with Streptococcus thermophilus, Food Sci. Biotechnol. 22 (2013) 1023–1032. https://doi.org/10.1007/s10068-013-0179-5.

[84] K. Kurita, Controlled functionalization of the polysaccharide chitin, Prog. Polym. Sci. 26 (2001) 1921–1971. https://doi.org/10.1016/S0079-6700(01)00007-7.

[85] A. Tolaimate, J. Desbrieres, M. Rhazi, A. Alagui, Contribution to the preparation of chitins and chitosans with controlled physico-chemical properties, Polymer (Guildf). 44 (2003) 7939–7952. https://doi.org/10.1016/J.POLYMER.2003.10.025.

[86] Broussignac P, High natural polymer known in the industry: chitosan, Chim Ind Genie Chim 99 (1968) 1241–1247.

[87] K. Piekarska, M. Sikora, M. Owczarek, J. Jóźwik-Pruska, M. Wiśniewska-Wrona, Chitin and Chitosan as Polymers of the Future—Obtaining, Modification, Life Cycle Assessment and Main Directions of Application, Polymers (Basel). 15 (2023) 793. https://doi.org/10.3390/polym15040793.

[88] J.L. Vidal, T. Jin, E. Lam, F. Kerton, A. Moores, Blue is the new green: Valorization of crustacean waste, Current Research in Green and Sustainable Chemistry 5 (2022) 100330. https://doi.org/10.1016/j.crgsc.2022.100330.

[89] E. Lizundia, F. Luzi, D. Puglia, Organic waste valorisation towards circular and sustainable biocomposites, Green Chemistry 24 (2022) 5429–5459. https://doi.org/10.1039/D2GC01668K.

[90] R. Smets, B. Verbinnen, I. Van De Voorde, G. Aerts, J. Claes, · Mik, V. Der Borght, Sequential Extraction and Characterisation of Lipids, Proteins, and Chitin from Black Soldier Fly (Hermetia illucens) Larvae, Prepupae, and Pupae, Waste Biomass Valorization 11 (2020) 6455–6466. https://doi.org/10.1007/s12649-019-00924-2.

[91] M. El-Sheikh, A. Badry, M. Abdelaal, A. Abd El-Aziz, 1-Preparation, Characterization, and Efficiency of Loading Leiurus quinquestriatus Venom on Chitosan Nanoparticles Extracted from Some Scorpions ., Egypt. Acad. J. Biol. Sci. B Zool. 14 (2022) 373–396. https://doi.org/10.21608/eajbsz.2022.272455.

[92] F. Arrouze, J. Desbrieres, S. Lidrissi Hassani, A. Tolaimate, Investigation of β-chitin extracted from cuttlefish: comparison with squid β-chitin, Polymer Bulletin 78 (2021) 7219–7239. https://doi.org/10.1007/s00289-020-03466-z.

[93] M. Kozma, B. Acharya, R. Bissessur, Chitin, Chitosan, and Nanochitin: Extraction, Synthesis, and Applications, Polymers (Basel). 14 (2022) 3989. https://doi.org/10.3390/polym14193989.

[94] B.T. Iber, N.A. Kasan, D. Torsabo, J.W. Omuwa, A review of various sources of chitin and chitosan in nature, J. Renew. Mater. 10 (2022) 1097–1123. https://doi.org/10.32604/JRM.2022.018142.

[95] N.A. Zainol Abidin, F. Kormin, N.A. Zainol Abidin, N.A.F. Mohamed Anuar, M.F. Abu Bakar, The Potential of Insects as Alternative Sources of Chitin: An Overview on the Chemical Method of Extraction from Various Sources, Int. J. Mol. Sci. 21 (2020) 4978. https://doi.org/10.3390/ijms21144978.

[96] A. Xiong, L. Ruan, K. Ye, Z. Huang, C. Yu, Extraction of Chitin from Black Soldier Fly (Hermetia illucens) and Its Puparium by Using Biological Treatment, . 13 (2023) 1424. https://doi.org/10.3390/life13071424.

[97] C. Pedrazzani, L. Righi, F. Vescovi, L. Maistrello, A. Caligiani, Black soldier fly as a New chitin source: Extraction, purification and molecular/structural characterization, LWT 191 (2024) 115618. https://doi.org/10.1016/j.lwt.2023.115618.

[98] I. Younes, M. Rinaudo, Chitin and Chitosan Preparation from Marine Sources. Structure, Properties and Applications, Mar. Drugs 13 (2015) 1133–1174. https://doi.org/10.3390/md13031133.

[99] FAO, Fishery and Aquaculture Country Profiles: The Kingdom of Morocco, Food and Agriculture Organization of the United Nations (2022).

[100] F. Arrouze, M. Essalhi, M. Rhazi, J. Desbrières, A. Tolaimate, Chitin and chitosan: Study of the possibilities of their production by valorization of the waste of crustaceans and cephalopods rejected in Essaouira, Journal of Materials and Environmental Sciences 8 (2017) 2251–2258.

[101] I. Junceda-Mena, E. García-Junceda, J. Revuelta, From the problem to the solution: Chitosan valorization cycle, Carbohydr. Polym. 309 (2023) 120674. https://doi.org/10.1016/j.carbpol.2023.120674.

[102] F. Devlieghere, A. Vermeulen, J. Debevere, Chitosan: antimicrobial activity, interactions with food components and applicability as a coating on fruit and vegetables, Food Microbiol. 21 (2004) 703–714. https://doi.org/10.1016/j.fm.2004.02.008.

[103] T. Sukmark, P. Rachtanapun, C. Rachtanapun, Antimicrobial Activity of Oligomer and Polymer Chitosan from Different Sources against Foodborne Pathogenic Bacteria, 2011.

[104] A. Saravanan, · V Parthasarathy, · P Senthil Kumar, Antimicrobial, antifungal, and antioxidant activities of the extracted chitosan from shrimp shell waste and its bioadsorption study of heavy metals from the aqueous solution, 14 (2024) 18109–18119. https://doi.org/10.1007/s13399-023-04078-z.

[105] C.-L. Ke, F.-S. Deng, C.-Y. Chuang, C.-H. Lin, M. Bardosova, polymers Antimicrobial Actions and Applications of Chitosan, (2021). https://doi.org/10.3390/polym13060904.

[106] V. Balaram, L. Copia, U.S. Kumar, J. Miller, S. Chidambaram, Pollution of water resources and application of ICP-MS techniques for monitoring and management—A comprehensive review, Geosystems and Geoenvironment 2 (2023) 100210. https://doi.org/10.1016/j.geogeo.2023.100210.

[107] G. Genchi, M.S. Sinicropi, G. Lauria, A. Carocci, A. Catalano, The Effects of Cadmium Toxicity, Int. J. Environ. Res. Public Health 17 (2020) 3782. https://doi.org/10.3390/ijerph17113782.

[108] M. Kitazawa, H.-W. Hsu, R. Medeiros, Copper Exposure Perturbs Brain Inflammatory Responses and Impairs Clearance of Amyloid-Beta, Toxicological Sciences 152 (2016) 194–204. https://doi.org/10.1093/toxsci/kfw081.

[109] N. Singh, B. Sharma, On the Mechanisms of Heavy Metal-Induced Neurotoxicity: Amelioration by Plant Products, Proceedings of the National Academy of Sciences, India Section B: Biological Sciences 91 (2021) 743–751. https://doi.org/10.1007/s40011-021-01272-9.

[110] B. Du, J. Zhou, B. Lu, C. Zhang, D. Li, J. Zhou, S. Jiao, K. Zhao, H. Zhang, Environmental and human health risks from cadmium exposure near an active lead-zinc mine and a copper smelter, China, Science of The Total Environment 720 (2020) 137585. https://doi.org/10.1016/J.SCITOTENV.2020.137585.

[111] H. Zengin, G. Toprak, G. Zengin, Investigation of adsorption performance of calcium oxide particles upon various treatments, Water Res. 243 (2023) 120380. https://doi.org/10.1016/j.watres.2023.120380.

[112] E. Solis-Toapanta, P. Fisher, C. Gómez, Growth Rate and Nutrient Uptake of Basil in Small-scale Hydroponics, HortScience 55 (2020) 507–514. https://doi.org/10.21273/HORTSCI14727-19.

[113] S. Agarwal, H. Dubey, C.L. Jain, A STUDY ON HYDROPONIC FARMING, International Journal for Multidisciplinary Research (IJFMR) 5 (2023). www.ijfmr.com.

[114] G. Crini, E. Lichtfouse, Advantages and disadvantages of techniques used for wastewater treatment, Environ. Chem. Lett. 17 (2019) 145–155. https://doi.org/10.1007/s10311-018-0785-9.

[115] M. Vakili, M. Rafatullah, B. Salamatinia, A.Z. Abdullah, M.H. Ibrahim, K.B. Tan, Z. Gholami, P. Amouzgar, Application of chitosan and its derivatives as adsorbents for dye removal from water and wastewater: A review, Carbohydr. Polym. 113 (2014) 115–130. https://doi.org/10.1016/j.carbpol.2014.07.007.

[116] M. Zhang, Y. Liu, Z. Yin, D. Feng, H. Lv, Preparation and adsorption properties of magnetic chitosan/sludge biochar composites for removal of Cu2+ ions, Sci. Rep. 13 (2023) 20937. https://doi.org/10.1038/s41598-023-46815-4.

[117] S. Shahraki, H. Samareh Delarami, Magnetic chitosan-(d-glucosimine methyl)benzaldehyde Schiff base for Pb+2 ion removal. Experimental and theoretical methods, Carbohydr. Polym. 200 (2018) 211–220. https://doi.org/10.1016/j.carbpol.2018.07.081.

[118] J. Wang, X. Guo, Adsorption kinetic models: Physical meanings, applications, and solving methods, J. Hazard. Mater. 390 (2020) 122156. https://doi.org/10.1016/j.jhazmat.2020.122156.

[119] A. Gougbedji, P. Agbohessou, P.A. Lalèyè, F. Francis, R.C. Megido, Inventaire des coproduits agricoles potentiellement utilisables pour la production de pupes de mouche Hermetia illucens (L. 1758) pour l'alimentation piscicole au Bénin, Tropicultura 38 (2020) 1–18. https://doi.org/10.25518/2295-8010.1587.

[120] R. Zhu, X. Zhang, Y. Wang, L. Zhang, C. Wang, F. Hu, C. Ning, G. Chen, Pectin oligosaccharides from hawthorn (Crataegus pinnatifida Bunge. Var. major): Molecular characterization and potential antiglycation activities, Food Chem. 286 (2019) 129–135. https://doi.org/10.1016/J.FOODCHEM.2019.01.215.

[121] X. Liu, X. Chen, H. Wang, Q. Yang, K. ur Rehman, W. Li, M. Cai, Q. Li, L. Mazza, J. Zhang, Z. Yu, L. Zheng, Dynamic changes of nutrient composition throughout the entire life cycle of black soldier fly, (2017). https://doi.org/10.1371/journal.pone.0182601.

[122] V. Bandura, L. Fialkovska, P. Osadchuk, Y. Levtrynskaia, A. Palvashova, INVESTIGATION OF PROPERTIES OF SUNFLOWER AND RAPESEED OILS

OBTAINED BY THE SOXHLET AND MICROWAVE EXTRACTION METHODS, Agraarteadus 33 (2022) 48–58. https://doi.org/10.15159/jas.22.17.

[123] M.M. Bradford, A rapid and sensitive method for the quantitation of microgram quantities of protein utilizing the principle of protein-dye binding, Anal. Biochem. 72 (1976) 248–254. https://doi.org/10.1016/0003-2697(76)90527-3.

[124] M.R. Kasaai, A review of several reported procedures to determine the degree of N-acetylation for chitin and chitosan using infrared spectroscopy, Carbohydr. Polym. 71 (2008) 497–508. https://doi.org/10.1016/J.CARBPOL.2007.07.009.

[125] M.L. Duarte, M.C. Ferreira, M.R. Marvão, J. Rocha, An optimised method to determine the degree of acetylation of chitin and chitosan by FTIR spectroscopy, Int. J. Biol. Macromol. 31 (2002) 1–8. https://doi.org/10.1016/S0141-8130(02)00039-9.

[126] R.H. Chen, M.L. Tsaih, Effect of temperature on the intrinsic viscosity and conformation of chitosans in dilute HCl solution, Int. J. Biol. Macromol. 23 (1998) 135–141. https://doi.org/10.1016/S0141-8130(98)00036-1.

[127] R. Rotaru, M. Savin, N. Tudorachi, C. Peptu, P. Samoila, L. Sacarescu, V. Harabagiu, Ferromagnetic iron oxide-cellulose nanocomposites prepared by ultrasonication, Polym. Chem. 9 (2018) 860–868. https://doi.org/10.1039/c7py01587a.

[128] N. Balázs, P. Sipos, Limitations of pH-potentiometric titration for the determination of the degree of deacetylation of chitosan, Carbohydr. Res. 342 (2007) 124–130. https://doi.org/10.1016/J.CARRES.2006.11.016.

[129] A. Tolaimate, J. Desbrières, M. Rhazi, A. Alagui, M. Vincendon, P. Vottero, On the influence of deacetylation process on the physicochemical characteristics of chitosan from squid chitin, Polymer (Guildf). 41 (2000) 2463–2469. https://doi.org/10.1016/S0032-3861(99)00400-0.

[130] Y.A. Hamdan, S. Elouali, N. Eladlani, B. Lefeuvre, H. Oudadesse, M. Rhazi, Investigation on Akis granulifera (Coleoptera, Sahlberg, 1823) as a potential source of chitin and chitosan: Extraction, characterization and hydrogel formation, Int. J. Biol. Macromol. 252 (2023) 126292. https://doi.org/10.1016/J.IJBIOMAC.2023.126292.

[131] T. Spranghers, M. Ottoboni, C. Klootwijk, A. Ovyn, S. Deboosere, B. De Meulenaer, J. Michiels, M. Eeckhout, P. De Clercq, S. De Smet, Nutritional composition of black soldier fly (Hermetia illucens) prepupae reared on different

organic waste substrates, J. Sci. Food Agric. 97 (2017) 2594–2600. https://doi.org/10.1002/jsfa.8081.

[132] E. Mirwandhono, M.I.A. Nasution, Yunilas, Extraction of chitin and chitosan black soldier fly (Hermetia illucens) prepupa phase on characterization and yield, IOP Conf. Ser. Earth Environ. Sci. 1114 (2022) 012019. https://doi.org/10.1088/1755-1315/1114/1/012019.

[133] T. Hahn, E. Tafi, N. Von Seggern, P. Falabella, R. Salvia, J. Thomä, · Eva Febel, M. Fijalkowska, E. Schmitt, L. Stegbauer, · Susanne Zibek, Purification of Chitin from Pupal Exuviae of the Black Soldier Fly Statement of Novelty, 13 (2022) 1993–2008. https://doi.org/10.1007/s12649-021-01645-1.

[134] S. Elkadaoui, M. Azzi, J. Desbrieres, J. Zim, Y. El Hachimi, A. Tolaimate, Valorization of Hermetia illucens breeding rejects by chitins and chitosans production. Influence of processes and life cycle on their physicochemical characteristics, Int. J. Biol. Macromol. 266 (2024) 131314. https://doi.org/10.1016/J.IJBIOMAC.2024.131314.

[135] H. Wang, K. ur Rehman, W. Feng, D. Yang, R. ur Rehman, M. Cai, J. Zhang, Z. Yu, L. Zheng, Physicochemical structure of chitin in the developing stages of black soldier fly, Int. J. Biol. Macromol. 149 (2020) 901–907. https://doi.org/10.1016/J.IJBIOMAC.2020.01.293.

[136] M.K. Lagat, S. Were, F. Ndwigah, V.J. Kemboi, C. Kipkoech, C.M. Tanga, microorganisms Antimicrobial Activity of Chemically and Biologically Treated Chitosan Prepared from Black Soldier Fly (Hermetia illucens) Pupal Shell Waste, (2021). https://doi.org/10.3390/microorganisms9122417.

[137] M. Triunfo, E. Tafi, A. Guarnieri, R. Salvia, C. Scieuzo, T. Hahn, S. Zibek, A. Gagliardini, L. Panariello, M.B. Coltelli, A. De Bonis, P. Falabella, Characterization of chitin and chitosan derived from Hermetia illucens, a further step in a circular economy process, (123AD). https://doi.org/10.1038/s41598-022-10423-5.

[138] I. Artilia, Z.Y. Dewi, W. Shofiani, W.N. Auli, N. Ahmad, Extraction and Characterization of Chitosan from Eco-Green <i>Hermetia Illucens</i> for Application in Dentistry, Key Eng. Mater. 965 (2023) 45–50. https://doi.org/10.4028/p-p8hENm.

[139] J.M. Paige, L. Ma, C. Chigbu, al -, Y. Niu, J. Sunarso, F. Liang, A. Nafisah, R. Mutia, A. Jayanegara, Chemical composition, chitin and cell wall nitrogen content of Black Soldier Fly (Hermetia illucens) larvae after physical and

biological treatment You may also like An Investigation of the Electrochemical Activity of (Ba/Sr)FeO 3-y Anodes A Comparative Study of Oxygen Reduction Reaction on Bi-and La-Doped SrFeO 3 Perovskite Cathodes Chemical composition, chitin and cell wall nitrogen content of Black Soldier Fly (Hermetia illucens) larvae after physical and biological treatment, IOP Conf. Ser. Mater. Sci. Eng. 546 (2019). https://doi.org/10.1088/1757-899X/546/4/042028.

[140] N.S. Liland, I. Biancarosa, P. Araujo, D. Biemans, C.G. Bruckner, R. Waagbø, B.E. Torstensen, E.-J. Lock, Modulation of nutrient composition of black soldier fly (Hermetia illucens) larvae by feeding seaweed-enriched media, (2017). https://doi.org/10.1371/journal.pone.0183188.

[141] Y. Ait Hamdan, S. Elouali, H. Oudadesse, B. Lefeuvre, M. Rhazi, Exploring the potential of chitosan/aragonite biocomposite derived from cuttlebone waste: Elaboration, physicochemical properties and in vitro bioactivity, Int. J. Biol. Macromol. 267 (2024) 131554. https://doi.org/10.1016/J.IJBIOMAC.2024.131554.

[142] A. Caligiani, A. Marseglia, G. Leni, S. Baldassarre, L. Maistrello, A. Dossena, S. Sforza, Composition of black soldier fly prepupae and systematic approaches for extraction and fractionation of proteins, lipids and chitin, Food Research International 105 (2018) 812–820. https://doi.org/10.1016/J.FOODRES.2017.12.012.

[143] C.-Y. Wong, S.-S. Rosli, Y. Uemura, Y.C. Ho, A. Leejeerajumnean, W. Kiatkittipong, C.-K. Cheng, M.-K. Lam, J.-W. Lim, Potential Protein and Biodiesel Sources from Black Soldier Fly Larvae: Insights of Larval Harvesting Instar and Fermented Feeding Medium, 12 (2019) 1570. https://doi.org/10.3390/en12081570.

[144] A. Nafary, S.A. Mousavi Nezhad, S. Jalili, Extraction and Characterization of Chitin and Chitosan from Tenebrio Molitor Beetles and Investigation of its Antibacterial Effect Against Pseudomonas aeruginosa., Adv. Biomed. Res. 12 (2023) 96. https://doi.org/10.4103/abr.abr_205_22.

[145] K. Mohan, T. Muralisankar, R. Jayakumar, C. Rajeevgandhi, A study on structural comparisons of α-chitin extracted from marine crustacean shell waste, Carbohydrate Polymer Technologies and Applications 2 (2021) 100037. https://doi.org/10.1016/j.carpta.2021.100037.

[146] M. Jang, B. Kong, Y. Jeong, C.H. Lee, J. Nah, Physicochemical characterization of α-chitin, β-chitin, and γ-chitin separated from natural resources, J. Polym. Sci. A Polym. Chem. 42 (2004) 3423–3432. https://doi.org/10.1002/pola.20176.

[147] S. Abolghassem, S. Molaei, S. Javanshir, Preparation of α-chitin-based nanocomposite as an effective biocatalyst for microwave aided domino reaction, Heliyon 5 (2019) e02036. https://doi.org/10.1016/j.heliyon.2019.e02036.

[148] J. Kumirska, M. Czerwicka, Z. Kaczyński, A. Bychowska, K. Brzozowski, J. Thöming, P. Stepnowski, Application of Spectroscopic Methods for Structural Analysis of Chitin and Chitosan, Mar. Drugs 8 (2010) 1567–1636. https://doi.org/10.3390/md8051567.

[149] N.M. Julkapli, Z. Ahmad, H.M. Akil, A.A. Bin Mohamed, X-Ray Diffraction Studies of Cross Linked Chitosan With Different Cross Linking Agents For Waste Water Treatment Application, in: 2010: pp. 106–111. https://doi.org/10.1063/1.3295578.

[150] S. Elouali, O. Dahbane, Y. Ait Hamdan, N. Eladlani, M. Rhazi, Exploring the potential use of chitosan derived from Hermetia illucens waste for olive oil mill wastewater treatment, EuroMediterr. J. Environ. Integr. (2024). https://doi.org/10.1007/s41207-024-00593-1.

[151] D. Purkayastha, S. Sarkar, Physicochemical Structure Analysis of Chitin Extracted from Pupa Exuviae and Dead Imago of Wild Black Soldier Fly (Hermetia illucens), 28 (2020) 445–457. https://doi.org/10.1007/s10924-019-01620-x.

[152] N.M. Farokhi, J.M. Milani, Z.R. Amiri, Production and comparison of structural, thermal and physical characteristics of chitin nanoparticles obtained by different methods, Sci. Rep. 14 (2024) 14594. https://doi.org/10.1038/s41598-024-65117-x.

[153] Y.A. Hamdan, H. Oudadesse, S. Elouali, N. Eladlani, B. Lefeuvre, M. Rhazi, Exploring the potential of chitosan from royal shrimp waste for elaboration of chitosan/bioglass biocomposite: Characterization and "in vitro" bioactivity, Int. J. Biol. Macromol. (2024) 134909. https://doi.org/10.1016/j.ijbiomac.2024.134909.

[154] M. Jang, B. Kong, Y. Jeong, C.H. Lee, J. Nah, Physicochemical characterization of α-chitin, β-chitin, and γ-chitin separated from natural resources, J. Polym. Sci. A Polym. Chem. 42 (2004) 3423–3432. https://doi.org/10.1002/pola.20176.

[155] M. Kaya, T. Baran, M. Asan-Ozusaglam, Y. Selim Cakmak, K. Ozcan Tozak, A. Mol, A. Mentes, G. Sezen, Extraction and Characterization of Chitin and Chitosan with Antimicrobial and Antioxidant Activities from Cosmopolitan Orthoptera Species (Insecta), Biotechnology and Bioprocess Engineering 20 (2015) 168–179. https://doi.org/10.1007/s12257-014-0391-z.

[156] Y.M. Chen, S. Pekdemir, I. Bilican, B. Koc-Bilican, B. Cakmak, A. Ali, L.S. Zang, M.S. Onses, M. Kaya, Production of natural chitin film from pupal shell of moth: Fabrication of plasmonic surfaces for SERS-based sensing applications, Carbohydr. Polym. 262 (2021) 117909. https://doi.org/10.1016/J.CARBPOL.2021.117909.

[157] C.S. Shin, D.Y. Kim, W.S. Shin, Characterization of chitosan extracted from Mealworm Beetle (Tenebrio molitor, Zophobas morio) and Rhinoceros Beetle (Allomyrina dichotoma) and their antibacterial activities, Int. J. Biol. Macromol. 125 (2019) 72–77. https://doi.org/10.1016/J.IJBIOMAC.2018.11.242.

[158] T. Marmier, C.R. Szczepanski, C. Candet, A. Zenerino, R.P. Godeau, G. Godeau, Investigation on Mecynorhina torquata Drury, 1782 (Coleoptera, Cetoniidae, Goliathini) cuticle: Surface properties, chitin and chitosan extraction, Int. J. Biol. Macromol. 164 (2020) 1164–1173. https://doi.org/10.1016/J.IJBIOMAC.2020.07.155.

[159] J. Ma, C. Xin, C. Tan, Preparation, physicochemical and pharmaceutical characterization of chitosan from Catharsius molossus residue, Int. J. Biol. Macromol. 80 (2015) 547–556. https://doi.org/10.1016/J.IJBIOMAC.2015.07.027.

[160] A. Gamage, N. Jayasinghe, P. Thiviya, M.L.D. Wasana, O. Merah, T. Madhujith, J.R. Koduru, Recent Application Prospects of Chitosan Based Composites for the Metal Contaminated Wastewater Treatment, Polymers (Basel). 15 (2023) 1453. https://doi.org/10.3390/polym15061453.

[161] A. Olohigbe, O. Etiosa, O. Wesley, Highly Deacetylated Chitosan as Low-cost Adsorbent Material for Removal of Heavy Metals from Water, Asian Journal of Physical and Chemical Sciences 5 (2018) 1–7. https://doi.org/10.9734/AJOPACS/2018/38599.

[162] S. Bensalem, B. Hamdi, S. Del Confetto, R. Calvet, Characterization of surface properties of chitosan/bentonite composites beads by inverse gas chromatography, Int. J. Biol. Macromol. 166 (2021) 1448–1459. https://doi.org/10.1016/J.IJBIOMAC.2020.11.024.

[163] F. Parthiban, S. Balasundari, A. Gopalakannan, K. Rathnakumar, S. Felix, Comparison of the Quality of Chitin and Chitosan from Shrimp, Crab and Squilla Waste, Current World Environment 12 (2017) 670–677. https://doi.org/10.12944/CWE.12.3.18.

[164] A. Islam, M.S. Islam, M.U.M.A. Zakaria, S.C. Paul, A.A. Mamun, Extraction and Worth Evaluation of Chitosan from Shrimp and Prawn Co-products, Am. J. Food Technol. 15 (2019) 43–48. https://doi.org/10.3923/ajft.2020.43.48.

[165] H. Zhu, H. Tang, F. Li, H. Sun, L. Tong, Effect of milling intensity on the properties of chitin, chitosan and chitosan films obtained from grasshopper, Int. J. Biol. Macromol. 239 (2023) 124249. https://doi.org/10.1016/J.IJBIOMAC.2023.124249.

[166] Y. Yu, X. Liu, J. Miao, K. Leng, Chitin from Antarctic krill shell: Eco-preparation, detection, and characterization, Int. J. Biol. Macromol. 164 (2020) 4125–4137. https://doi.org/10.1016/J.IJBIOMAC.2020.08.244.

[167] A. Hassainia, H. Satha, S. Boufi, Chitin from Agaricus bisporus: Extraction and characterization, Int. J. Biol. Macromol. 117 (2018) 1334–1342. https://doi.org/10.1016/j.ijbiomac.2017.11.172.

[168] K. Mohan, A.R. Ganesan, T. Muralisankar, R. Jayakumar, P. Sathishkumar, V. Uthayakumar, R. Chandirasekar, N. Revathi, Recent insights into the extraction, characterization, and bioactivities of chitin and chitosan from insects, Trends Food Sci. Technol. 105 (2020) 17–42. https://doi.org/10.1016/J.TIFS.2020.08.016.

[169] L. Soetemans, M. Uyttebroek, L. Bastiaens, Characteristics of chitin extracted from black soldier fly in different life stages, Int. J. Biol. Macromol. 165 (2020) 3206–3214. https://doi.org/10.1016/J.IJBIOMAC.2020.11.041.

[170] K. Piekarska, M. Sikora, M. Owczarek, J. Jóźwik-Pruska, M. Wiśniewska-Wrona, Chitin and Chitosan as Polymers of the Future—Obtaining, Modification, Life Cycle Assessment and Main Directions of Application, Polymers (Basel). 15 (2023) 793. https://doi.org/10.3390/polym15040793.

[171] N. Isobe, Y. Kaku, S. Okada, S. Kawada, K. Tanaka, Y. Fujiwara, R. Nakajima, D. Bissessur, C. Chen, Identification of Chitin Allomorphs in Poorly Crystalline Samples Based on the Complexation with Ethylenediamine, Biomacromolecules 23 (2022) 4220–4229. https://doi.org/10.1021/acs.biomac.2c00714.

[172] S. Ling, D.L. Kaplan, M.J. Buehler, Nanofibrils in nature and materials engineering, Nat. Rev. Mater. 3 (2018) 18016. https://doi.org/10.1038/natrevmats.2018.16.

[173] F. Breish, C. Hamm, S. Andresen, Nature's Load-Bearing Design Principles and Their Application in Engineering: A Review, Biomimetics 9 (2024) 545. https://doi.org/10.3390/biomimetics9090545.

[174] B. Cho, S.-J. Jang, H. Hwang, T. Kim, Convergent Evolution of Armor: Thermal Resistance in Deep-Sea Hydrothermal Vent Crustaceans, Biology (Basel). 13 (2024) 956. https://doi.org/10.3390/biology13120956.

[175] Z.W. White, F.J. Vernerey, Armours for soft bodies: how far can bioinspiration take us?, Bioinspir. Biomim. 13 (2018) 041004. https://doi.org/10.1088/1748-3190/aababa.

[176] H. Ning, C. Monroe, S. Gibbons, B. Gaskey, P. Flater, A review of helicoidal composites: From natural to bio-inspired damage tolerant materials, International Materials Reviews 69 (2024) 181–228. https://doi.org/10.1177/09506608241252498.

[177] K. Stamm, B.D. Saltin, J.-H. Dirks, Biomechanics of insect cuticle: an interdisciplinary experimental challenge, Applied Physics A 127 (2021) 329. https://doi.org/10.1007/s00339-021-04439-3.

[178] V. Perricone, E. Sarmiento, A. Nguyen, N.C. Hughes, D. Kisailus, The convergent design evolution of multiscale biomineralized structures in extinct and extant organisms, Commun. Mater. 5 (2024) 227. https://doi.org/10.1038/s43246-024-00669-z.

[179] N. Lee, P.R. Berthelson, V. Nguyen, M. Garrett, A.K. Brinda, R.D. Moser, M.F. Horstemeyer, H. Rhee, R.K. Prabhu, Microstructure and nanomechanical properties of the exoskeleton of an ironclad beetle (Zopherus haldemani), Bioinspir. Biomim. 16 (2021) 036005. https://doi.org/10.1088/1748-3190/abe27b.

[180] S. Elouali, Y. Ait Hamdan, S. Benali, P. Lhomme, M. Gosselin, J.M. Raquez, M. Rhazi, Extraction of chitin and chitosan from Hermetia illucens breeding waste: A greener approach for industrial application, Int. J. Biol. Macromol. 285 (2025) 138302. https://doi.org/10.1016/J.IJBIOMAC.2024.138302.

[181] Y.-S. Wang, M. Shelomi, Review of Black Soldier Fly (Hermetia illucens) as Animal Feed and Human Food, Foods 6 (2017) 91. https://doi.org/10.3390/foods6100091.

[182] H.P.S. Makkar, G. Tran, V. Heuzé, P. Ankers, State-of-the-art on use of insects as animal feed, Anim. Feed Sci. Technol. 197 (2014) 1–33. https://doi.org/10.1016/j.anifeedsci.2014.07.008.

[183] S. Kumari, P.K. Rath, Extraction and Characterization of Chitin and Chitosan from (Labeo rohit) Fish Scales, Procedia Materials Science 6 (2014) 482–489. https://doi.org/10.1016/j.mspro.2014.07.062.

[184] X. Liu, J. Zhang, K.Y. Zhu, Chitin in Arthropods: Biosynthesis, Modification, and Metabolism, in: 2019: pp. 169–207. https://doi.org/10.1007/978-981-13-7318-3_9.

[185] I.F.M. Rumengan, P. Suptijah, S. Wullur, A. Talumepa, Characterization of chitin extracted from fish scales of marine fish species purchased from local markets in North Sulawesi, Indonesia, IOP Conf. Ser. Earth Environ. Sci. 89 (2017) 012028. https://doi.org/10.1088/1755-1315/89/1/012028.

[186] P. Ramasamy, N. Subhapradha, V. Shanmugam, A. Shanmugam, Extraction, characterization and antioxidant property of chitosan from cuttlebone Sepia kobiensis (Hoyle 1885), Int. J. Biol. Macromol. 64 (2014) 202–212. https://doi.org/10.1016/j.ijbiomac.2013.12.008.

[187] M. Kaya, T. Baran, A. Mentes, M. Asaroglu, G. Sezen, K.O. Tozak, Extraction and Characterization of α-Chitin and Chitosan from Six Different Aquatic Invertebrates, Food Biophys. 9 (2014) 145–157. https://doi.org/10.1007/s11483-013-9327-y.

[188] M. Kaya, T. Baran, Description of a new surface morphology for chitin extracted from wings of cockroach (Periplaneta americana), Int. J. Biol. Macromol. 75 (2015) 7–12. https://doi.org/10.1016/j.ijbiomac.2015.01.015.

[189] H.F.G. Barbosa, D.S. Francisco, A.P.G. Ferreira, É.T.G. Cavalheiro, A new look towards the thermal decomposition of chitins and chitosans with different degrees of deacetylation by coupled TG-FTIR, Carbohydr. Polym. 225 (2019) 115232. https://doi.org/10.1016/j.carbpol.2019.115232.

[190] R.L. Lavall, O.B.G. Assis, S.P. Campana-Filho, β-Chitin from the pens of Loligo sp.: Extraction and characterization, Bioresour. Technol. 98 (2007) 2465–2472. https://doi.org/10.1016/j.biortech.2006.09.002.

[191] S. Kumari, P. Rath, A. Sri Hari Kumar, T.N. Tiwari, Extraction and characterization of chitin and chitosan from fishery waste by chemical method, Environ. Technol. Innov. 3 (2015) 77–85. https://doi.org/10.1016/j.eti.2015.01.002.

[192] M. Rinaudo, S. Pérez, From Chitin to Chitosan, 2019. https://www.glycopedia.eu/e-chapters/chitin-chitosan/article/abstract-introduction.

[193] M. Kaya, M. Mujtaba, E. Bulut, B. Akyuz, L. Zelencova, K. Sofi, Fluctuation in physicochemical properties of chitins extracted from different body parts of honeybee, Carbohydr. Polym. 132 (2015) 9–16. https://doi.org/10.1016/j.carbpol.2015.06.008.

[194] B. Kaczmarek, A. Sionkowska, A.M. Osyczka, Physicochemical properties of scaffolds based on mixtures of chitosan, collagen and glycosaminoglycans with nano-hydroxyapatite addition, Int. J. Biol. Macromol. 118 (2018) 1880–1883. https://doi.org/10.1016/j.ijbiomac.2018.07.035.

[195] A. Baxter, M. Dillon, K.D.A. Taylor, Improved method for i.r. determination of the degree of N-acetylation of chitosan, Int. J. Biol. Macromol. 14 (1992).

[196] E.S. Abdou, K.S.A. Nagy, M.Z. Elsabee, Extraction and characterization of chitin and chitosan from local sources, Bioresour. Technol. 99 (2008) 1359–1367. https://doi.org/10.1016/J.BIORTECH.2007.01.051.

[197] Y. Wang, Y. Chang, L. Yu, C. Zhang, X. Xu, Y. Xue, Z. Li, C. Xue, Crystalline structure and thermal property characterization of chitin from Antarctic krill (Euphausia superba), Carbohydr. Polym. 92 (2013) 90–97. https://doi.org/10.1016/J.CARBPOL.2012.09.084.

[198] B. Focher, P.L. Beltrame, A. Naggi, G. Torri, Alkaline N-deacetylation of chitin enhanced by flash treatments. Reaction kinetics and structure modifications, Carbohydr. Polym. 12 (1990) 405–418. https://doi.org/10.1016/0144-8617(90)90090-F.

[199] J. Blackwell, Structure of β-chitin or parallel chain systems of poly-β-(1→4)- *N* -acetyl- <scp>D</scp> -glucosamine, Biopolymers 7 (1969) 281–298. https://doi.org/10.1002/bip.1969.360070302.

[200] A. Domard, A perspective on 30 years research on chitin and chitosan, Carbohydr. Polym. 84 (2011) 696–703. https://doi.org/10.1016/j.carbpol.2010.04.083.

[201] W. Arbia, L. Arbia, L. Adour, A. Amrane, Chitin Extraction from Crustacean Shells Using Biological Methods-A Review, Food Technol. Biotechnol. 51(1) (2013) 12–25.

[202] F.Z. Aboudamia, M. Kharroubi, M. Neffa, F. Aatab, S. Hanoune, M. Bouchdoug, A. Jaouad, Potential of discarded sardine scales (*Sardina pilchardus*) as chitosan sources, J. Air Waste Manage. Assoc. 70 (2020) 1186–1197. https://doi.org/10.1080/10962247.2020.1813840.

[203] M. Yadav, P. Goswami, K. Paritosh, M. Kumar, N. Pareek, V. Vivekanand, Seafood waste: a source for preparation of commercially employable chitin/chitosan materials, Bioresour. Bioprocess. 6 (2019) 8. https://doi.org/10.1186/s40643-019-0243-y.

[204] M. Lavertu, Z. Xia, A.N. Serreqi, M. Berrada, A. Rodrigues, D. Wang, M.D. Buschmann, A. Gupta, A validated 1H NMR method for the determination of the degree of deacetylation of chitosan, J. Pharm. Biomed. Anal. 32 (2003) 1149–1158. https://doi.org/10.1016/S0731-7085(03)00155-9.

[205] L.D. Fernando, M.C. Dickwella Widanage, J. Penfield, A.S. Lipton, N. Washton, J.-P. Latgé, P. Wang, L. Zhang, T. Wang, Structural Polymorphism of Chitin and Chitosan in Fungal Cell Walls From Solid-State NMR and Principal Component Analysis, Front. Mol. Biosci. 8 (2021). https://doi.org/10.3389/fmolb.2021.727053.

[206] M.R. Kasaai, A review of several reported procedures to determine the degree of N-acetylation for chitin and chitosan using infrared spectroscopy, Carbohydr. Polym. 71 (2008) 497–508. https://doi.org/10.1016/J.CARBPOL.2007.07.009.

[207] F.A. Al Sagheer, M.A. Al-Sughayer, S. Muslim, M.Z. Elsabee, Extraction and characterization of chitin and chitosan from marine sources in Arabian Gulf, Carbohydr. Polym. 77 (2009) 410–419. https://doi.org/10.1016/j.carbpol.2009.01.032.

[208] A. Guarnieri, M. Triunfo, C. Scieuzo, D. Ianniciello, E. Tafi, T. Hahn, S. Zibek, R. Salvia, A. De Bonis, P. Falabella, Antimicrobial properties of chitosan from different developmental stages of the bioconverter insect Hermetia illucens, Sci. Rep. 12 (2022) 8084. https://doi.org/10.1038/s41598-022-12150-3.

[209] S. Kumari, S.H. Kumar Annamareddy, S. Abanti, P. Kumar Rath, Physicochemical properties and characterization of chitosan synthesized from fish scales, crab and shrimp shells, Int. J. Biol. Macromol. 104 (2017) 1697–1705. https://doi.org/10.1016/j.ijbiomac.2017.04.119.

[210] E.M. Dahmane, M. Taourirte, N. Eladlani, M. Rhazi, Extraction and Characterization of Chitin and Chitosan from Parapenaeus longirostris from Moroccan Local Sources, International Journal of Polymer Analysis and Characterization 19 (2014) 342–351. https://doi.org/10.1080/1023666X.2014.902577.

[211] A.Y. Alyami, A. Mahmood, Synthesis, characterization and application of chitosan functionalized and functional graphene oxide membranes for desalination of water by pervaporation, Environ. Res. 251 (2024) 118589. https://doi.org/10.1016/j.envres.2024.118589.

[212] N. Eladlani, E.M. Dahmane, M. Rhazi, M. Taourirte, Nanoparticles and whiskers-based chitosan films for Cr complexation, Environ. Chem. Lett. 13 (2015) 105–110. https://doi.org/10.1007/s10311-014-0488-9.

[213] H. Yi, R. Patel, K.D. Patel, L.-S. Bouchard, A. Jha, A.W. Perriman, M. Patel, Conducting polymer-based scaffolds for neuronal tissue engineering, J. Mater. Chem. B 11 (2023) 11006–11023. https://doi.org/10.1039/D3TB01838E.

[214] S. Boulila, H. Oudadesse, R. Kallel, F. Ghrab, B. Lefeuvre, T. Boudawara, A. Elfeki, H. Elfeki, The performance of a scaffold bioglass–chitosan in the treatment of bone defect, Polymer Bulletin 75 (2018) 5567–5586. https://doi.org/10.1007/s00289-018-2342-x.

[215] Y.A. Hamdan, H. Oudadesse, L. Jawad, K. Smimih, H. Kabdy, S. Elouali, N. Eladlani, M. Rhazi, Chitosan-Based Biomaterials for Tissue Engineering of Glial Cells, in: 2023: pp. 416–441. https://doi.org/10.4018/978-1-6684-9675-6.ch021.

[216] Y.A. Hamdan, B. El-Mansoury, S. Elouali, K. Rachmoune, A. Belbachir, H. Oudadesse, M. Rhazi, A review of chitosan polysaccharides: Neuropharmacological implications and tissue regeneration, Int. J. Biol. Macromol. (2024) 135356. https://doi.org/10.1016/J.IJBIOMAC.2024.135356.

[217] Y.A. Hamdan, S. Elouali, A. Ben Maloui, B. El-Mansoury, H. Oudadesse, M. Rhazi, Chitosan and its derivatives as potential neuro-protective agents for the treatment of Parkinson's disease, 2023. https://doi.org/10.4018/978-1-6684-5156-4.ch015.

[218] H. EL Knidri, J. Dahmani, A. Addaou, A. Laajeb, A. Lahsini, Rapid and efficient extraction of chitin and chitosan for scale-up production: Effect of process parameters on deacetylation degree and molecular weight, Int. J. Biol. Macromol. 139 (2019) 1092–1102. https://doi.org/10.1016/j.ijbiomac.2019.08.079.

[219] T. Fahmy, A. Sarhan, Characterization and molecular dynamic studies of chitosan–iron complexes, Bulletin of Materials Science 44 (2021) 142. https://doi.org/10.1007/s12034-021-02434-1.

[220] S. Elouali, J. Elarabi, F. El Amerany, Y. Ait Hamdan, N. Eladlani, S. Benali, H. Lamtai, E.H. El Mouden, J.-M. Raquez, M. Rhazi, Chitosan-enhanced hydroponic cultivation of Ocimum basilicum L.: a sustainable approach for improved growth, quality and antioxidant activity, EuroMediterr. J. Environ. Integr. 10 (2025) 4551–4564. https://doi.org/10.1007/s41207-025-00809-y.

[221] S.N. Ghanem, M.I. Marzouk, M.E. Tawfik, S.B. Eskander, Spectroscopic approaches for structural analysis of extracted chitosan generated from chitin deacetylated for escalated periods, BMC Chem. 19 (2025) 214. https://doi.org/10.1186/s13065-025-01558-3.

[222] V. Georgieva, D. Zvezdova, L. Vlaev, Non-isothermal kinetics of thermal degradation of chitosan, Chem. Cent. J. 6 (2012) 81. https://doi.org/10.1186/1752-153X-6-81.

[223] A. Verardi, R. Lamanna, C. Sposato, S. Samperna, D. Mammolenti, G. Coppola, O. Mileti, C.G. Lopresto, S. Palazzo, P. Sangiorgio, Impact of thermal pre-treatment on the extraction efficiency and physicochemical profile of chitin from blue crab (*Callinectes sapidus*) carapace, Int. J. Biol. Macromol. 347 (2026) 150802. https://doi.org/10.1016/j.ijbiomac.2026.150802.

[224] N. El Messaoudi, J. Georgin, D.S.P. Franco, M. Yılmazoğlu, B. Temur, Y. Miyah, M. Benjelloun, A.M. Al-Msiedeen, Composites based on porphyran as an adsorbent for environmentally friendly water treatment, React. Funct. Polym. 220 (2026) 106616. https://doi.org/10.1016/j.reactfunctpolym.2025.106616.

[225] D. Humelnicu, E.S. Dragan, M. Ignat, M.V. Dinu, A Comparative Study on Cu2+, Zn2+, Ni2+, Fe3+, and Cr3+ Metal Ions Removal from Industrial Wastewaters by Chitosan-Based Composite Cryogels, Molecules 25 (2020) 2664. https://doi.org/10.3390/molecules25112664.

[226] S. Panja, S. Hanson, C. Wang, EDTA-Inspired Polydentate Hydrogels with Exceptionally High Heavy Metal Adsorption Capacity as Reusable Adsorbents for Wastewater Purification, ACS Appl. Mater. Interfaces 12 (2020) 25276–25285. https://doi.org/10.1021/acsami.0c03689.

[227] L. Mu, G. Shi, H. Fang, Hydrated cation–π interactions of π-electrons with hydrated Mg2+ and Ca2+ cations, J. Chem. Phys. 160 (2024). https://doi.org/10.1063/5.0210995.

[228] Y. Liu, M. Shi, S. Fang, Q. Zhang, Q. Wu, N. Li, D. Lin, Superoleophobic Hierarchical Honeycomb Hydrogels for Effective Heavy Metal Removal in Crude Oil Emulsion, ACS Appl. Mater. Interfaces 17 (2025) 16187–16201. https://doi.org/10.1021/acsami.4c21809.

[229] K. Wang, F. Zhang, K. Xu, Y. Che, M. Qi, C. Song, Modified magnetic chitosan materials for heavy metal adsorption: a review, RSC Adv. 13 (2023) 6713–6736. https://doi.org/10.1039/D2RA07112F.

[230] N.N.A. Kadir, M. Shahadat, S. Ismail, Formulation study for softening of hard water using surfactant modified bentonite adsorbent coating, Appl. Clay Sci. 137 (2017) 168–175. https://doi.org/10.1016/j.clay.2016.12.025.

[231] Z. Wang, Z. Feng, L. Yang, M. Wang, Effective Removal of Calcium and Magnesium Ions from Water by a Novel Alginate–Citrate Composite Aerogel, Gels 7 (2021) 125. https://doi.org/10.3390/gels7030125.

[232] A.R.N. Pontillo, S. Koutsoukos, T. Welton, A. Detsi, Investigation of the influence of natural deep eutectic solvents (NaDES) in the properties of chitosan-stabilised films, Mater. Adv. 2 (2021) 3954–3964. https://doi.org/10.1039/D0MA01008A.

[233] M. Akram, Z. Bano, S.U.A. Bhutto, M.K. Majeed, J. Pan, L. Li, M. Xia, F. Wang, Enhanced nickel (II) removal from aqueous media using magnesium-Punica granatum linn based adsorbent: Mechanism and performance, J. Mol. Liq. 431 (2025) 127808. https://doi.org/10.1016/j.molliq.2025.127808.

[234] S. Subramaniam, K.Y. Foo, E.N. Md Yusof, A.H. Jawad, L.D. Wilson, S. Sabar, Hydrothermal synthesis of phosphorylated chitosan and its adsorption performance towards Acid Red 88 dye, Int. J. Biol. Macromol. 193 (2021) 1716–1726. https://doi.org/10.1016/J.IJBIOMAC.2021.11.009.

[235] H. Jim, Préparation, caractérisation, performances et mécanisme d'adsorption de l'oxyde de magnésium réticulé mésoporeux à surface spécifique élevée sur le Pb(II) dans les eaux usées, Préparation, Caractérisation, Performances et Mécanisme d'adsorption de l'oxyde de Magnésium Réticulé Mésoporeux à Surface Spécifique Élevée Sur Le Pb(II) Dans Les Eaux Usées (2024). https://meixi-mgo.com/preparation-of-mesoporous-magnesium-oxide/ (accessed February 13, 2026).

[236] M.A.A. Shahmirzadi, S.S. Hosseini, N.R. Tan, Enhancing removal and recovery of magnesium from aqueous solutions by using modified zeolite and bentonite and process optimization, Korean Journal of Chemical Engineering 33 (2016) 3529–3540. https://doi.org/10.1007/s11814-016-0218-z.

[237] Z. Zhang, T. Wang, H. Zhang, Y. Liu, B. Xing, Adsorption of Pb(II) and Cd(II) by magnetic activated carbon and its mechanism, Science of The Total Environment 757 (2021) 143910. https://doi.org/10.1016/j.scitotenv.2020.143910.

[238] L. Velarde, M.S. Nabavi, E. Escalera, M.-L. Antti, F. Akhtar, Adsorption of heavy metals on natural zeolites: A review, Chemosphere 328 (2023) 138508. https://doi.org/10.1016/j.chemosphere.2023.138508.

[239] J. Sun, Y. Liu, S. Hu, M. Yu, J. Lu, Adsorption Behavior of Cr3+ from Model Water by NaOH/Fe(III) Modified Clinoptilolite Zeolite, in: 2023: pp. 315–324. https://doi.org/10.1007/978-981-19-5783-3_25.

[240] T. Zhang, Y. Wang, Y. Kuang, R. Yang, J. Ma, S. Zhao, Y. Liao, H. Mao, Adsorptive removal of Cr 3+ from aqueous solutions using chitosan microfibers immobilized with plant polyphenols as biosorbents with high capacity and selectivity, Appl. Surf. Sci. 404 (2017) 418–425. https://doi.org/10.1016/j.apsusc.2017.02.018.

[241] L. Zhou, S. Zhang, K. Zhang, D. Ren, X. Zhang, Adsorption Performance and Mechanism of Cu2+ Adsorption from Aqueous Solution by Olivine Loaded with Magnesium Oxide Micro Rods, Water Air Soil Pollut. 236 (2025) 354. https://doi.org/10.1007/s11270-025-07981-5.

[242] J. Li, Y. Wei, L. Zou, S. Li, Y. Luo, Study on the Adsorption Mechanism of Cu^{2+} by ZnAl-LDH-Containing Exchangeable Interlayer Chloride Ions, Langmuir 40 (2024) 23754–23765. https://doi.org/10.1021/acs.langmuir.4c02644.

[243] Y. Gao, Y. Guan, J. Liang, L. Yu, Y. Ye, S. Chen, J. Lv, D. Cheng, Mechanism of Cu2+ selective adsorption by copper sulfide in hybrid capacitive deionization with hydrophobic binder, Process Safety and Environmental Protection 202 (2025) 107742. https://doi.org/10.1016/j.psep.2025.107742.

[244] H. Faqhiri, M. Hannula, M. Kellomäki, M.T. Calejo, J. Massera, Effect of Melt-Derived Bioactive Glass Particles on the Properties of Chitosan Scaffolds, J. Funct. Biomater. 10 (2019) 38. https://doi.org/10.3390/j™10030038.

[245] M. Rhazi, J. Desbrières, A. Tolaimate, M. Rinaudo, P. Vottero, A. Alagui, M. El Meray, Influence of the nature of the metal ions on the complexation with chitosan., Eur. Polym. J. 38 (2002) 1523–1530. https://doi.org/10.1016/S0014-3057(02)00026-5.

[246] N. Eladlani, E.M. Dahmane, A. Ouahrouch, M. Rhazi, M. Taourirte, Recovery of Chromium(III) from Tannery Wastewater by Nanoparticles and Whiskers of Chitosan, J. Polym. Environ. 26 (2018) 152–157. https://doi.org/10.1007/s10924-016-0926-9.

[247] J. Oliva, J. De Pablo, J.L. Cortina, J. Cama, C. Ayora, Removal of cadmium, copper, nickel, cobalt and mercury from water by Apatite II™: Column experiments, J. Hazard. Mater. 194 (2011) 312–323. https://doi.org/10.1016/J.JHAZMAT.2011.07.104.

[248] Z. Wang, Z. Feng, L. Yang, M. Wang, Effective Removal of Calcium and Magnesium Ions from Water by a Novel Alginate–Citrate Composite Aerogel, Gels 7 (2021) 125. https://doi.org/10.3390/gels7030125.

[249] M. Rhazi, J. Desbrières, A. Tolaimate, M. Rinaudo, P. Vottero, A. Alagui, Contribution to the study of the complexation of copper by chitosan and oligomers, Polymer (Guildf). 43 (2002) 1267–1276. https://doi.org/10.1016/S0032-3861(01)00685-1.

[250] Near East Foundation, Innovative Entrepreneurs Making an Impact, Https://Neareast.Org/Innovative-Entrepreneurs-Making-an-Impact/ (2024).